ARTICLE IN PRESS

Physics Reports xxx (xxxx) xxx

Contents lists available at ScienceDirect

Physics Reports

journal homepage: www.elsevier.com/locate/physrep

Characterising the Higgs boson with ATLAS data from the LHC Run-2

The ATLAS Collaboration[1]

ARTICLE INFO

Article history:
Received 15 May 2024
Received in revised form 15 October 2024
Accepted 1 November 2024
Available online xxxx
Editor: Giulia Zanderighi

This work is dedicated to the memory of Prof. Peter Ware Higgs, whose groundbreaking research on broken symmetries and mass generation predicted the boson that is the focus of this Report.

Keywords:
Higgs boson
Standard model physics

ABSTRACT

The Higgs boson was discovered by the ATLAS and CMS Collaborations in 2012 using data from Run 1 of the Large Hadron Collider (2010–2012). In Run 2 (2015–2018), about 140 fb^{-1} of proton–proton collisions at a centre-of-mass energy of 13 TeV were collected by the ATLAS experiment. This review presents the most important Run 2 results obtained by the ATLAS Collaboration regarding the properties of the Higgs boson and its interactions with other particles. The performed studies significantly enhance the understanding of the Higgs boson, while hunting for deviations from the predictions of the Standard Model of particle physics.

Contents

[1] See Appendix for more details.

https://doi.org/10.1016/j.physrep.2024.11.001

Please cite this article as:, Characterising the Higgs boson with ATLAS data from the LHC Run-2, Physics Reports (2024), https://doi.org/10.1016/j.physrep.2024.11.001.

1. Introduction

One of the main motivations for building the Large Hadron Collider (LHC) was to investigate the nature of electroweak symmetry breaking. After the discovery of the Higgs boson [1,2] by the ATLAS and CMS Collaborations [3,4], the focus has shifted to the measurement of its properties. Ever since, an important goal has been to determine whether the Higgs boson can be a portal to so-far undiscovered phenomena.

This report summarises the expansive Higgs boson analysis programme performed by the ATLAS Collaboration with the data recorded during Run 2 of the LHC (2015−2018) and discusses the wealth of exciting results available at the time of its publication. Unless otherwise specified, all results are based on the full Run 2 data sample, corresponding to 140 fb^{-1} of proton–proton (pp) collisions recorded with the ATLAS detector [5]. For detailed discussions of technical aspects of the conducted analyses, the reader is referred to the original publications, which are cited throughout the report. Searches for exotic Higgs boson decays and additional Higgs bosons are covered elsewhere [6].

1.1. The Higgs mechanism

The Standard Model of particle physics (SM) is a relativistic quantum field theory based on gauge symmetries that describes the elementary particles and their interactions [7–10]. Seemingly forbidden by gauge invariance, massive W and Z bosons are enabled by electroweak symmetry breaking. In its simplest form, electroweak symmetry breaking is realised through the introduction of a complex doublet scalar field, which manifests itself in a neutral scalar boson, the Higgs boson [11–15]. While the Higgs field potential itself is invariant under the SU(2) transformation, its shape allows for spontaneous symmetry breaking, which keeps the gauge symmetries intact but leads to a vacuum expectation value that is non-zero and non-invariant under SU(2). Interactions between the Higgs field and the fermions, the Yukawa interactions, give rise to the masses of the fermions. The Yukawa couplings and the Higgs boson mass are free parameters in the SM.

The LHC offers a unique opportunity to study the Higgs sector and therefore the nature of electroweak symmetry breaking. With the measurement of the Higgs boson mass, the SM Higgs sector is fully determined by experimentally measured parameters. Measurements of the Higgs boson couplings to other particles and the Higgs boson self-coupling are of particular importance. The Yukawa sector describes a completely new boson–fermion interaction that is the only interaction in the SM that distinguishes between particles of different masses and therefore flavours. The Higgs boson self-coupling is mainly probed through double Higgs boson production and is an important parameter of the Higgs field potential, which is related to the structure of the vacuum and governs the properties of the electroweak phase transition in the early universe [16,17].

The SM Higgs boson is a scalar boson: spin zero and its interactions are even under charge–parity (CP) conjugation. In pp collisions, the main Higgs boson production mechanisms predicted by the SM are gluon–gluon fusion (ggF), vector-boson fusion (VBF), and associated production with vector bosons (VH, where V represents a W or Z boson), top- or bottom-quark pairs ($t\bar{t}H$, $b\bar{b}H$), or a single top quark (tH). The different production processes can be tagged through dedicated selection criteria, taking advantage of the particular signatures of the different final states. They are shown, together with the main predicted decay processes, in Fig. 1. The corresponding diagrams for double Higgs boson production through the ggF and VBF mechanisms are shown in Fig. 2. The expected width of the SM Higgs boson for a mass of 125 GeV is 4.1 MeV [18].

1.2. SM predictions for Higgs boson production and decay

Complementing the measurement programme at the LHC, there is an intense effort ongoing to calculate Higgs boson production cross-sections and branching ratios, as well as their associated uncertainties, to the best possible accuracy in various phase space regions. Furthermore, Monte Carlo (MC) simulations are developed to optimise the experimental data analysis and to compare observed and expected results. These differential predictions are more challenging and therefore only available at lower precision than the total production cross-sections.

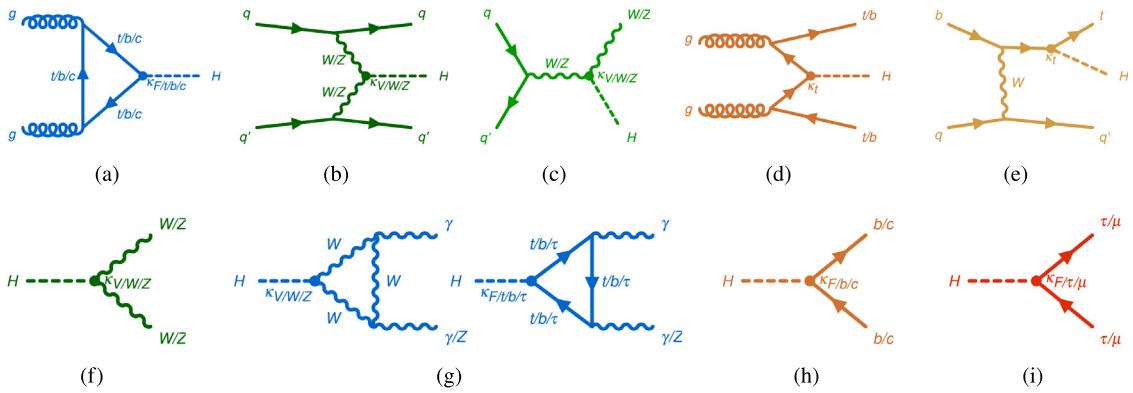

Fig. 1. Top: Higgs boson production via (a) gluon–gluon fusion, (b) vector-boson fusion, and (c) associated production with vector bosons, (d) top- or bottom-quark pairs, or (e) a single top quark. Bottom: Higgs boson decays into (f) a pair of vector bosons, (g) a pair of photons or a Z boson and a photon, (h) a pair of quarks, and (i) a pair of charged leptons [19].

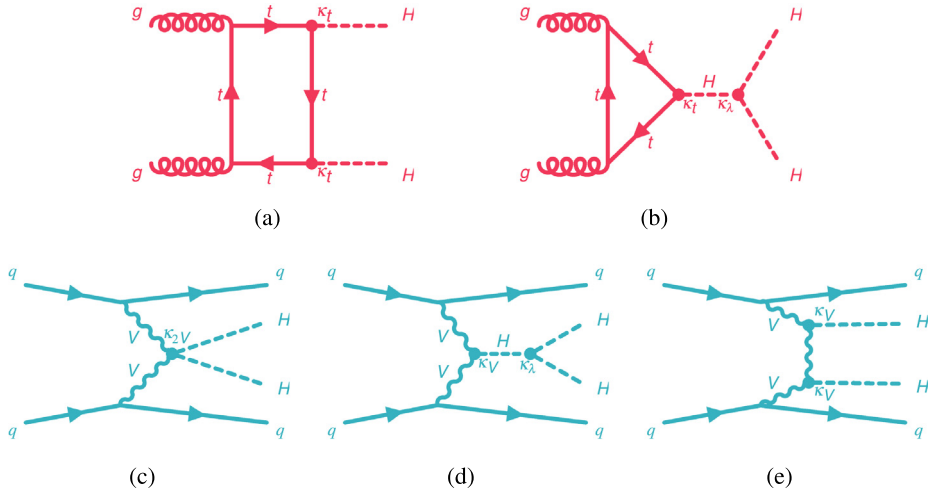

Fig. 2. Examples of leading-order Feynman diagrams for Higgs boson pair production in the (a and b) ggF HH and (c, d and e) VBF HH modes.

Table 1
SM predictions of Higgs boson production cross-sections for a Higgs boson mass of 125.09 GeV in pp collisions at a centre-of-mass energy of $\sqrt{s} = 13$ TeV. The values are based on Refs. [21–33] for ggF, Refs. [34–36] for VBF, Refs. [37–45] for WH and ZH, Refs. [46–49] for $t\bar{t}H$, Refs. [50–52] for $b\bar{b}H$, and Refs. [53,54] for tH. They are compiled in Ref. [18].

Process	Precision in QCD	Precision in EW	Cross-section [pb]	Fraction [%]
ggF	N^{3}LO	NLO	$48.5^{+2.7}_{-3.6}$	87.2
VBF	approx. NNLO	NLO	3.78 ± 0.08	6.8
$qq \to WH$	NNLO	NLO	1.37 ± 0.03	2.44
$qq \to ZH$	NNLO	NLO	$0.76^{+0.01}_{-0.02}$	1.35
$gg \to ZH$	NLO	LO	$0.12^{+0.03}_{-0.02}$	0.22
$t\bar{t}H$	NLO	NLO	$0.51^{+0.03}_{-0.05}$	0.92
$b\bar{b}H$	NNLO	LO	$0.49^{+0.10}_{-0.12}$	0.88
tH	NLO	LO	$0.092^{+0.006}_{-0.011}$	0.16

SM Higgs boson production cross-sections are calculated for the different production modes shown in Fig. 1(a)–(e). The total cross-sections are listed in Table 1, including the achieved accuracy in the electroweak (EW) and strong (QCD) coupling constant, i.e., tree-level or leading order (LO), next-to-leading order (NLO), next-to-next-to leading order (NNLO), etc. They are calculated assuming a Higgs boson mass of 125.09 GeV. This value is based on the combined Higgs boson mass measurement by the ATLAS and CMS Collaborations in the LHC Run 1 [20].

The SM predicts the double Higgs boson production cross-section to be more than a thousand times smaller than single Higgs boson production: $\sigma_{\text{ggF } HH} = 31.0^{+2.1}_{-7.2}$ fb [18,55–64], computed at NNLO in QCD including approximated mass top effects, and $\sigma_{\text{VBF } HH} = 1.73 \pm 0.04$ fb, at N^{3}LO in QCD, for a Higgs boson mass of 125 GeV [65–67].

Branching fractions, or decay probabilities for the different Higgs boson decays, as depicted in Fig. 1(f)–(i), also depend on the Higgs boson mass. For a mass of 125.09 GeV, the SM predicts that decays into W bosons have a branching fraction of 22%, Z bosons of 3%, photons (γ) of 0.2%, and Z boson and photon of 0.2%. Decays into fermion pairs have the following branching ratios: bottom quarks 58%, charm quarks 3%, τ leptons 6%, and muons 0.02% [68–72].

For most of the analyses discussed in this report, samples were produced with MC generators as follows: ggF events were simulated using the Powheg NNLOPS program [33,73–77], which provides NNLO accuracy in QCD. The other production modes were simulated with the Powheg generator [73–75,78–80] at an accuracy of NLO in QCD, except for $b\bar{b}H$ and tH, which were simulated using the MadGraph5_aMC@NLO generator, also at NLO accuracy in QCD [81]. In the majority of cases, the Pythia program is used to simulate decays and to model the effects of parton showering, hadronisation and the underlying event. To evaluate modelling uncertainties, alternative samples showered with the Herwig program are used. The effect of multiple interactions in the same and neighbouring LHC bunch crossings (pile-up) was modelled by overlaying the original hard-scattering event with simulated inelastic pp events. The generated events were passed through a simulation of the ATLAS detector [82] using Geant4 [83].

1.3. The LHC run 1 legacy: From the discovery of the Higgs boson to the first property measurements

1.3.1. The Higgs boson discovery

By 2012, both the LEP collider at CERN and the Tevatron collider at Fermilab had searched for the Higgs boson and excluded the existence of a SM Higgs boson with a mass below 114.4 GeV [84] or between 149 and 182 GeV [85] at 95% confidence level (CL). SM consistency fits based on precision electroweak measurements hinted at a Higgs boson with a mass of $\sim 90 \pm 30$ GeV [86,87].

Due to record centre-of-mass energies and a steady increase in collected pp data, Run 1 of the LHC saw a continuous widening of the excluded mass ranges for a SM Higgs boson, except for masses around 125 GeV, where, during the 2011 and 2012 data taking, the data recorded by the ATLAS and CMS detectors showed an excess over the background-only hypothesis.

On July 4th, 2012, based on approximately 10 fb^{-1} of recorded LHC data each, the ATLAS and CMS Collaborations individually announced the discovery of a neutral boson with a mass of about 125 GeV [1,2]. As shown in Fig. 3, multiple decay channels contributed to the combined significance of the excess, which exceeded the five standard deviation (σ) discovery threshold. The ones with the highest significances were the $\gamma\gamma$ and four-lepton ($ZZ^* \to 4\ell$, $\ell = e, \mu$) final states, which provide an excellent invariant mass resolution and favourable signal-to-background ratios, as well as the $WW^* \to e\nu\mu\nu$ final state. Fig. 4 shows the observed excess in the $\gamma\gamma$ and 4ℓ invariant mass distributions, and in the transverse mass distribution for the $H \to WW^* \to e\nu\mu\nu$ decay channel, where the transverse momentum of the neutrinos is estimated through the missing transverse momentum in the detector. This results in the wider distribution seen in Fig. 4(c). The transverse mass is defined as $m_{\text{T}} = \sqrt{(E_{\text{T}}^{\ell\ell} + E_{\text{T}}^{\text{miss}})^2 - |\vec{p}_{\text{T}}^{\,\ell\ell} + \vec{p}_{\text{T}}^{\,\text{miss}}|^2}$, where $\vec{p}_{\text{T}}^{\,\ell\ell}$ is the transverse momentum vector of the dilepton system, $\vec{p}_{\text{T}}^{\,\text{miss}}$ is the missing transverse momentum vector with magnitude $E_{\text{T}}^{\text{miss}}$, and $E_{\text{T}}^{\ell\ell}$ is the square root of sum in quadrature of the magnitude of $\vec{p}_{\text{T}}^{\,\ell\ell}$ and the invariant mass of the dilepton system.

1.3.2. First measurements of the Higgs boson properties

The data produced by the LHC and recorded by the ATLAS and CMS detectors in Run 1, in particular the 20 fb^{-1} of data at 8 TeV centre-of-mass energy recorded in 2012, allowed the first measurements of the properties of the newly discovered particle.

A Higgs boson mass measurement in the $H \to ZZ^* \to 4\ell$ and $H \to \gamma\gamma$ decay channels, combining ATLAS and CMS data, resulted in a value of $m_H = 125.09 \pm 0.24$ GeV [20]. This value is used as input to almost all measurements performed by the ATLAS Collaboration based on the LHC Run 2 data. In most measurements, the effect of the associated uncertainty is negligible.

Combining ATLAS and CMS Higgs boson measurements from Run 1 in all accessible production and decay channels, the Higgs boson signal yield relative to the SM prediction, also called signal strength μ, was measured to be 1.09 ± 0.11 [88]. Each experiment observed, with more than 5σ significance, the ggF production process and the decays into two Z bosons, two W bosons, and two photons. The combination also allowed observation of VBF production and decays into two τ-leptons. Assuming SM coupling structures, the couplings of the Higgs boson to the gauge bosons were measured with an accuracy of $\sim$10%, to top quarks and τ-leptons with $\sim$17%, and to bottom quarks with $\sim$30%.

Differential cross-section measurements were performed in the $H \to \gamma\gamma$, $H \to ZZ^* \to 4\ell$, and $H \to WW^* \to e\nu\mu\nu$ decay channels [89–92], analysing Higgs boson kinematics and properties of associated hadronic jet production.

First statements could also be made in Run 1 regarding the spin and CP properties of the newly discovered particle. The fact that decays into two bosons were observed clearly characterises the particle as a boson, with the diphoton decay excluding the spin-1 possibility [93,94]. Spin and CP studies of diboson decays [95] confronted the scalar hypothesis with several alternative spin scenarios, including non-SM spin-0 and spin-2 models with universal and non-universal couplings

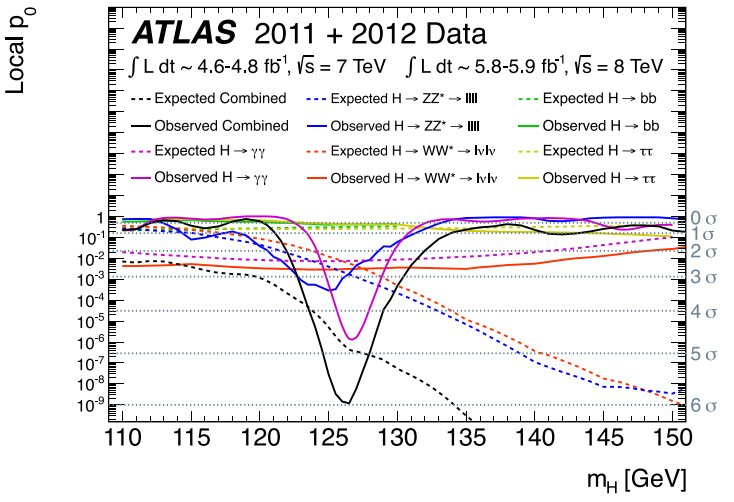

Fig. 3. Left vertical axis: The p-value, i.e., the probability for a background-only experiment to be more like the signal than the observation, for individual decay channels and their statistical combination. Right vertical axis: The translation to standard deviations. The horizontal axis shows the Higgs boson mass hypothesis [1].

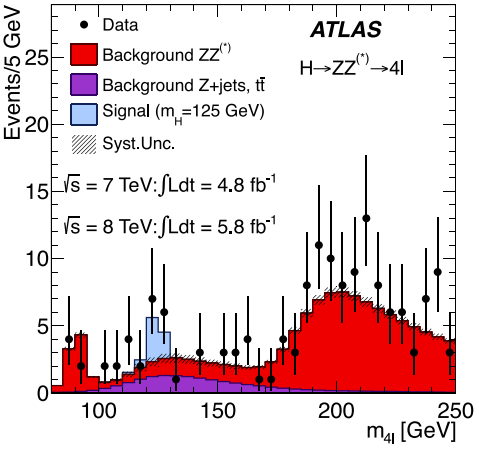

(a)

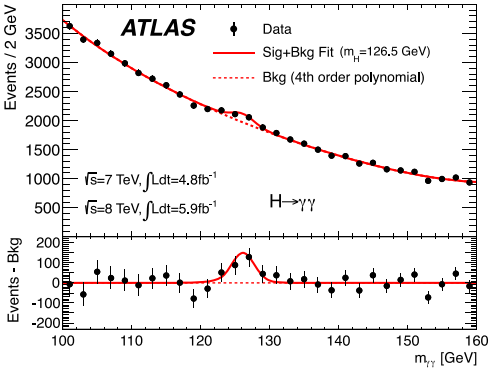

(b)

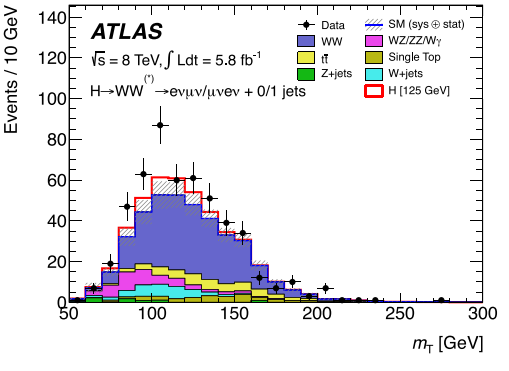

(c)

Fig. 4. Invariant mass distributions in the (a) $ZZ^* \to 4\ell$ and (b) $\gamma\gamma$ final states, and (c) the transverse mass in the $WW^* \to e\nu\mu\nu$ final state, showing the excesses in data events over the background-only hypotheses that led to the discovery of the Higgs boson [1].

to fermions and vector bosons. All tested alternative models were excluded in favour of the SM Higgs boson hypothesis at a CL of more than 99.9%. No sign of CP violation was found in VBF production with τ-lepton decays [96].

An upper limit was set on the width of the Higgs boson by the ATLAS Collaboration of 22.7 MeV [97], which corresponds to roughly six times the SM expectation. This assumed that the signal strength on the Higgs boson peak and off-shell is the same [98–101].

Within the achieved statistical and systematic uncertainties, all measurements in Run 1 agreed with the predictions for a SM Higgs boson.

In Run 2 of the LHC, the ATLAS detector recorded 140 fb^{-1} of pp collision data. For this data sample, the SM predicts a total of ∼9 million Higgs bosons produced at the ATLAS interaction point, of which 0.3% are experimentally accessible [19]. Making use of this unprecedented amount of data, the goals for Run 2 included a more precise determination of the Higgs boson mass and width (see Section 2), and of fiducial and differential cross-sections (see Section 3). Measurements of the Higgs boson couplings to fermions, in particular the direct observation of the Yukawa couplings to third generation quarks (see Section 4) were eagerly anticipated, as were the searches for rare decays (see Sections 4 and 5). The larger data sample also allowed increased precision on the measured Higgs boson production cross-sections and couplings to other particles (see Section 6) and the study of the CP properties of both the boson and fermion couplings (see Section 7). Finally, enormous progress was made regarding the search for Higgs boson pair production and the constraints on the Higgs boson self-coupling (see Section 8).

2. Higgs boson mass and width

2.1. Higgs boson mass

The SM predicts the existence of a Higgs boson but not its mass, which therefore has to be measured experimentally. Once the mass of the Higgs boson is known, together with the masses of fermions, the SM production cross-section and branching ratios can be calculated. They can then be checked experimentally to search for deviations from SM predictions due to potential new phenomena. The value of the Higgs boson mass also affects the SM predictions of the effective weak mixing angle and, logarithmically, the W boson mass (see e.g., Ref. [102]). Moreover, the shape and energy evolution of the Higgs potential are directly related to the Higgs boson mass, which therefore determines the stability of the electroweak vacuum [16,103].

Among the various decay modes, $H \to \gamma\gamma$ and $H \to ZZ^* \to 4\ell$ play a special role in the characterisation of the Higgs boson and in particular the measurement of its mass. Both final states are fully reconstructable, provide an excellent mass resolution, and are accompanied by well-understood backgrounds. Among the two, $H \to \gamma\gamma$ yields more signal events, while $H \to ZZ^* \to 4\ell$ benefits from a higher signal-to-background ratio.

The $H \to \gamma\gamma$ decay channel [104] allows the direct observation of a narrow mass peak over a smooth background that can be determined directly from the collected data. The typical mass resolution in the ATLAS detector is 1.7 GeV for a Higgs boson mass of 125 GeV. The main background process is non-resonant $\gamma\gamma$ production with a smaller contribution of about 25% from γ+jet and dijet processes where one or two of the hadronic jets are misidentified as photons. In the $H \to \gamma\gamma$ analysis, the Higgs boson properties (e.g., signal yield, mass) are measured in events with at least two isolated and well-identified photon candidates. The selection efficiency for events with a SM Higgs boson decaying into two photons is about 36%. Depending on the measurement being performed, events are classified into different categories to improve the specific sensitivity to a given observable. In the case of the Higgs boson mass measurement, the selected events are classified into 14 categories with different signal-to-background ratios, invariant mass resolutions and photon energy scale uncertainties.

The invariant diphoton mass distribution ($m_{\gamma\gamma}$) of the simulated signal in each category is found to be very well described by a double-sided Crystal Ball [105] probability density function. The normalisation factors of the signal, one for each category, are treated as free parameters in the fit to reduce the model-dependence of the measurement. In each category, the $m_{\gamma\gamma}$ distribution of the background processes is represented by either an exponential function, a power-law function, or the exponential of a second-order polynomial.

One key aspect of the mass measurement in the $H \to \gamma\gamma$ channel is the careful control of the systematic uncertainties, mainly arising from the photon energy scale. A significant effort was devoted during Run 2 to substantially reduce these uncertainties, resulting in a decrease of a factor close to four compared to the mass measurement performed with the initial 36 fb^{-1} of LHC Run 2 data [106]. This improvement in the photon energy scale calibration was achieved through a better understanding of the energy response across the longitudinal layers of the ATLAS electromagnetic calorimeter and a new correction implemented in the extrapolation of the electron energy scale measured in $Z \to ee$ events to photons [107]. The impact of the photon energy scale uncertainty on the mass measurement was reduced to 83 MeV. Systematic uncertainties related to the choice of the function used to describe the background are also taken into account, with a minor impact on the mass measurement, but more relevant for analyses targeting the measured signal yield. The measured mass of the Higgs boson in the $H \to \gamma\gamma$ final state using the full Run 2 data sample is $m_H = 125.17 \pm 0.11(\text{stat.}) \pm 0.09(\text{syst.})$ GeV. The measurement is statistically limited, hence opening the possibility for substantial improvements with the future LHC runs. The diphoton invariant mass distribution of all selected data events, weighted according to the signal-to-background ratio in the respective category, and the fitted functions are shown in Fig. 5(a).

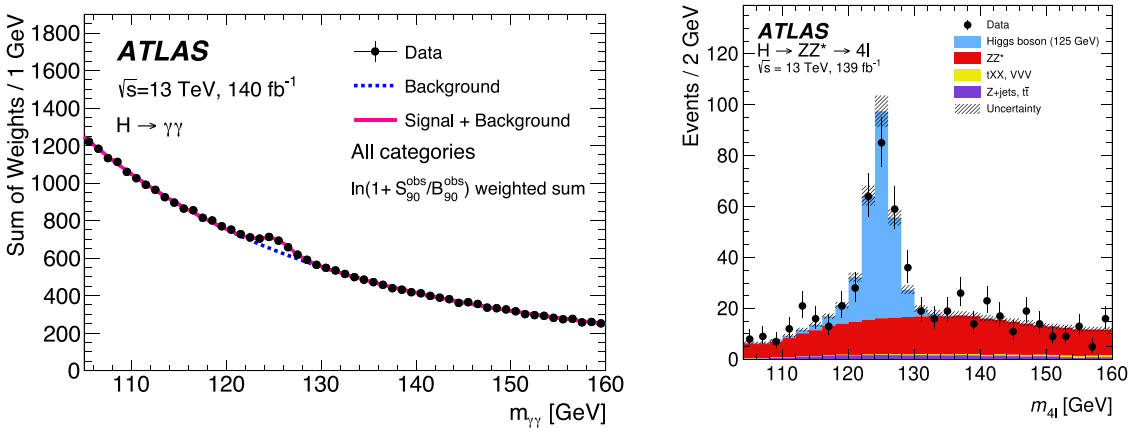

Fig. 5. (a) Weighted diphoton invariant mass distribution of all selected data events, overlaid with the result of the fit [104]. (b) Four-lepton invariant mass distribution of the selected events in data compared with the simulation [108].

***H → ZZ* → 4ℓ* decays** [108] are reconstructed by requiring two pairs of oppositely charged same-flavour isolated electrons or muons in the final state. One of the two pairs, the leading lepton pair is required to have an invariant mass compatible with that of the Z boson. The events are split into four sub-channels according to the flavour of the leading and subleading lepton pair (4μ, $2e2\mu$, $2\mu2e$, $4e$). The selection efficiency ranges between 31% and 16%, depending on the sub-channel. The dominant background process is non-resonant $ZZ \to 4\ell$ production, which is suppressed in this specific measurement by using a neural network (NN) based classifier. The measurement of the Higgs boson mass is carried out by simultaneously fitting the reconstructed invariant mass of the four-lepton system ($m_{4\ell}$) in the four sub-channels using an unbinned maximum-likelihood approach. The resolution of $m_{4\ell}$ varies from approximately 1.5 GeV to 2.1 GeV. The signal model comprises a double-sided Crystal Ball probability density function, with the mean of its Gaussian core determined as a function of m_H and the standard deviation expressed as a function of the predicted event-level resolution. In the fitting procedure, the normalisations of the signal and background components are treated as free parameters for each of the four sub-channels.

Fig. 5(b) shows the four-lepton invariant mass distribution of the selected events in data compared with the simulation. The Higgs boson mass measured in the $H \to ZZ^* \to 4\ell$ channel using the Run 2 data sample is $m_H = 124.99 \pm 0.18(\text{stat.}) \pm 0.04(\text{syst.})$ GeV, with the dominant source of systematic uncertainty arising from the uncertainties in the muon momentum scale, resolution and sagitta bias correction (28 MeV) and the electron energy scale (19 MeV).

The combination of the mass measurements performed with the $H \to \gamma\gamma$ and $H \to ZZ^* \to 4\ell$ channels using Run 1 and Run 2 [20] data results in a Higgs boson mass of $m_H = 125.11 \pm 0.09(\text{stat.}) \pm 0.06(\text{syst.})$ GeV [109], which corresponds to an experimental precision of 0.09%. With the current precision achieved in the Higgs boson mass, the impact of its uncertainty on the Higgs boson production cross-sections and branching ratios is below 1%. A summary plot of the Higgs boson mass measurements performed in Run 1 and Run 2 and their combination is shown in Fig. 6.

2.2. Higgs boson width

Once the mass of the Higgs boson is known, the SM allows the width to be computed. For a Higgs boson with a mass of 125 GeV, the expected width is only $\Gamma_H = 4.1$ MeV [18]. Any deviation from this value would indicate the presence of phenomena beyond the SM, e.g., Higgs boson decays into so-far unknown particles.

Due to the experimental mass resolution in the most precise channels ($H \to \gamma\gamma$ and $H \to ZZ^* \to 4\ell$) of the order of 1−2 GeV, a direct measurement of the SM width of the Higgs boson is not achievable from the detected lineshapes. Similarly, the corresponding lifetime is so short that the decay length is extremely small, well beyond the experimental resolution on the reconstruction of the displaced vertex from the beam spot. In addition, the width cannot be extracted from the rate measurement in the different decay channels because only cross-section times branching-ratio measurements are possible at the LHC. However, in 2012, a different method was proposed, which relies on measuring on-shell and off-shell Higgs boson production [98–101]. In the SM, despite the small total width, about 10% of the $gg \to H^* \to VV$ ($V = W, Z$) events are produced with an invariant mass larger than twice the vector bosons masses. In particular, the vector bosons from the Higgs boson decay and the top quarks running in the ggF production loop can be on-shell above the thresholds of $2m_V$ and $2m_t$, respectively. On-shell Higgs boson production is inversely proportional to the width, e.g., for ggF production with the Higgs boson decaying into two V bosons

$$\sigma^{\text{on-shell}}_{gg\to H\to VV} \propto \frac{g^2_{ggF,\text{on-shell}} g^2_{HVV,\text{on-shell}}}{\Gamma_H m_H}, \tag{1}$$

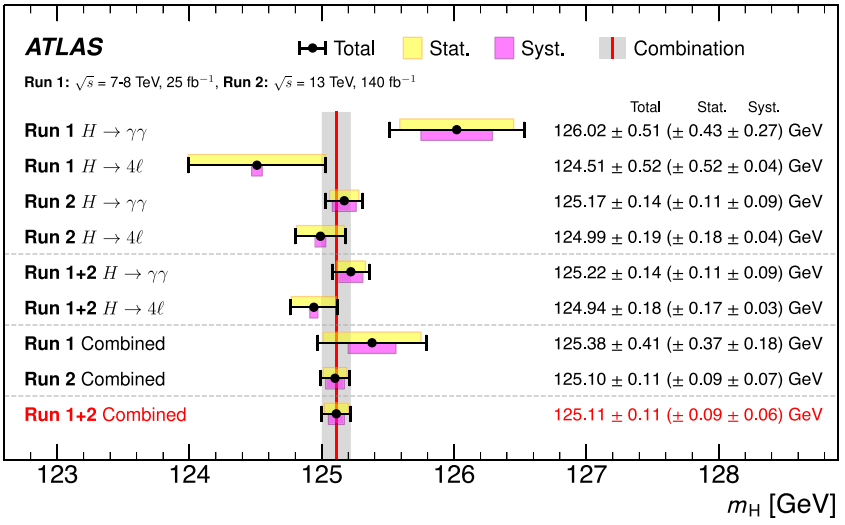

Fig. 6. ATLAS Higgs boson mass measurement combining LHC Run 1 and Run 2 results in the $H \to \gamma\gamma$ and $H \to ZZ^* \to 4\ell$ final states [109].

where $g_{ggF,\mathrm{on-shell}}$ and $g_{HVV,\mathrm{on-shell}}$ are the on-shell couplings associated with the Higgs boson production and decay. On the other hand, off-shell Higgs boson production has negligible dependence on the width, e.g.,

$$\sigma^{\mathrm{off-shell}}_{gg\to H\to VV} \propto \frac{g^2_{ggF,\mathrm{off-shell}} g^2_{HVV,\mathrm{off-shell}}}{m^2_{VV}}. \tag{2}$$

Similar expressions apply to electroweak production, where the g_{ggF} coupling is replaced by the g_{HVV} coupling. If the effective couplings have a known relationship (e.g., the one predicted in the SM) in the on-shell and off-shell regimes, the ratio of the off-shell to the on-shell production allows the determination of Γ_H.

The off-shell Higgs boson signal cannot be treated independently of the $gg \to VV$ background due to significant negative interference between the two processes [98]. For a given off-shell signal strength $\mu_{\mathrm{off-shell}}$, the expected number of events as a function of the invariant mass of the diboson system, m_{VV}, is positive and corresponds to the sum of the $gg \to VV$ background, the off-shell signal, which is proportional to $\mu_{\mathrm{off-shell}}$, and the (negative) interference term, which is proportional to $\sqrt{\mu_{\mathrm{off-shell}}}$. Additionally, when extracting the width of the Higgs boson, it must also be assumed that any new phenomena affecting the off-shell signal strength and the off-shell couplings do not modify the relative phase of the interfering signal and background processes. The full Run 2 data sample is used to study off-shell Higgs boson production and set an upper limit on the width of the Higgs boson through the $ZZ \to 4\ell$ and $ZZ \to 2\ell 2\nu$ final states [110], which were identified as the most sensitive channels in Run 1 [111].

The $ZZ \to 4\ell$ analysis selects events with two same-flavour oppositely charged dilepton pairs and a four-lepton invariant mass above the on-shell ZZ production threshold. The mass of each dilepton pair is required to be compatible with that of a Z boson. The signal regions are designed to be sensitive to both the electroweak and ggF production modes, considering only events with $m_{4\ell} > 220$ GeV, while events with $180 < m_{4\ell} < 220$ GeV are used to constrain the normalisation of the dominant $qq \to ZZ$ process. To enhance the signal sensitivity, a multi-class dense NN is used to distinguish among the off-shell Higgs boson signal, the interfering background and non-interfering background. Two separate NNs are trained for ggF and electroweak-induced signals. The NN's output is employed to define the final observable, serving as a discriminating variable in the corresponding signal region. Fig. 7(a) shows the observed distribution of the NN based discriminant in the ggF signal region compared with the SM expectations.

In the $ZZ \to 2\ell 2\nu$ final state, the presence of neutrinos prevents the kinematic reconstruction of m_{ZZ}. The discriminating variable used to enhance sensitivity to the off-shell production of the Higgs boson is therefore the transverse mass, computed from the transverse components of the momenta, defined as

$$m^{ZZ}_{\mathrm{T}} \equiv \sqrt{\left(\sqrt{m^2_Z + (p^{\ell\ell}_{\mathrm{T}})^2} + \sqrt{m^2_Z + (E^{\mathrm{miss}}_{\mathrm{T}})^2}\right)^2 - \left|\vec{p}^{\,\ell\ell}_{\mathrm{T}} + \vec{p}^{\,\mathrm{miss}}_{\mathrm{T}}\right|^2}, \tag{3}$$

which is reconstructed from the mass of the Z boson m_Z, the transverse momentum vector of the dilepton system $\vec{p}^{\,\ell\ell}_{\mathrm{T}}$ and the missing transverse momentum vector $\vec{p}^{\,\mathrm{miss}}_{\mathrm{T}}$, along with their respective magnitudes. Signal events are selected by requiring two oppositely charged electron or muon candidates with a dilepton invariant mass compatible with the Z boson mass and high $E^{\mathrm{miss}}_{\mathrm{T}}$, vetoing events with a third lepton. Additional selection criteria are optimised to maximise the signal significance relative to the main backgrounds, which include ZZ, WZ, WW, top-quark, and W/Z+jets processes. Fig. 7(b) shows the observed m^{ZZ}_{T} distribution compared with the SM prediction in the ggF signal region.

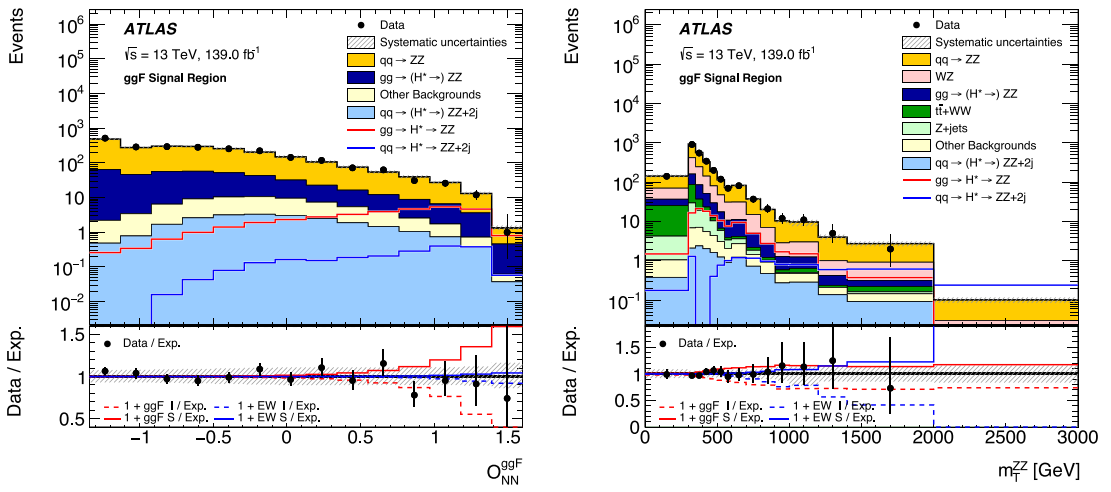

Fig. 7. (a) Observed and expected distribution of the NN-based observable sensitive to the off-shell production in the 4ℓ channel in the ggF signal region [110]. (b) Observed and expected transverse mass distribution in the $2\ell 2\nu$ channel in the ggF signal region [110].

Combining the 4ℓ and $2\ell 2\nu$ channels, the ratio of the off-shell Higgs boson production rate to its SM prediction (μ_{offshell}) is measured. The data are found to be consistent with SM predictions, rejecting the hypothesis of no off-shell Higgs boson production ($\mu_{\text{offshell}} = 0$) with an observed (expected) statistical significance of 3.3 (2.2)σ, thus providing experimental evidence for this process. In addition, these results are combined with the on-shell Higgs boson measurements in the $H \to ZZ^* \to 4\ell$ channel [112], obtaining an indirect measurement of the width of the Higgs boson of $\Gamma_H = 4.5^{+3.0}_{-2.5}$ MeV, in agreement with the SM expectation, and observed (expected) lower and upper limits on the total width of $0.5\ (0.1) < \Gamma_H < 10.2\ (10.6)$ MeV at 95% CL.

3. Fiducial and differential cross-sections

Fiducial and differential cross-section measurements allow the characterisation of the Higgs boson through production- and decay-related distributions. They are usually performed inclusively over all production modes. Compared to measurements of event yields, these cross-section measurements have the advantage that they can be easily interpreted and used by physicists outside the ATLAS Collaboration, as they include corrections for detector effects.

In each final state, a fiducial phase space is chosen to reduce the extrapolation from the measured phase space and therefore the model dependence of the measurement. The fiducial phase space is defined at particle level, i.e., based on generated stable particles, approximating the selection of reconstructed events. After selecting the events, the extraction of the signal event yields and the correction to the fiducial phase space are performed simultaneously using a likelihood fit.

3.1. Fiducial and total cross-sections

Higgs boson production cross-sections are measured in the $\gamma\gamma$ and $ZZ^* \to 4\ell$ final states. The event selections are very similar to those discussed in Section 2, but the events are not separated into different categories. The Higgs boson production cross-section times branching ratio measured in the $\gamma\gamma$ fiducial volume is 67 ± 6 fb [113], while the cross-section times branching ratio measured in the $ZZ^* \to 4\ell$ fiducial volume is 3.28 ± 0.32 fb [114]. Both results are in agreement with the SM predictions (64 ± 4 fb and 3.41 ± 0.18 fb, respectively [18]), and achieve a precision of about 10%.

To allow the combination of the $ZZ^* \to 4\ell$ and $\gamma\gamma$ measurements [115], total cross-sections are extracted by extrapolating from the fiducial to the total phase space, also correcting for the branching fractions. The combination improves the statistical power by roughly doubling the analysed data sample, as the lower cross-section times branching fraction of the $ZZ^* \to 4\ell$ decay channel is balanced by a better signal-over-background ratio compared to the $\gamma\gamma$ measurement. On the other hand, the combination increases the model-dependence of the result. The extrapolation factors rely on SM predictions and uncertainties related to the measured cross-sections of the different Higgs boson production modes are taken into account. The reduction in statistical uncertainties is significantly larger than the additional uncertainties due to the extrapolation, which are at the per-cent level. The cross-sections measured at different centre-of-mass energies are presented in Fig. 8, together with the SM prediction. For pp collisions at 13 TeV centre-of-mass energy, the measured cross-section is $55.5 \pm 3.2(\text{stat.})^{+2.4}_{-2.2}(\text{syst.}) = 55.5^{+4.0}_{-3.8}$ pb, achieving a precision of about 7%. Good agreement with the SM prediction (55.6 ± 2.2 pb [18]) is observed.

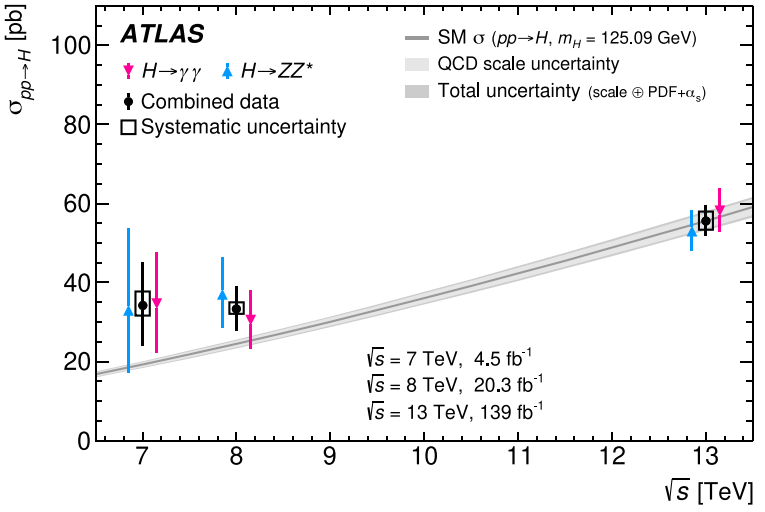

Fig. 8. Total $pp \to H + X$ cross-sections measured at centre-of-mass energies of 7, 8 and 13 TeV in the $ZZ^* \to 4\ell$ and $\gamma\gamma$ decay channels, and their combination, compared with SM predictions [115].

3.2. Differential cross-sections

Measurements of differential cross-sections allow probing of Higgs boson kinematics, such as the Higgs boson transverse momentum p_{T}^{H} and rapidity, and other aspects of Higgs boson production and decay, such as the number and properties of the associated hadronic jets. The $ZZ^* \to 4\ell$ and $\gamma\gamma$ differential cross-section measurements are performed individually and combined, to benefit from the reduced statistical uncertainties. As for the total cross-section, the necessary extrapolation introduces additional model-dependent uncertainties.

For each observable, a likelihood fit performs the extraction of the signal event yields in each bin. It uses dedicated factors for the correction of measurement inefficiencies, a migration matrix for the unfolding of resolution effects, and the measured luminosity to determine the cross-sections. No regularisation is applied. In addition to the experimental and background uncertainties, uncertainties related to the model dependence of the unfolding are included.

The p_{T}^{H} distribution of the Higgs boson is one of the most interesting observables to measure as it could be sensitive to different phenomena beyond the SM (BSM). It could differ from the SM prediction if the Higgs boson were produced together with an invisible particle or if so-far unknown particles contributed to the ggF loop. In addition, the p_{T}^{H} distribution, the overall production rate and the $H \to \gamma\gamma$ branching fraction are sensitive to the Yukawa couplings of the Higgs boson to the bottom and charm quarks. Both the contributions of these quarks to the loop-induced ggF production and $b\bar{b}$ and $c\bar{c}$ initiated Higgs boson production play an important role. The p_{T}^{H} would also be modified by the presence of new dynamics. Constraints on non-SM interactions can be set within an effective field theory model, as shown in Section 6. A combined measurement of p_{T}^{H}, extrapolated to the total phase space, is shown in Fig. 9(a). The binning was chosen to adequately capture the shape of the distribution for the subsequent interpretations. A precision of 20% is achieved in some regions. Fig. 9(b) shows the observed limits at 95% CL on the Yukawa coupling-strength modifiers of the bottom and charm quarks, defined as the ratios of the measured Yukawa couplings to their SM values [116], based on the shape and normalisation of the p_{T}^{H} distribution. The combination of these constraints with those from the $H \to b\bar{b}$ and $H \to c\bar{c}$ analyses is discussed in Section 4.

Fig. 10 shows the rapidity of the Higgs boson measured in the $H \to \gamma\gamma$ decay channel and the invariant mass of the off-shell Z boson in the $H \to ZZ^* \to 4\ell$ decay channel. The rapidity of the Higgs boson is sensitive to the parton distribution functions of the colliding protons, and is also influenced by QCD radiative corrections. The invariant mass of the off-shell Z boson would be modified by the presence of a 'dark' Z boson mixing with the SM [117,118]. It is also sensitive to anomalous couplings and can be interpreted in the pseudo-observable framework [119]. The two results are a subset of the measured distributions, which cover a broad range of observables, ranging from Higgs boson kinematics to properties of the associated hadronic jets and of the Higgs boson decay products.

Despite the missing information from the neutrinos in the final state and thanks to the relatively high branching ratio, it is also possible to measure differential cross-sections in the $WW^* \to e\nu\mu\nu$ final state [120,121]. In this channel, the measurements are not performed inclusively, but separately for ggF and VBF production. Events are selected if they contain two oppositely charged, different-flavour leptons (electrons or muons). Further requirements are applied to ensure a non-negligible missing transverse momentum in the event. To suppress $\tau\tau$ background from the Υ meson, or from an off-shell photon or Z boson (Drell–Yan) a minimum requirement on the invariant mass of the two leptons is applied. After the event selection, the dominant backgrounds to the Higgs boson signal are non-resonant WW production, top

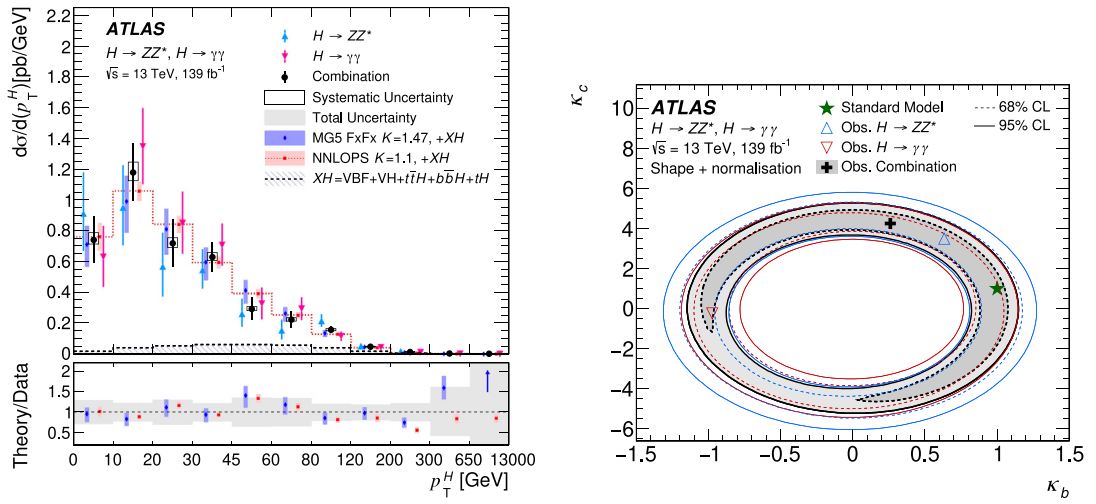

(a) (b)

Fig. 9. (a) Higgs boson transverse momentum measured in the $ZZ^* \to 4\ell$ and $\gamma\gamma$ decay channels, and their combination, compared with two SM ggF predictions, which are scaled to the total expected N^{3}LO cross-section and added to the predictions for the other production modes. (b) Observed limits at 95% CL on the Yukawa coupling-strength modifiers based on both the shape and normalisation of the Higgs boson transverse momentum distribution. The SM prediction and the observed best-fit values are also indicated [115].

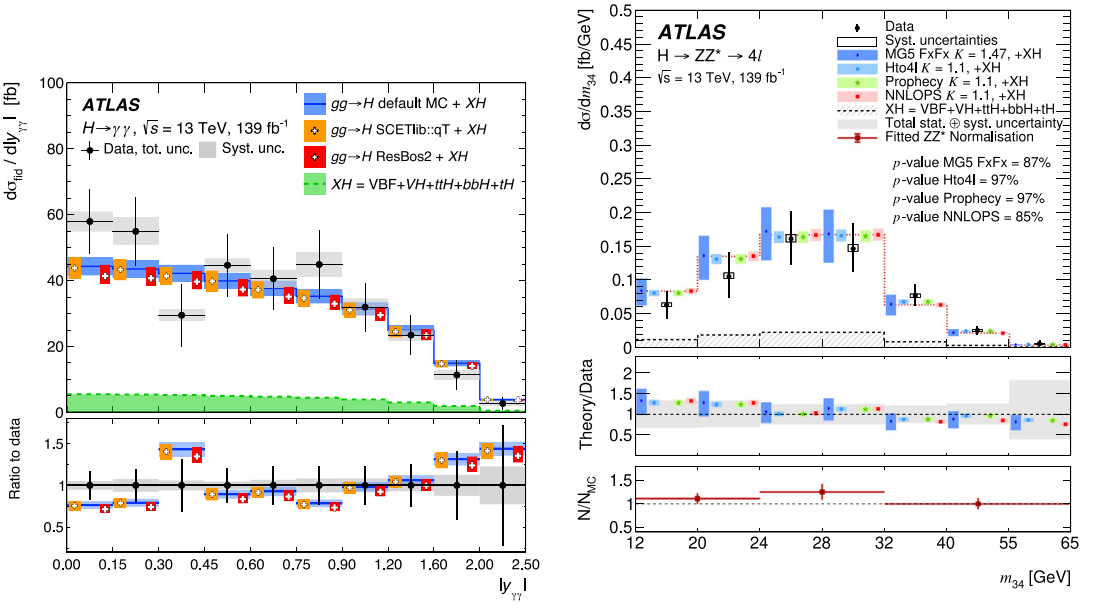

(a) (b)

Fig. 10. (a) The rapidity of the Higgs boson measured in the $H \to \gamma\gamma$ decay channel [113], and (b) the invariant mass of the off-shell Z boson in the $H \to ZZ^* \to 4\ell$ decay channel [114]. The measurements are compared with different SM ggF predictions that are added to predictions for the other production modes. For the invariant mass, the ggF predictions are scaled to the total N^{3}LO cross-sections.

pair production, the Drell–Yan process, and jets that are misidentified as leptons. Dedicated control regions are created that are enriched in these background processes. They are used in the subsequent fit to extract correction factors to the estimated yields, which are extracted from MC for most backgrounds. To estimate the background from events with jets misidentified as leptons, correction factors are determined from data and applied to the corresponding control region. In the VBF analysis, an additional control region enriched in ggF events is added to the fit to estimate this background. In the ggF analysis, the small contributions from other Higgs boson production modes are estimated by using simulated

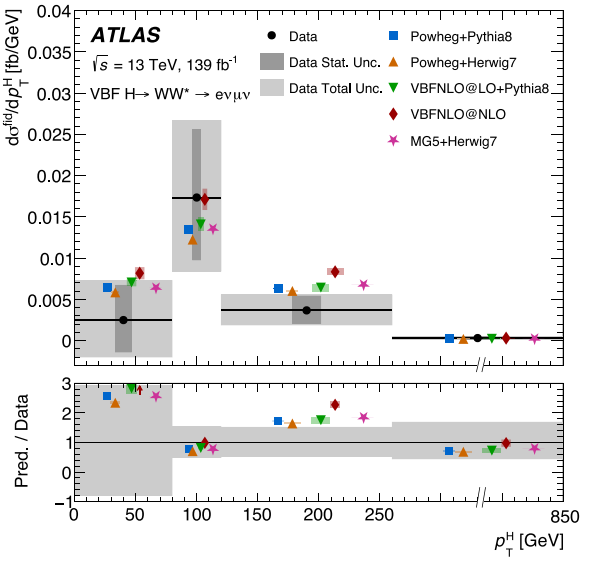

Fig. 11. Higgs boson transverse momentum measured for VBF production in the $WW^* \to e\nu\mu\nu$ decay channel compared with different SM predictions [121].

events scaled to the expected SM cross-sections. The unfolding is performed by inverting the response matrix. In the ggF analysis, a Tikhonov regularisation term [122] is included in the likelihood to avoid large statistical fluctuations. Fig. 11 shows p_{T}^{H} measured for VBF production in the $WW^* \to e\nu\mu\nu$ decay channel.

Good agreement is seen between all measured differential cross-sections and the state-of-the-art SM predictions.

4. Higgs boson couplings to fermions

4.1. Observation of the Higgs boson couplings to third generation fermions: τ-leptons, top and bottom quarks

In the SM, fermions obtain their masses by interacting with the Higgs field via the Yukawa coupling. One of the major achievements during Run 2 of the LHC was the direct confirmation of the Yukawa couplings to third generation fermions. This was accomplished by studying the fermionic decays of the Higgs boson and the associated production of the Higgs boson with pairs of top quarks.

The observation of Higgs boson decays into two τ-leptons was established during Run 1 through a combination of measurements by the ATLAS and CMS Collaborations, with a significance of 5.5σ [88]. ATLAS achieved a single-experiment observation using 36.1 fb^{-1} of Run 2 data in combination with Run 1 data [123].

All combinations of hadronic and leptonic τ-lepton decays are considered. They are treated as separate analysis channels due to differences in their background composition. In all channels, the dominant background is the $Z \to \tau\tau$ process. Therefore, the best sensitivity can be achieved for topologies in which Z boson production is suppressed, such as Lorentz-boosted ggF and VBF production. The relative contributions from other backgrounds, primarily from top-quark and vector-boson decays, as well as from misidentified leptonic or hadronic τ-lepton decays, vary considerably depending on the τ-lepton decay mode. The invariant mass of the $\tau\tau$ system is used to discriminate between Higgs boson and Z boson production and to extract the signal yield, making the mass resolution extremely important. An algorithm is employed that determines the most probable $\tau\tau$ mass for the event, assuming that the measured missing transverse momentum originates from neutrinos in a resonant $\tau\tau$ final state [124]. Several categories are defined based on the Higgs boson production mode, particularly probing VBF and boosted Higgs boson production via ggF. The normalisations of the major backgrounds are constrained using data from different control regions. The yields of the $Z \to \tau\tau$ background are estimated directly from a fit to the final discriminating variable.

In Fig. 12(a), the reconstructed invariant mass of the $\tau\tau$ system is shown for all signal regions using the 2015–2016 ATLAS data sample [123]. The $H \to \tau\tau$ signal is established with an observed (expected) significance of 4.4σ (4.1σ), which increases to 6.4σ (5.4σ) when combined with the Run 1 results.

With the data collected by the end of Run 2, it is possible to probe the $H \to \tau\tau$ cross-section in the four major production modes (ggF, VBF, VH, and $t\bar{t}H$), and as a function of the kinematic properties of the events in ggF and electroweak production processes [125]. In Fig. 12(b), the reconstructed invariant mass of the $\tau_{\mathrm{lep}}\tau_{\mathrm{had}}$ pair is shown, where one τ-lepton decays leptonically and one hadronically. The measured cross-sections times branching ratio for $|y_H| < 2.5$ in the dominant ggF and VBF production modes are $2.65 \pm 0.41(\mathrm{stat.})^{+0.91}_{-0.67}(\mathrm{syst.})$ pb and $0.197 \pm 0.028(\mathrm{stat.})^{+0.032}_{-0.026}(\mathrm{syst.})$ pb

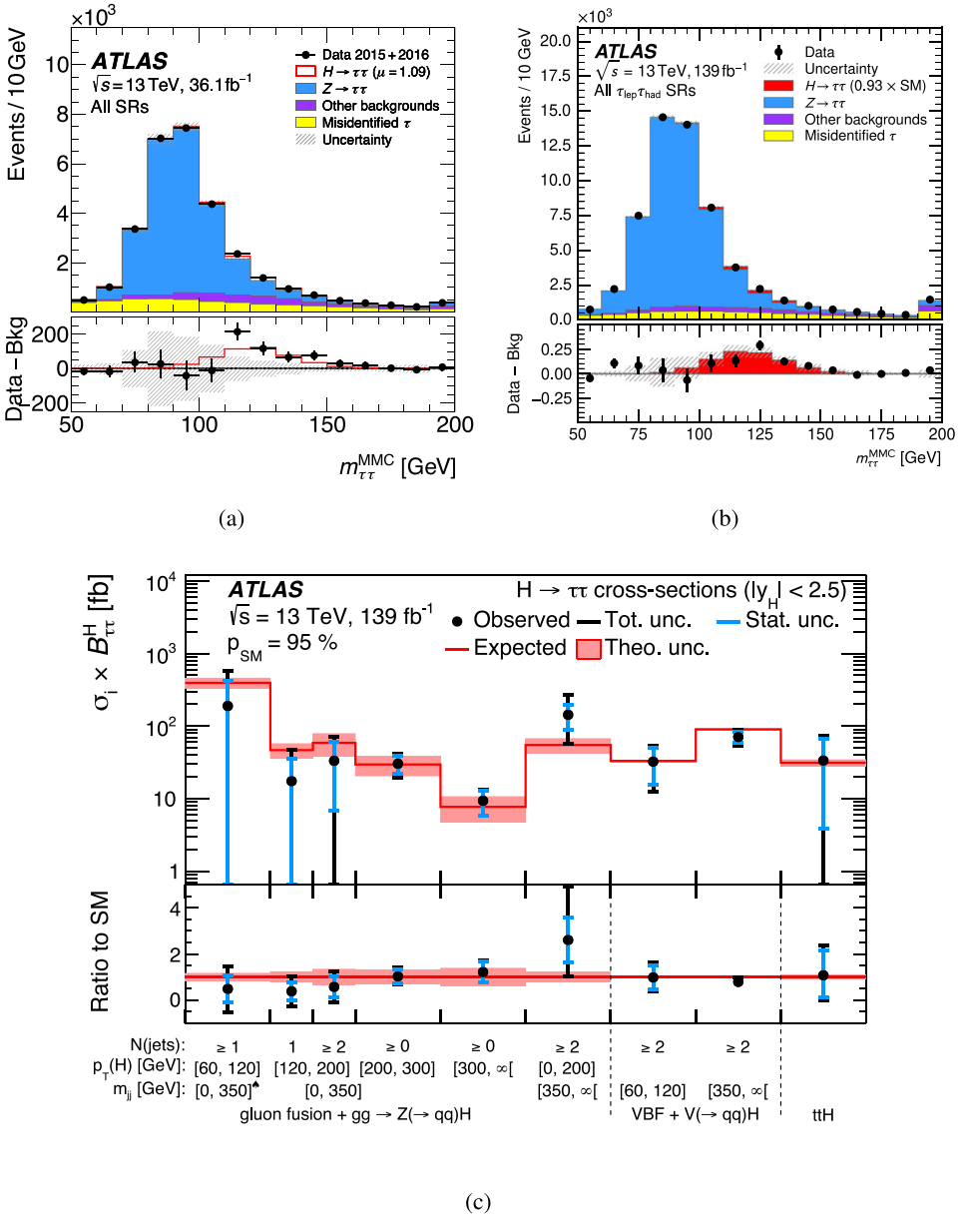

Fig. 12. (a) The invariant mass of the $\tau\tau$ system for all combinations of τ-lepton decays using 36.1 fb^{-1} of data [123]. (b) The same observable considering only signal regions with one τ-lepton decaying leptonically and one decaying hadronically for 139 fb^{-1} of data [125]. (c) The measured cross-sections times branching ratio in nine different kinematic regions compared with the SM expectations [125].

respectively, in agreement with the SM expectations. Cross-sections of the production of a Higgs boson decaying into τ-leptons are measured as a function of p_{T}^{H}, the number of jets produced in association with the Higgs boson, and the invariant mass of the two leading jets m_{jj}, as shown in Fig. 12(c). The achieved statistical and systematic uncertainties are 24% for the electroweak production of the Higgs boson with two jets and m_{jj} greater than 350 GeV and about 40% for the boosted ggF production.

The observation of $t\bar{t}H$ production [126] was an important breakthrough. Since the strength of the Yukawa interaction is proportional to the fermion mass, the predicted Yukawa coupling of the top quark is the largest one in the SM, with a value close to unity. Indirect constraints on this coupling were already obtained through ggF production and Higgs boson decays into photons, which occur via quantum loops (Fig. 1). In the SM, the dominant contribution to the former arises from diagrams featuring the top quark or the bottom quark in the loop, along with their interference. Meanwhile, in the latter case, the primary contribution is due to the W boson in the loop or the top quark [127]. However,

so-far unknown phenomena could affect these loops, therefore a direct measurement through $t\bar{t}H$ production is necessary to disentangle and probe potential BSM effects.

The presence of complex final states and large irreducible backgrounds, combined with a small predicted rate (about 1% of the total Higgs boson production), makes the measurement of $t\bar{t}H$ challenging. Different analyses using up to 79.8 fb^{-1} of Run 2 data and targeting various Higgs boson decay channels were combined, leading to the observation of this production mode in 2018 [126].

The search for $t\bar{t}H$ production via $H \to b\bar{b}$ decays [128] benefits from the large Higgs boson branching fraction to bottom quarks, but suffers from sizeable backgrounds, primarily from events with a top quark pair and additional heavy-flavour jets, which are also challenging to model. Events are selected in which one or both top quarks decay semileptonically. The events are further categorised using the jet multiplicity and the probability that a certain jet originates from a bottom quark (b-tagging). This allows nine signal-enriched regions to be defined, with a maximum purity at the level of about 5%, and ten background-enriched control regions. Multivariate discriminants based on kinematic variables are trained for each region to further enhance the signal-to-background separation. The signal yield is extracted through a global fit in which the normalisation of the $t\bar{t}$ +heavy flavour background components is allowed to float freely. An excess over the background-only hypothesis is observed (expected) with a significance of 1.4σ (1.6σ) with the 2015–2016 data sample, corresponding to 36.1 fb^{-1} of Run 2 data.

Searching for $t\bar{t}H$ production, the $H \to WW^*$, $H \to \tau\tau$, and the $H \to ZZ^*$ decays are difficult to disentangle, as they lead to similar final states featuring the presence of multiple leptons. Therefore, they are treated together in a common $t\bar{t}H, H \to$ multilepton analysis [129]. The $t\bar{t}H$, $H \to ZZ^* \to 4\ell$ contribution is studied in a dedicated analysis and minimised to be negligible in the $t\bar{t}H, H \to$ multilepton analysis with a selection based on the four-lepton invariant mass. Events are categorised into seven orthogonal categories based on the number of light leptons and hadronically decaying τ-lepton candidates. The $t\bar{t}$ background is suppressed by requiring two leptons with the same charges or at least three leptons of any charges. The defined categories have different background compositions and a wide range of total yields and signal purities. The irreducible background is predominantly composed of SM processes with prompt leptons, such as $t\bar{t}W$, $t\bar{t}Z$, and diboson production. Control regions are used to extract the normalisation for these backgrounds and estimate the backgrounds with non-prompt light leptons and mis-identified hadronically decaying τ-lepton candidates. Dedicated multivariate discriminants are employed in most of the signal regions to further enhance the signal-to-background separation. In Fig. 13(a), the observed and expected yields in the signal regions and control regions are shown. A combined profile likelihood fit across all regions extracts the signal with an observed (expected) significance of 4.1σ (2.8σ) with the 2015–2016 data sample, corresponding to 36.1 fb^{-1} of Run 2 data.

The $t\bar{t}H$, $H \to ZZ^* \to 4\ell$ final state is treated in a dedicated analysis [126], separating events in which both top quarks decay hadronically from events in which at least one top quark decays semileptonically and employing a boosted decision tree (BDT) in each region. Due to the small Higgs boson branching ratio to four leptons, the expected rates are very low. The expected background contamination is also small. The simulation predicts 0.6 signal events, and an expected significance of 1.2σ. No events are observed with 79.8 fb^{-1} of Run 2 data.

The $t\bar{t}H$ analysis using $H \to \gamma\gamma$ decays [126] benefits from a very clean signature, with a peak in the invariant mass distribution of the diphoton system over a smooth background, but it suffers from a low rate. The main background processes are non-resonant diphoton production and other Higgs boson production modes. Regarding the associated top quark decays, this analysis distinguishes between leptonic events (where at least one light lepton is present) and hadronic channels. BDTs are employed in various analysis categories to separate the signal from backgrounds. As shown in Fig. 13(b), the signal is extracted from signal-plus-background fits to the $\gamma\gamma$ invariant mass distribution, with the background constrained by the mass sidebands. The resulting observed (expected) significance is 4.1σ (3.7σ) with 79.8 fb^{-1} of Run 2 data.

Combining the various decay modes, along with the results obtained using the Run 1 data, an observed (expected) significance of 6.3σ (5.1σ) for $t\bar{t}H$ production is achieved with 36.1−79.8 fb^{-1} of Run 2 data [126]. Assuming SM branching fractions, the total $t\bar{t}H$ production cross-section at 13 TeV is measured to be $670 \pm 90(\text{stat.})^{+110}_{-100}(\text{syst.})$ fb, in agreement with the SM prediction. Fig. 13(c) shows the combined event yields in all analysis categories as a function of $\log_{10}(S/B)$, where S and B are the expected signal and background yields extracted from the fit, with a clearly visible signal-like excess over the background at high $\log_{10}(S/B)$.

Exploiting the full Run 2 data sample, it is possible to make cross-section measurements as a function of p_{T}^{H} in $t\bar{t}H$ production, both in the $H \to \gamma\gamma$ [131] and $H \to b\bar{b}$ [130] final states. Fig. 13(d) shows the results obtained in the $H \to b\bar{b}$ final state.

The observation of Higgs boson decays into bottom-quark pairs in 2018 was another significant milestone in the understanding of Higgs boson interactions [132]. This observation provides direct evidence of the Yukawa coupling of the Higgs boson with down-type quarks.

The $H \to b\bar{b}$ decay has the largest branching ratio in the SM at about 58%. However, inclusive $H \to b\bar{b}$ searches are very challenging at the LHC due to backgrounds arising from multijet production that are orders of magnitudes larger than Higgs boson production. The most sensitive analysis is based on VH production, where events are categorised according to the number of charged leptons (muons or electrons) from the vector boson decays. Events containing zero or two leptons target ZH production, while events with one lepton target WH production. All events are required to have at least two jets, of which exactly two must have a high probability to originate from bottom quarks. The primary background sources

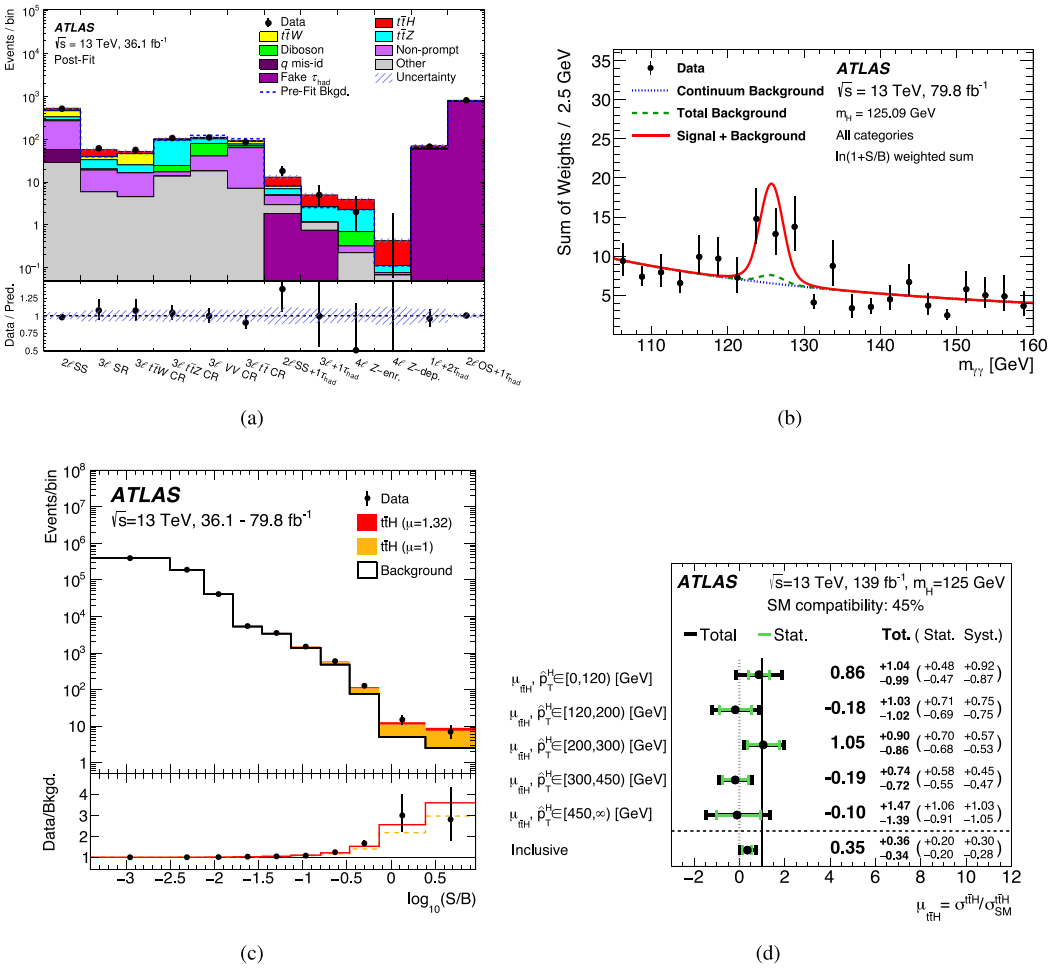

Fig. 13. (a) Comparison of the data to the prediction in the different signal and control regions of the $t\bar{t}H$, $H \to$ multilepton analysis, after the fit is performed [129]. (b) The diphoton invariant mass distribution in the $t\bar{t}H, H \to \gamma\gamma$ analysis [126]. (c) Event yields as a function of $\log_{10}(S/B)$ for data, background and a Higgs boson signal for all decay channels considered, using up to 79.8 fb^{-1} of data, leading to the observation of $t\bar{t}H$ production [126]. (d) Measured $t\bar{t}H$ production cross-sections normalised to the SM expectation as function of p_{T}^{H} in the $H \to b\bar{b}$ final state [130].

are V+jets and $t\bar{t}$ production, and their normalisation is constrained using dedicated control regions. The separation between the signal and background is achieved using the invariant mass of the $b\bar{b}$ system $m_{b\bar{b}}$ and several other kinematic observables, such as the transverse momentum of the vector boson. These observables are used as input to BDTs in the different signal regions. Based on the first 79.8 fb^{-1} of Run 2 data, the analysis yields an observed significance for VH, $H \to b\bar{b}$ production of 4.9σ (4.2σ expected). Combining this result with the searches for $H \to b\bar{b}$ in other Higgs boson production modes, a significance of 5.4σ is observed, with an expectation of 5.5σ. Furthermore, the combination of this result with the other searches for VH production provides the first observation of this process with a significance of 5.3σ (4.8σ expected).

In addition, an analysis without multivariate discriminants (cut-based analysis) is performed as a cross-check. In this case, $m_{b\bar{b}}$ is used as the discriminating variable and additional selection criteria are employed, e.g., on the separation between the two b-tagged jets, to increase the purity of the signal regions. The VZ process with the Z boson decaying into $b\bar{b}$ offers a powerful validation of the cut-based analysis, as this process closely resembles the Higgs boson signal except for the lower invariant mass of the $b\bar{b}$ system. Fig. 14(a) shows the invariant mass distribution of the $b\bar{b}$ system after subtracting all backgrounds except for the VZ process, using the first 79.8 fb^{-1} of data in Run 2. The VZ contribution is clearly visible, along with a significant excess at higher $m_{b\bar{b}}$ values due to VH production.

The full Run 2 data sample allows further improvements in the $VH, H \to b\bar{b}$ measurements [133], yielding a measured signal strength relative to the SM prediction of $\mu_{VH}^{bb} = 1.02^{+0.12}_{-0.11}(\mathrm{stat.})^{+0.14}_{-0.13}(\mathrm{syst.})$. Fig. 14(b) shows the observed and predicted discriminant distribution used to separate the Higgs boson signal from the backgrounds in one of the signal regions. In addition, cross-sections of associated production of a Higgs boson decaying into bottom quark pairs and a vector boson decaying into leptons are measured as a function of the vector boson transverse momentum in kinematic

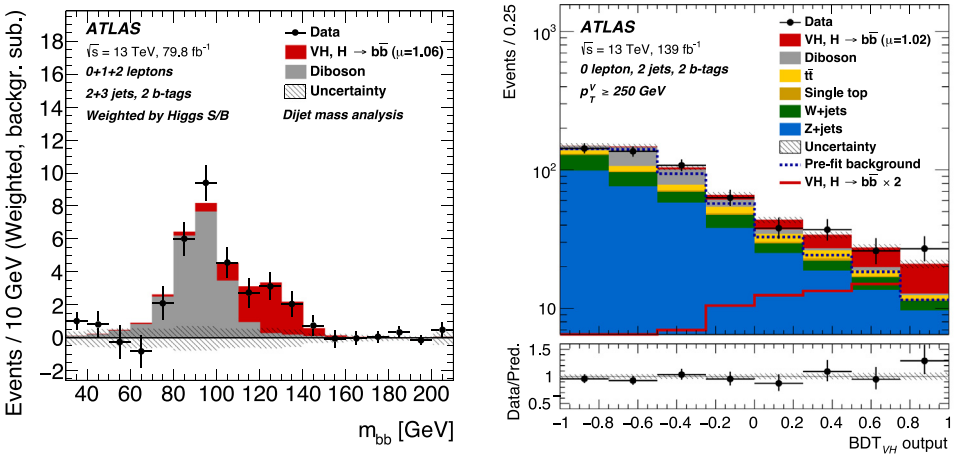

(a) (b)

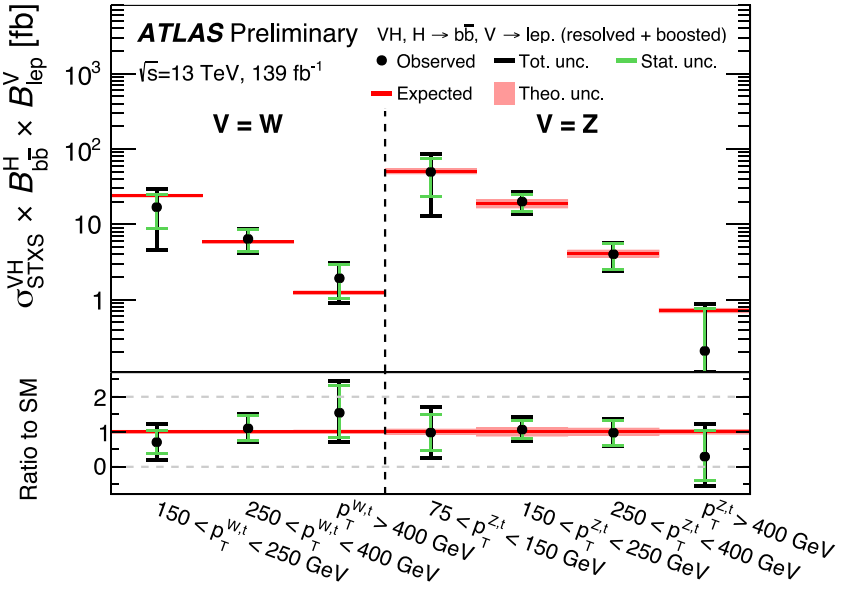

(c)

Fig. 14. (a) The S/B weighted $b\bar{b}$ invariant mass distribution for the cut-based $VH, H \to b\bar{b}$ analysis after the subtraction of all backgrounds but the WZ and ZZ diboson processes, based on Run 2 data collected up to 2017 [132]. (b) Observed and predicted distribution for one of the 14 BDTs used to separate the Higgs boson signal from the background processes in the $VH, H \to b\bar{b}$ analysis performed with the full Run 2 data sample [133]. (c) The production cross-section of the Higgs boson times the $H \to b\bar{b}$ and $V \to$ leptons branching ratios as a function of the transverse momentum of the vector boson p_{T}^{V} [134].

fiducial volumes, with uncertainties ranging from 30% in the highest p_{T}^{V} region ($p_{\mathrm{T}}^{V} > 250$ GeV) to 85% in the lowest (75 GeV $< p_{\mathrm{T}}^{Z} <$ 150 GeV).

For transverse momenta of the Higgs boson above about 300 GeV, the decay products of the Higgs boson in the $VH, H \to b\bar{b}$ process cannot always be reconstructed through two jets with a small radius parameter R ($R = 0.4$). The collimated Higgs boson decay products may however be reconstructed as a single jet with a large radius parameter ($R = 1$). This boosted region is particularly interesting due to its sensitivity to BSM physics at high energy scales. The measured signal strength for the $VH, H \to b\bar{b}$ events reconstructed as a single large-radius jet with $p_{\mathrm{T}}^{V} > 250$ GeV with the full Run 2 data is $\mu_{VH}^{b\bar{b}} = 0.72^{+0.39}_{-0.36}$ [135].

A combination of the $VH, H \to b\bar{b}$ measurements targeting different transverse momentum regions by reconstructing the Higgs boson as two individual jets [133] or a single large-radius jet [135] is also performed [134]. The overlap between the two analyses is addressed by switching from the former to the latter at a p_{T}^{V} of 400 GeV. Cross-sections are measured

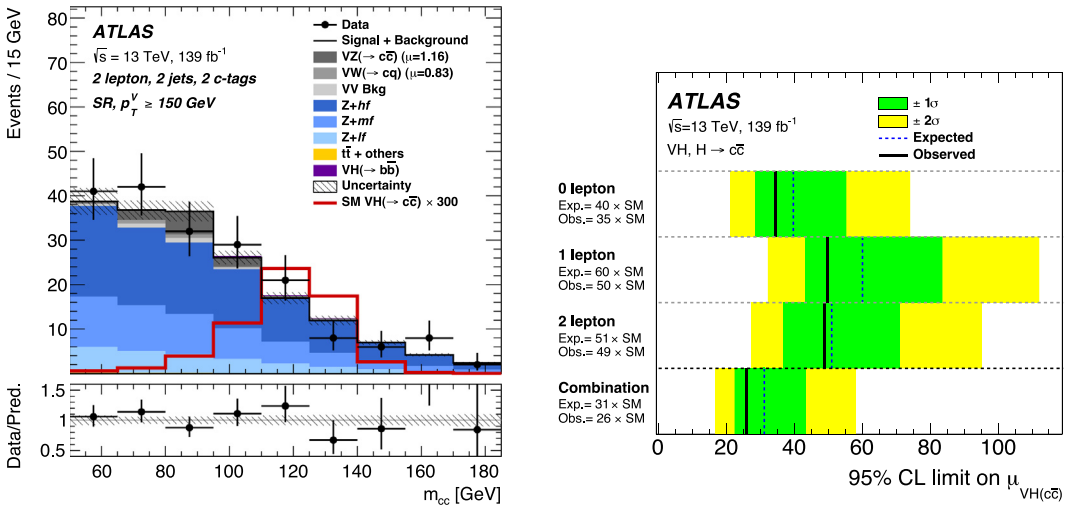

(a) (b)

Fig. 15. (a) Invariant mass distribution of the two charm-tagged jets in a selected signal region of the $H \to c\bar{c}$ analysis [116]. The $H \to c\bar{c}$ signal is also shown, scaled by 300 times the SM prediction. (b) The observed and expected 95% CL upper limits on the VH, $H \to c\bar{c}$ signal strength in the different analysis categories and for the combined fit [116].

as function of the transverse momentum of the W and Z bosons and found to be compatible with the SM expectations, as shown in Fig. 14(c).

Higgs bosons decaying into bottom-quark pairs are also studied in the VBF production mode [136], resulting in a measured yield of $0.95^{+0.38}_{-0.36}$ times the one predicted by the SM with the full Run 2 data sample, corresponding to an observed (expected) significance of 2.6σ (2.8σ).

Run 2 data are also exploited to study the inclusive production of the Higgs boson at high transverse momentum in the $H \to b\bar{b}$ decay channel [137]. The observed (expected) 95% CL upper limit on the Higgs boson production cross-section for $p_{\mathrm{T}}^{H} > 1$ TeV is 9.6 (7.4) fb, while the SM cross-section in the same kinematic region is 0.13 fb.

4.2. Higgs boson couplings to the second generation fermions: $H \to c\bar{c}$ and $H \to \mu\mu$

One of the challenges tackled during Run 2 was the investigation of the Yukawa interactions of the Higgs boson with the fermions of the second generation. As the Yukawa interaction is the only known fundamental interaction that distinguishes between fermion generations, the study of the couplings beyond the third generation is crucial.

Higgs boson decays into charm quark–antiquark pairs are usually searched for in events compatible with VH production [116]. As in the $H \to b\bar{b}$ case, this production mode provides the possibility for efficient triggering and background rejection through the leptonic decays of the associated W or Z bosons. Nevertheless, the analysis of $H \to c\bar{c}$ encounters several additional challenges. The branching ratio for Higgs boson decays into charm quark–antiquark pairs is $\mathcal{B}(H \to c\bar{c}) = 2.89\%$, approximately 20 times smaller than the branching ratio for Higgs boson decays into bottom quark–antiquark pairs. In addition, charm-hadron decays have less distinct signatures compared to those of bottom-hadron decays due to the shorter lifetime of charm hadrons. A dedicated algorithm requires jets to have a high probability to originate from charm quarks while vetoing jets likely to originate from bottom quarks, allowing the possibility to statistically combine the $H \to c\bar{c}$ and $H \to b\bar{b}$ analyses. This configuration gives an average efficiency of 27% to tag c-jets in simulated $t\bar{t}$ events, with b- and light-jet misidentification rates of 8% and 1.6%, respectively. Similarly to the $H \to b\bar{b}$ analysis, events are classified according to the number of charged leptons in the events. Additional cuts are applied in the various categories to suppress the V+jet, $t\bar{t}$ and diboson backgrounds. The VH, $H \to c\bar{c}$ signal and background yields are obtained through a simultaneous fit to the invariant mass of the charm-tagged jets ($m_{c\bar{c}}$). The analysis strategy is validated by the simultaneous measurement of diboson processes with one of the bosons decaying into at least one charm quark. Fig. 15(a) shows the observed $m_{c\bar{c}}$ distribution in data compared with the SM prediction for one of the analysis categories. The upper limit on the VH, $H \to c\bar{c}$ signal strength for each of the vector boson decay channels considered in the analysis is shown in Fig. 15(b), and their combination yields an observed (expected) upper limit on the VH, $H \to c\bar{c}$ signal strength of 26 (31) at 95% CL.

A statistical combination of the $H \to c\bar{c}$ and $H \to b\bar{b}$ analyses is performed to simultaneously constrain the coupling-strength modifiers κ_b and κ_c, which are defined as the ratios of the measured Yukawa couplings to their SM values [116]. The combination ensures a reduced model dependency of the result, as, even after the $H \to c\bar{c}$ analysis selection, the VH, $H \to b\bar{b}$ process is expected to be two to eight times larger than the VH, $H \to c\bar{c}$ contribution, depending on the signal

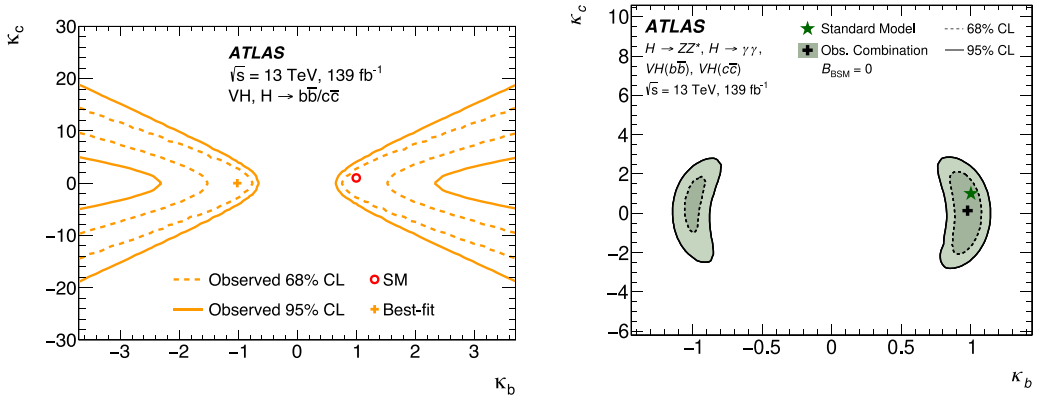

(a) (b)

Fig. 16. (a) The observed constraints on κ_b and κ_c at 68% and 95% CL from a fit to multivariate discriminants used to identify VH events with Higgs bosons decaying into $b\bar{b}$ or $c\bar{c}$, assuming no decays into BSM particles [116]. (b) Observed contours for the κ_b and κ_c parameters from a simultaneous fit to the p_{T}^{H} distributions measured in $H \to \gamma\gamma$ and $H \to ZZ^* \to 4\ell$ decays and to the multivariate discriminants in (a) [115].

region. The observed bounds in the κ_c–κ_b plane are shown in Fig. 16(a). The observed (expected) upper limit on the ratio yields $|\kappa_c/\kappa_b| < 4.5$ (5.1) at 95% CL. This bound is slightly smaller than the m_b/m_c ratio [138], indicating that the Higgs boson to charm-quark coupling is weaker than the Higgs boson to bottom-quark coupling. The direct limits on the κ_b and κ_c coupling-strength modifiers are combined with the ones from the fiducial differential cross-section measurements of p_{T}^{H} in the $H \to \gamma\gamma$ and $H \to ZZ^* \to 4\ell$ final states (Section 3). The resulting constraints are shown in Fig. 16(b) [115].

The $H \to \mu\mu$ decay channel presents a unique opportunity to investigate the interactions of the Higgs boson with second-generation fermions. Despite its low SM branching ratio (approximately 2.17×10^{-4}), the expected sensitivity in this decay channel surpasses the $H \to c\bar{c}$ decay channel, thanks to the lower background contamination and the better invariant mass resolution. Considerable effort was dedicated to further enhance the sensitivity of this decay channel during Run 2 [139], capitalising particularly on continuous improvements in analysis techniques and muon reconstruction.

Events are selected that contain two isolated muons with opposite charges and high transverse momenta, reconstructed within the acceptance of the ATLAS muon spectrometer. The dominant background is the Drell–Yan process. The selected events are then categorised using multivariate techniques that exploit kinematic and topological differences among the various Higgs boson production modes and background processes, typically resulting in a signal-to-background ratio (S/B) ranging from 0.1% to 8% in the 120 GeV $< m_{\mu\mu} <$ 130 GeV window.

Thanks to the excellent muon momentum resolution, the resonant behaviour of the Higgs boson signal in the $m_{\mu\mu}$ distribution can be utilised after categorisation to extract the signal yield and determine background normalisation and shape parameters, as shown in Fig. 17. The resolution of the $m_{\mu\mu}$ resonance is improved by including photons from QED final-state radiation through which muons can lose a significant fraction of their energy. The signal is modelled using a double-sided Crystal Ball function, with the width of the Gaussian component ranging from 2.6 to 3.2 GeV depending on the specific category.

The observed (expected) significance over the background-only hypothesis for a Higgs boson with a mass of 125.09 GeV is 2.0σ (1.7σ). The best-fit value of the signal strength parameter, defined as the ratio of the observed signal yield to the one expected in the SM, is $\mu = 1.2 \pm 0.6$.

5. Search for rare loop-induced decays of the Higgs boson

Higgs boson decays into two leptons and a photon can occur at tree level through the Yukawa coupling of a Higgs boson to leptons, or through quantum loops of virtual particles. Representative Feynman diagrams are shown in Fig. 18. The corresponding invariant mass distributions of the electron pair in $H \to ee\gamma$ decays are presented in Fig. 19. Due to the small Yukawa couplings to electrons, the tree-level diagram in Fig. 18(a) is only relevant for $H \to \mu\mu\gamma$. Rare loop processes are interesting to study, as they could be modified by so-far undiscovered particles modifying the branching ratios [140]. Furthermore, the three-particle final state might in the future allow CP studies of the corresponding couplings [141,142].

ATLAS has performed searches for Higgs boson decays into two leptons and a photon, with $m_{\ell\ell}$ below 30 GeV, mostly targeting the decay into a virtual photon and a photon [143], as well for decays with $m_{\ell\ell}$ close to the Z pole [144], dominated by decays into a Z boson and a photon. Searches for Higgs bosons decaying into a meson and a photon [145] are not discussed here, as the SM branching ratios are too small to be detectable at the LHC (see instead Ref. [6]).

Events with a photon and two electrons or two muons are selected. For the low-$m_{\ell\ell}$ analysis, the invariant mass of the two leptons $m_{\ell\ell}$ is required to be smaller than 30 GeV. For the $Z\gamma$ analysis, the dilepton invariant mass must be

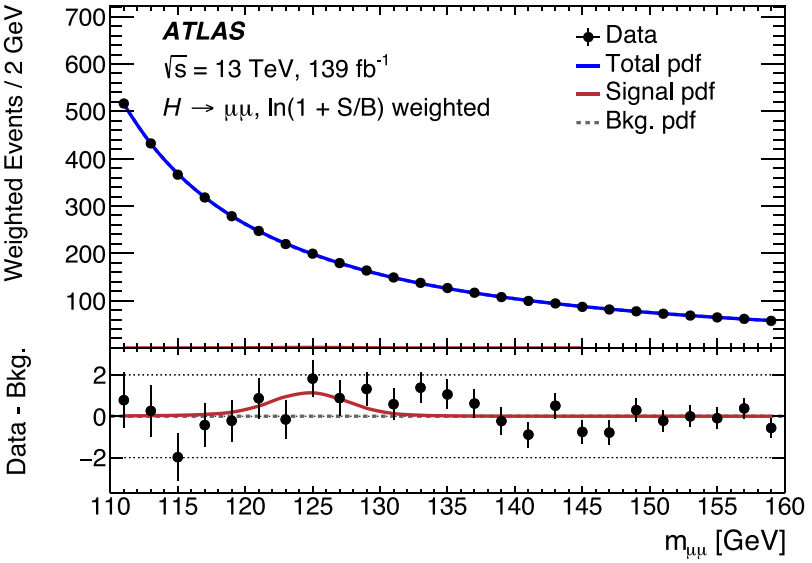

Fig. 17. Dimuon invariant mass spectrum in all analysis categories observed in data, with the events and probability density functions (pdfs) weighted by $\ln(1+S/B)$ [139] where S corresponds to the observed signal yield in the 120 GeV $< m_{\mu\mu} <$ 130 GeV window and B is the background yield in the same window, both derived by the fit to the data.

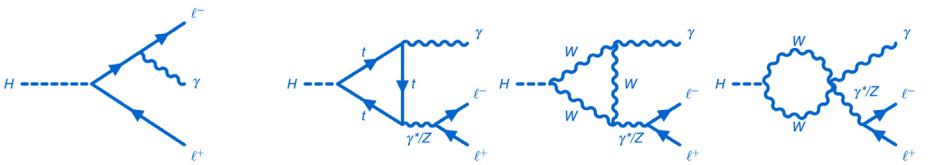

Fig. 18. Representative Feynman diagrams of Higgs boson decays into two leptons and a photon.

within 10 GeV of the Z boson mass. In the $ee\gamma$ final state, for low invariant masses and high transverse momenta of the dielectron system, the two electromagnetic showers can overlap in the calorimeter. Therefore, the search for low-$m_{\ell\ell}$ final states also considers events if they contain a photon and an object that is compatible with two very close electrons. In addition to the categorisation into lepton final states, further categorisations are introduced, guided by the different signal-to-background ratios of the various Higgs boson production modes: categories targeting VBF production, $\ell\ell\gamma$ final states with high transverse momenta, and the remainder. In each of the two dilepton mass ranges, a simultaneous parameterised fit is performed over the $m_{\ell\ell\gamma}$ mass distributions in all categories, to extract the number of signal events. As in the $\gamma\gamma$ final state, uncertainties in the choice of fit function for the background are included. Overall, statistical uncertainties are dominant. Fig. 20 shows the $m_{\ell\ell\gamma}$ distributions, with each data event weighted by a category-dependent weight that depends on the signal-to-background ratio in a window around the resonance peak.

Testing the low-$m_{\ell\ell}$ regime, evidence for the $H \to \ell\ell\gamma$ process is found with a significance of 3.2σ over the background-only hypothesis, compared with an expected significance of 2.1σ for the SM prediction. The best-fit value of the signal-strength parameter is $\mu = 1.5 \pm 0.5$. The Higgs boson production cross-section times the $H \to \ell\ell\gamma$ branching ratio for $m_{\ell\ell\gamma} < 30$ GeV is determined to be $8.7^{+2.8}_{-2.7}$ fb.

In the search for the $Z\gamma$ process, the observed (expected) significance is 2.2σ (1.2σ). The best-fit value for the $H \to Z\gamma$ signal strength is found to be $\mu = 2.0\ ^{+1.0}_{-0.9}$. As the analysis is limited by the small expected number of signal events, a combination is performed with the CMS analysis [146], effectively doubling the data sample, which pushes the significance above the evidence threshold: 3.4σ with an expectation of 1.6σ. The corresponding best-fit signal strength is $\mu = 2.2 \pm 0.7$ [147].

6. Cross-sections and couplings from combined fits

Higgs boson measurements with different decay signatures can be combined to extract as complete a portrait of the Higgs boson as possible [19]. The combination harnesses the statistical power of an unprecedented number of Higgs boson measurements to extract inclusive cross-sections and cross-sections for different production processes and

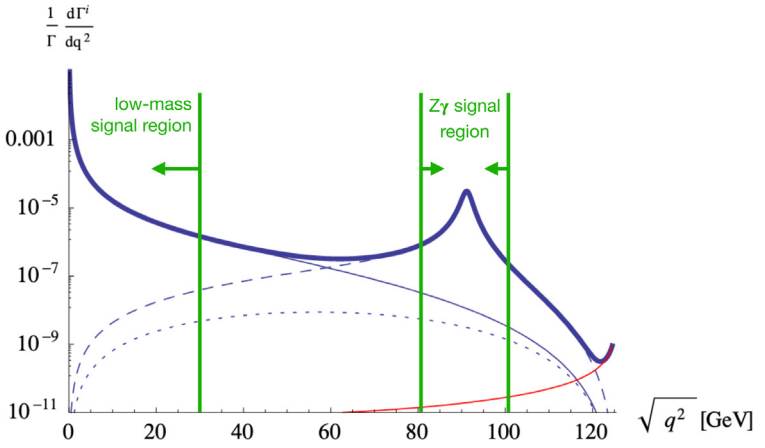

Fig. 19. Distribution of the invariant mass of the two electrons in $H \to ee\gamma$ decays [148]. The red line shows the tree level diagram, the dashed line the decay into a Z boson and a photon, and the thin blue line the decay into a virtual photon and a photon. The dotted line comes from four-point box diagrams, not discussed here. The low-$m_{\ell\ell}$ and $Z\gamma$ signal regions used in the ATLAS analyses are indicated by vertical lines.

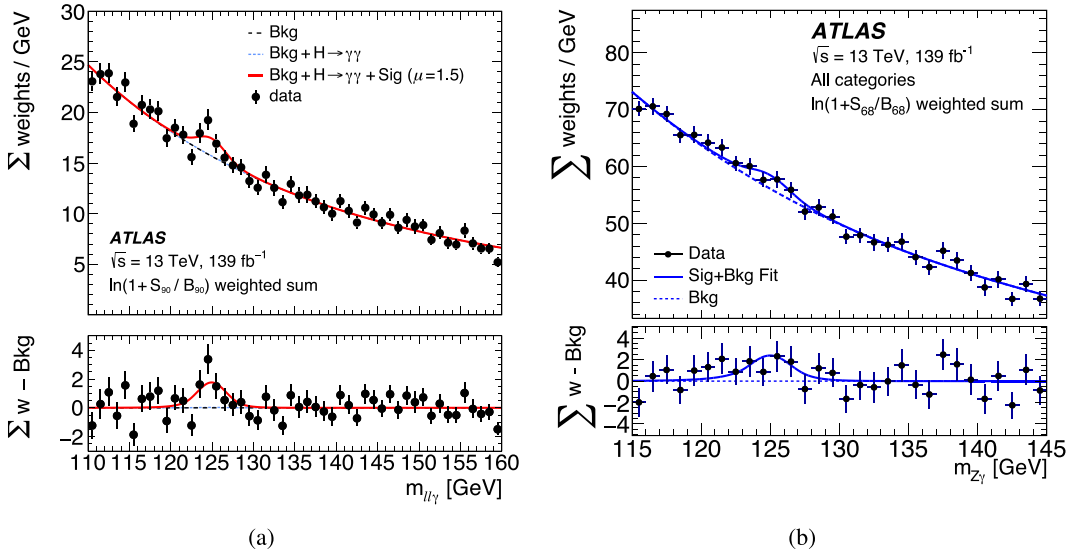

Fig. 20. (a) The $m_{\ell\ell\gamma}$ distributions for the low-$m_{\ell\ell}$ analysis [143], and (b) the $Z\gamma$ analysis [144], where every data event is reweighted by a category-dependent weight, $\ln(1+S_X/B_X)$, with X = 90% (68%) for the low-$m_{\ell\ell}$ ($Z\gamma$) analysis. Here, S_X is the number of signal events in the smallest window containing X% of the expected signal, and B_X is the expected number of background events in the same window.

kinematic regions. Each production–decay process is sensitive to different combinations of Higgs boson couplings to other fundamental particles, and the combination allows all accessible couplings to be constrained simultaneously.

Analyses in the following Higgs boson decay channels are considered in the combination: $H \to \gamma\gamma$ [131], $H \to ZZ^* \to 4\ell$ [112], $H \to WW^* \to e\nu\mu\nu$ [149,150], $H \to Z\gamma \to \ell\ell\gamma$ [144], $H \to b\bar{b}$ [130,133,135–137], $H \to \tau\tau$ [125], $H \to \mu\mu$ [139], $H \to c\bar{c}$ [116]. They provide measurements in different Higgs boson production modes and phase space regions. A complementary analysis of the $t\bar{t}H$ process, sensitive to WW^*, ZZ^* and $\tau\tau$ final states is included, as well [129]. Furthermore, searches for Higgs bosons decaying into invisible particles, such as dark matter candidates, are considered, most notably those targeting the VBF and ZH production mechanisms [151,152]. These are included in a subset of the fits.

The statistical analysis of the data is based on a combined likelihood function, calculated by forming the product of the likelihood functions describing each of the input measurements [153]. A multitude of results can be extracted from the combination of the different analyses. Each result is obtained under certain assumptions, as detailed below.

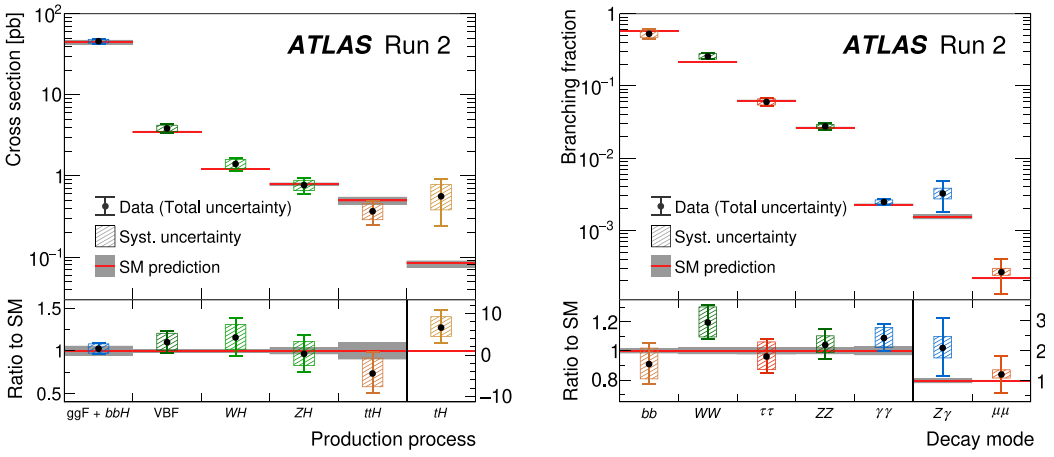

Fig. 21. (a) Observed and predicted Higgs boson production cross-sections, assuming SM values for the branching ratios. (b) Observed and expected branching fractions assuming SM values for the cross-sections [19].

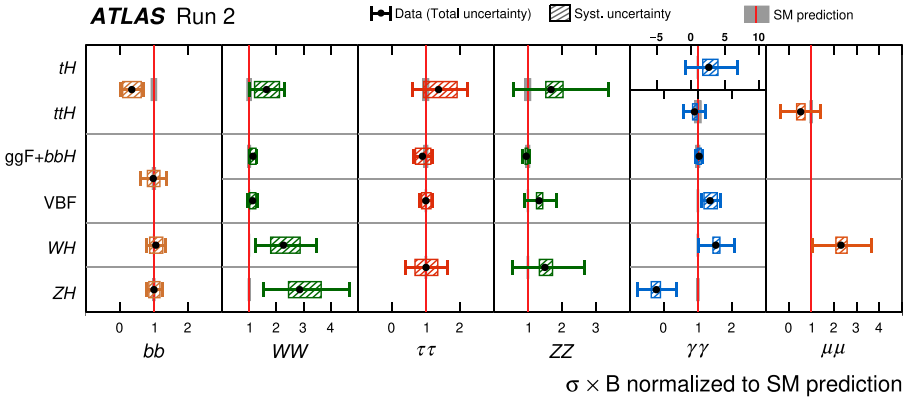

Fig. 22. Observed event rate divided by predicted SM event rate for different combinations of Higgs boson production and decay processes [19].

6.1. Global signal strength, production cross-sections and decay branching ratios

Assuming each production–decay process scales with the same global signal strength μ, the measured number of produced Higgs bosons relative to the SM prediction is
$\mu = 1.05 \pm 0.06 = 1.05 \pm 0.03(\text{stat.}) \pm 0.03(\text{exp.}) \pm 0.04(\text{sig.th.}) \pm 0.02(\text{bkg.th.})$, where the total uncertainty is split into statistical, experimental and theoretical uncertainties (signal and background).

The cross-sections of the different Higgs boson production processes are measured assuming SM values for the decay branching fractions and vice versa, as shown in Fig. 21. All major production modes are now observed, including the *WH* and *ZH* processes individually. An unprecedented upper limit at 95% CL was observed for *tH* production: 15 times the SM cross-section (7 times expected), with a strong correlation between the $t\bar{t}H$ and *tH* measurements. Fig. 22 shows the observed event rate divided by the predicted SM event rate for different combinations of Higgs boson production and decay processes. This measurement does not require any assumptions on cross-sections or branching ratios and nicely illustrates the sensitivity of the analyses in the different decay channels. Excellent overall agreement is observed with the SM predictions over multiple orders of magnitude.

6.2. Higgs boson couplings to other particles

To extract the couplings of the Higgs boson to other particles, a formalism has to be introduced. In the κ-framework [127], the cross-section times the branching fraction for an individual measurement is parameterised in terms of multiplicative coupling-strength modifiers that do not change kinematic distributions but only the strength of the coupling to a given particle compared to that expected in the SM. For example, the partial width of the decay into two bottom

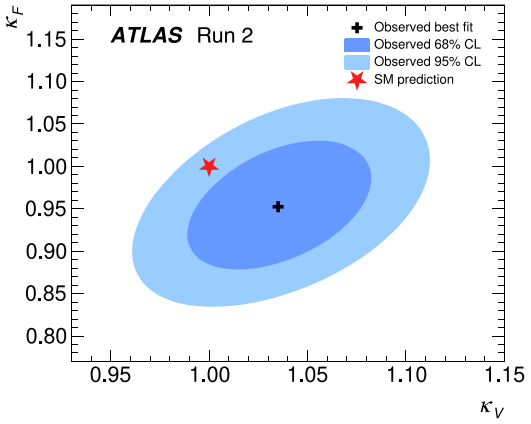

Fig. 23. Fit in the κ_F–κ_V plane, showing the best fit value and the 68% and 95% CL regions [19]. This fit is performed assuming that there are no BSM contributions to invisible or undetected Higgs boson decays.

quarks is parameterised as $\Gamma_b/\Gamma_b^{\mathrm{SM}} = \kappa_b^2$. Care is taken to adjust the total width of the Higgs boson accordingly, and in some fits BSM contributions to undetected or invisible decays are included, where undetected decays are hidden by large backgrounds. For production and decays through quantum loops (e.g., ggF and $H \to \gamma\gamma$), either effective coupling-strength modifiers are introduced (κ_g and κ_γ), or the loops are resolved into the different particle contributions according to the SM.

Assuming all coupling-strength modifiers to fermions (κ_F) scale the same way, as do all modifiers to vector bosons (κ_V), one can perform a two-dimensional fit in κ_F and κ_V, finding the best fit value and the 68% and 95% CL regions, as shown in Fig. 23. Here, the loops are assumed to be as in the SM with no BSM contributions to undetected or invisible decays allowed. The SM value lies within the 95% CL region.

Still resolving the loop-induced processes according to the SM and not allowing for additional decays, the coupling-strength modifiers for individual particles can be fit separately. The reduced coupling-strength modifiers are defined as $\sqrt{\kappa_V g_V/2v} = \sqrt{\kappa_V}(m_V/v)$ for weak bosons with a mass m_V, and $\kappa_F g_F = \kappa_F m_F/v$ for fermions with a mass m_F, where g_V and g_F are the corresponding absolute coupling strengths and $v = (\sqrt{2}G_{\mathrm{F}})^{-\frac{1}{2}} \sim 246$ GeV is the vacuum expectation value of the Higgs field, which can be derived from the measurement of the Fermi constant G_{F} [154]. Fig. 24 shows these reduced coupling-strength modifiers as a function of the particle masses. The SM predicts a striking diagonal line, encapsulating the essence of the SM Higgs Lagrangian, which agrees very well with the measured values over about three orders of magnitude. Two versions of the fit are performed, as the sensitivity of the analyses to the charm quark coupling is still rather low. In one, the modification to the charm quark coupling is fixed to be the same as for the top quark coupling, and in the other, the charm quark coupling is a free parameter.

Finally, a fit is performed allowing for new contributions to the loop-induced processes by using effective coupling-strength modifiers for the gluon, photon and $Z\gamma$ couplings. Fig. 25 shows the results of two fits: allowing (and not allowing) for undetected and invisible non-SM contributions to the branching ratios. When these contributions are allowed, the searches for invisibly decaying Higgs bosons produced via VBF or ZH production are included in the fit, $\kappa_V \leq 1$ is imposed to avoid degeneracies, and upper limits are set at 95% CL on the undetected and invisible branching fractions to non-SM particles. It can be seen that allowing for undetected and invisible BSM contributions does not change the fitted coupling-strength modifiers significantly. The modifiers for the coupling strength to top-quark, bottom-quark and τ-lepton are measured with uncertainties ranging from about 7% to 12%, to W and Z bosons with uncertainties of about 6%, and for the effective loop-induced coupling strength to photons and gluons with 6% and 7%, respectively. The upper limit on the invisible (undetected) BSM branching ratio is 0.13 (0.12), improving on the direct searches alone (see Ref. [6]).

6.3. Production cross-sections in different kinematic regions and their interpretation

A comprehensive study is performed measuring cross-sections separately per production mechanism in different phase space regions, referred to as simplified template cross-sections (STXS) [18,155–157]. The STXS framework has been designed to maximise the sensitivity of Higgs boson cross-section measurements to BSM effects, while minimising their theory dependence and allowing for the combination of analyses in different decay channels. The measurements and the SM predictions are shown in Fig. 26. Different kinematic regimes are targeted, for example Higgs bosons produced with high transverse momenta, which could be modified by BSM phenomena at high energies. Selections are also made based on the properties of the hadronic jets in the events, for example separating VBF- and VH-enriched $qq \to Hqq$ production. The measured cross-sections could reveal phenomena beyond the SM that are not observable

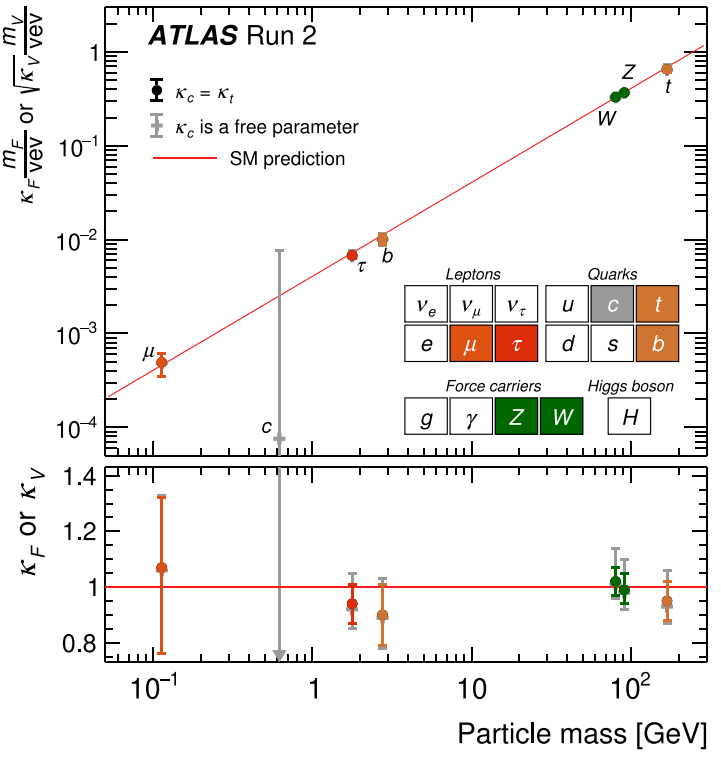

Fig. 24. Higgs boson coupling-strength modifiers and their uncertainties versus the particle masses, compared with the SM prediction [19]. For the bottom and the top quark, the masses are evaluated at a scale corresponding to that of the Higgs boson mass. Loop-induced processes are resolved according to the SM predictions, and no decays into non-SM particles are allowed.

through measurements of the coupling strengths. Furthermore they can be used as a basis for electroweak fits and BSM interpretations.

The measurement of the production cross-sections in different kinematic regions, separated by decay mode, is interpreted in the SM effective field theory (SMEFT) [158]. This allows effects of unknown phenomena at energy scales Λ that are large compared to the vacuum expectation value of the Higgs field, and that reduce to the SM at lower energies, to be searched for without having to rely on a specific model. A complete set of higher-order-in-mass operators invariant under the SM gauge group is built from the SM fields [159]. They are scaled by Wilson-coefficients, which are zero in the SM. If dimension-five operators are ignored, because they violate lepton number conservation, the leading contributions to physical observables are expected to come from dimension-six operators, which can describe CP-even or CP-odd couplings. There are several complete sets (bases), of these dimension-six operators e.g., the Warsaw [160–162], Higgs [18,163] and HISZ [164] bases.

Here, the Warsaw basis is used, and only CP-even operators are considered (see Section 7 for searches for CP-odd effects). When parameterising the cross-section times branching ratios through SMEFT, the series needs to be truncated by construction. Two different choices are considered: keeping only the linear terms of the new operators (proportional to Λ^{-2}), or including quadratic terms (proportional to Λ^{-4}) as well, along with products of different Wilson coefficients. The second choice is more complete, but also less consistent as it does not include terms from dimension-eight operators with the same suppression factor. The input measurements do not allow constraints to be put on all relevant Wilson coefficients simultaneously. The solution chosen in this analysis is a rotated basis, which allows linear combinations that combine operators with similar predicted effects on the measurements [165].

Fig. 27 shows the fitted values of the rotated coefficients for the linear and the linear+quadratic fit, including their uncertainties. All coefficients are compatible with the SM expectation of zero. The strongest constraints can be found on coefficients which affect SM processes that are suppressed by small Yukawa couplings or include quantum loops. The operators corresponding to $c_{eH,22}$, $c_{eH,33}$, c_{bH} are effectively modifiers of the Higgs Yukawa coupling to muons, τ-leptons and bottom quarks, respectively, while non-zero values of c_{Hq} would modify VH production. The eigenvectors $e^{[i]}_{\text{ggF}}$ encapsulate changes to the ggF production and $e^{[i]}_{H\gamma\gamma,Z\gamma}$ could affect the $H \to \gamma\gamma$ and $H \to Z\gamma$ decays.

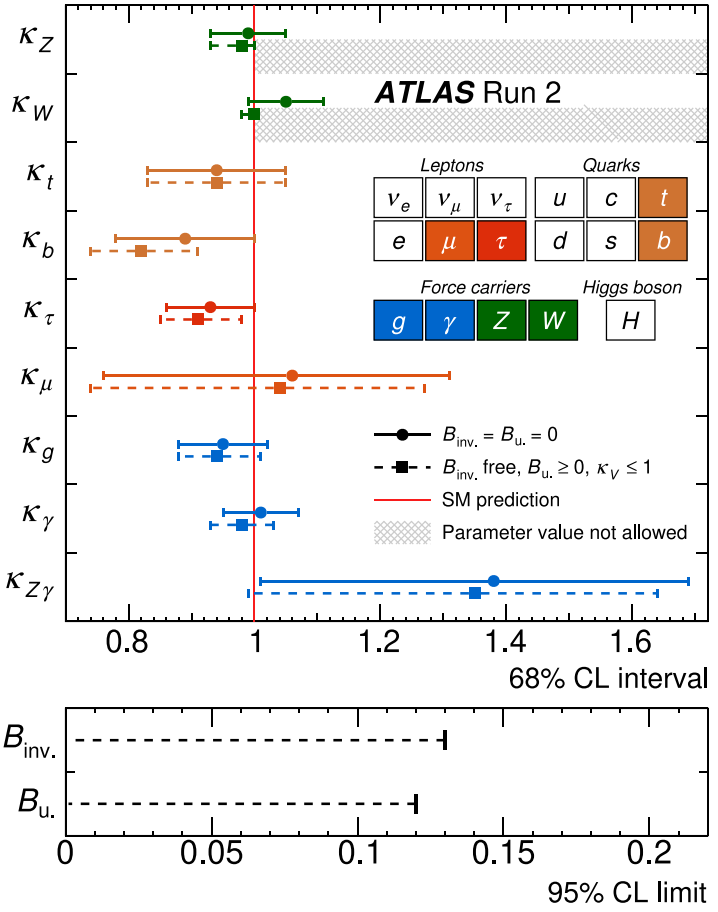

Fig. 25. Coupling-strength modifiers and their uncertainties per particle type with effective gluon, photon and $Z\gamma$ couplings, assuming the BSM contribution to undetected and invisible branching fractions to be zero (solid lines), and allowing them to contribute to the width of the Higgs boson (dashed lines). For the second case, the undetected branching ratio is assumed to be larger or equal to zero, and κ_V is assumed to be smaller or equal to one. Limits on the undetected and invisible branching fractions to non-SM particles are shown in the bottom panel [19].

7. Study of CP properties and search for anomalous interactions

In the SM, the Higgs boson is a CP-even scalar with the following quantum numbers: $J^{CP} = 0^{++}$. Any sign of CP-odd couplings in the production or decay of the Higgs boson would be an unambiguous indication of BSM phenomena. Moreover, it would provide a so-far unknown source of CP violation that could play a fundamental role in explaining the matter–antimatter asymmetry in the universe.

CP-odd Higgs boson couplings to other particles can be described by adding corresponding terms to the SM Lagrangian [159,166,167]. Couplings to bosons and fermions are investigated separately, also probing for mixtures between pure CP-odd and CP-even couplings. While a CP-odd component of the vector-boson couplings to the Higgs boson would be naturally suppressed by the scale at which BSM physics becomes relevant [159,168], this suppression does not happen for Yukawa couplings, where CP-odd Higgs−fermion couplings may be significant already at tree level [166,167].

7.1. CP properties in interactions with vector bosons

Higgs boson couplings to vector bosons are usually parameterised in the SMEFT framework (see Section 6). In the Warsaw basis, there are three relevant dimension-six operators describing CP-odd interactions at the *HVV* vertex, scaled by the following Wilson coefficients: $c_{H\tilde{B}}$, $c_{H\tilde{W}B}$, and $c_{H\tilde{W}}$. Adding these CP-odd operators to the Lagrangian, and assuming the coefficients of the CP-even dimension-six operators to be zero, the new matrix element can be written as the sum of the SM matrix element $\mathcal{M}_{SM}$ and the CP-odd BSM Matrix element $\mathcal{M}_{BSM}$. The HISZ basis also contains three coefficients to describe CP-odd interactions. By setting $\tilde{d} = \tilde{d}_B$ and the third coefficient to zero, the HISZ basis allows the strength of

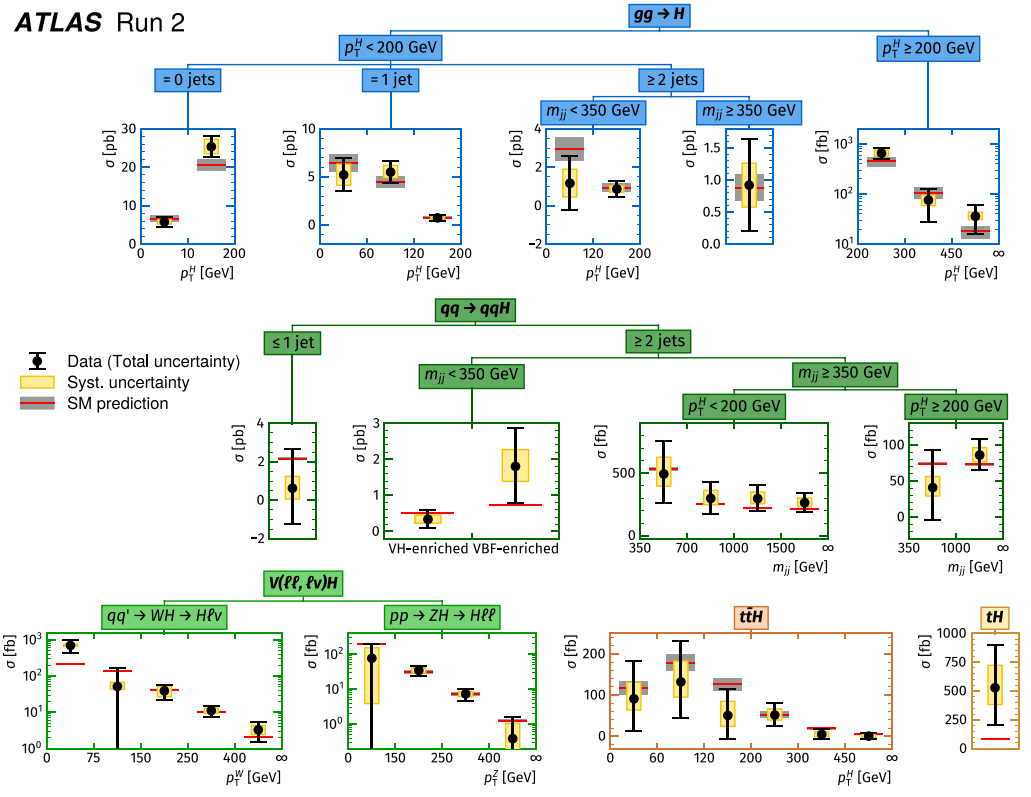

Fig. 26. Observed and predicted Higgs boson production cross-sections in different kinematic regions [19].

CP violation to be described by a single parameter $\tilde{d}$, through

$$\mathcal{M} = \mathcal{M}_{SM} + \tilde{d} \cdot \mathcal{M}_{BSM},$$

where the dependence on $\tilde{d}$ has explicitly been factored out [96,169].

Experimentally, Higgs boson couplings to vector bosons can be probed in Higgs boson production (most prominently the VBF production mode) and Higgs boson decays into Z or W bosons. BSM effects on couplings can be probed by measuring cross-sections in different kinematic regions (see Section 6) and with CP-sensitive observables (this section), which, compared to the cross-section measurements specifically target CP-odd BSM effects.

The CP-sensitive observable of choice is the matrix-element-based 'Optimal Observable' [170–172], defined as

$$\mathcal{OO} = \frac{2Re(\mathcal{M}^*_{SM}\mathcal{M}_{BSM})}{|\mathcal{M}_{SM}|^2}.$$

This distribution is symmetric with a mean value of zero for a CP-even Higgs boson and becomes asymmetric when contributions from CP-odd BSM couplings are present. In the measurements discussed below, only the shape of the distribution is considered, such that exclusively CP-odd BSM effects are probed.

The Optimal Observable for a given VBF event is calculated based on matrix elements extracted from MC simulations at LO in QCD. From the data, the four-momenta of the Higgs boson and the two VBF jets are used as input to $\mathcal{OO}$. The momentum fractions of the initial-state partons are extracted by making use of the energy–momentum conservation in the collision, taking into account all possible quark flavour combinations as predicted by the parton distribution function [173].

The CP properties are probed in VBF production for Higgs bosons decaying into two τ-leptons [173], two photons [174], four leptons [169], or two W bosons [121]. The $H \to ZZ^* \to 4\ell$ analysis also makes use of the decay characteristics, which are accessed through the reconstructed four-momenta of the decay leptons, to extract CP information.

In the $H \to \tau\tau$ decay channel, the variable $\mathcal{OO}$ is measured in bins of a BDT that is trained to distinguish the VBF signal from the background of non-Higgs and non-VBF processes. A simultaneous fit is performed over these signal regions and a number of control regions, enriched in the most important background processes, to extract the strength of a possible CP-odd parameter $\tilde{d}$.

In the $H \to \gamma\gamma$ decay channel, two BDTs are trained to suppress ggF and non-Higgs contributions creating a sample enriched in VBF events. To estimate the remaining background, the signal yield is extracted from a combined unbinned

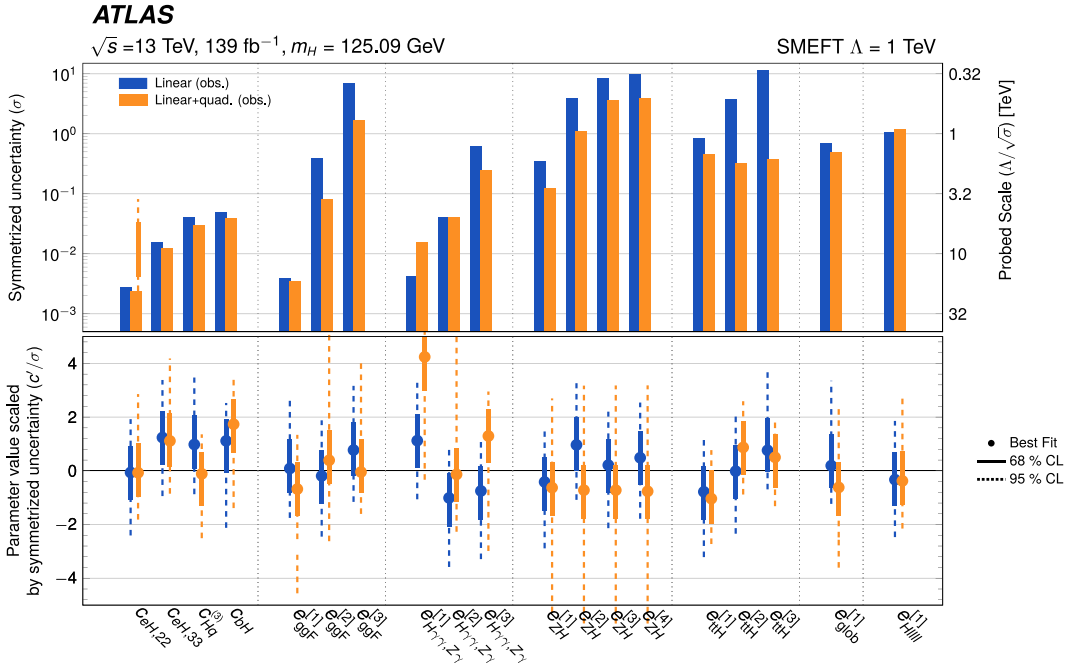

Fig. 27. Comparison of the observed parameters of the rotated basis with the SMEFT model that keeps only terms linear in the new operators (blue) and the model including quadratic terms (orange), where all other coefficients and nuisance parameters are profiled, i.e., set to the values that maximise the likelihood [158]. The top panel shows the symmetrised 68% CL uncertainty σ of each parameter measurement (left vertical axis) and the corresponding energy scale $\Lambda/\sqrt{\sigma}$, Λ = 1 TeV that is probed (right vertical axis). The bottom panel shows the measured parameter value, 68% (solid) and 95% (dashed) CL intervals, divided by the symmetrised uncertainty shown in the top panel.

maximum-likelihood fit applied to the $m_{\gamma\gamma}$ distribution of the observed data in each bin of $\mathcal{OO}$ (see Fig. 28). Using the $H \to \gamma\gamma$ channel, constraints are extracted for $\tilde{d}$ and, separately, for the Wilson coefficient of the relevant operator $c_{H\tilde{W}}$ in the Warsaw basis.

In order to extract a constraint on $c_{H\tilde{W}}$ in the $H \to ZZ^* \to 4\ell$ decay channel, both the VBF production and properties of the $H \to ZZ^* \to 4\ell$ decay are used. A NN is trained by creating samples depleted or enriched in VBF, and a fit is performed simultaneously over the different regions. The Wilson coefficients $c_{H\tilde{B}}$ and $c_{H\tilde{W}B}$, and $\tilde{d}$ are extracted from the decays. Each coefficient is fitted separately, based on a dedicated Optimal Observable.

The measurements of differential VBF cross-sections in the $H \to WW^* \to e\nu\mu\nu$ decay channel, discussed in Section 3, are used to constrain the Wilson coefficients $c_{H\tilde{W}}$, $c_{H\tilde{B}}$, and $c_{H\tilde{W}B}$ [121]. The distribution of the azimuthal angle difference between the two jets produced together with the Higgs boson is used as discriminant observable.

No deviation from a pure CP-even coupling is found in any of the studies. Fig. 29 summarises some of the resulting constraints on the Wilson coefficients in both the Warsaw and HISZ bases.

The CP properties of the effective Higgs–gluon coupling are studied in the $H \to WW^* \to e\nu\mu\nu$ decay channel [175]. The Lagrangian can be extended by a CP-odd term as

$$\mathcal{L}_{Hgg} = -\frac{g_{Hgg}}{4}\kappa_{gg}(\cos\alpha\, G^a_{\mu\nu}G^{a,\mu\nu} + \sin\alpha\, G^a_{\mu\nu}\tilde{G}^{a,\mu\nu})H, \tag{4}$$

where $G^a_{\mu\nu}$ is the gluon field strength tensor, $\tilde{G}^{a,\mu\nu} = G^a_{\rho\sigma}\epsilon^{\mu\nu\rho\sigma}/2$ is the dual tensor, g_{Hgg} is the effective coupling for the SM CP-even ggF interaction, κ_{gg} is the coupling-strength modifier for the effective Higgs−gluon interaction and α is the CP-mixing angle, which is zero in the SM. The azimuthal angle difference between the two jets produced together with the Higgs boson is used as CP-sensitive observable. Events are selected with two jets and kinematics compatible with the ggF production mode. A BDT is applied to reduce the background contamination and control regions are defined for the most important backgrounds. A maximum-likelihood fit over all considered regions is performed. Using the angular distribution and the overall rate, a value of $\tan\alpha = 0.0 \pm 0.4(\text{stat.}) \pm 0.3(\text{syst.})$ is obtained for the tangent of the mixing angle for CP-even and CP-odd contributions.

The $H \to WW^* \to e\nu\mu\nu$ decay channel also allows the Higgs boson coupling to longitudinally and transversely polarised W and Z bosons to be studied separately [175]. The azimuthal angle difference between the jets and the production rates in the signal regions are used. To probe both production and decay, events are selected that are compatible with the VBF production mode. The polarisation-dependent coupling-strength modifiers are defined as the ratios of the measured polarisation-dependent coupling strengths to those predicted by the SM, and are determined to be $a_L = 0.91^{+0.10}_{-0.18}(\text{stat.})^{+0.09}_{-0.17}(\text{syst.})$ and $a_T = 1.2 \pm 0.4(\text{stat.})^{+0.2}_{-0.3}(\text{syst.})$, compatible with the SM value of 1.

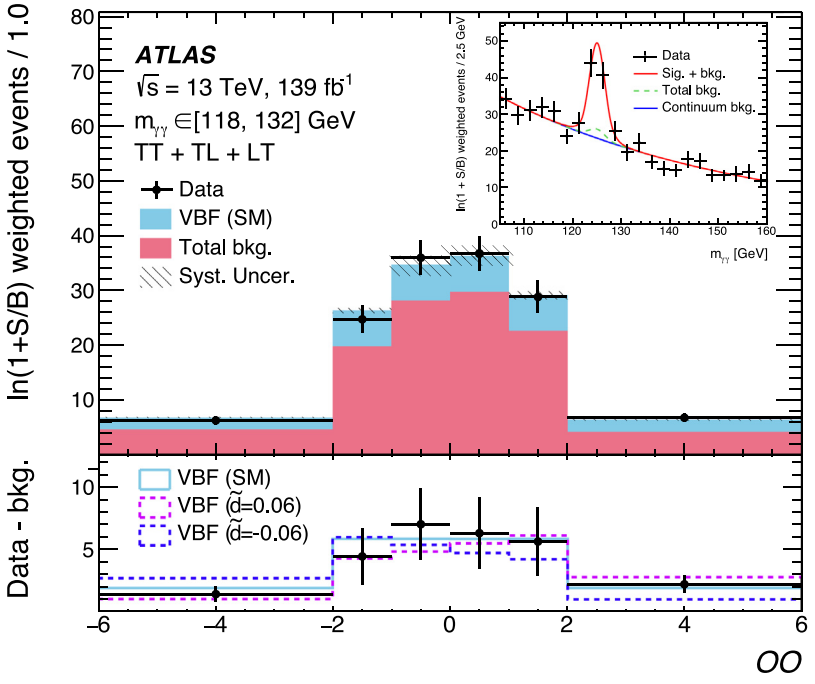

Fig. 28. Distribution of the Optimal Observable in the $H \to \gamma\gamma$ decay channel, for events enriched in the VBF production mode, with $118 < m_{\gamma\gamma} < 132$ GeV [174]. The total background includes events from non-VBF Higgs production. The bottom panel contains the background-subtracted distribution for data as well as the prediction for the SM and for two non-zero values of $\tilde{d}$. The invariant mass distribution is shown in the inset on the top right. Category-dependent weights are applied.

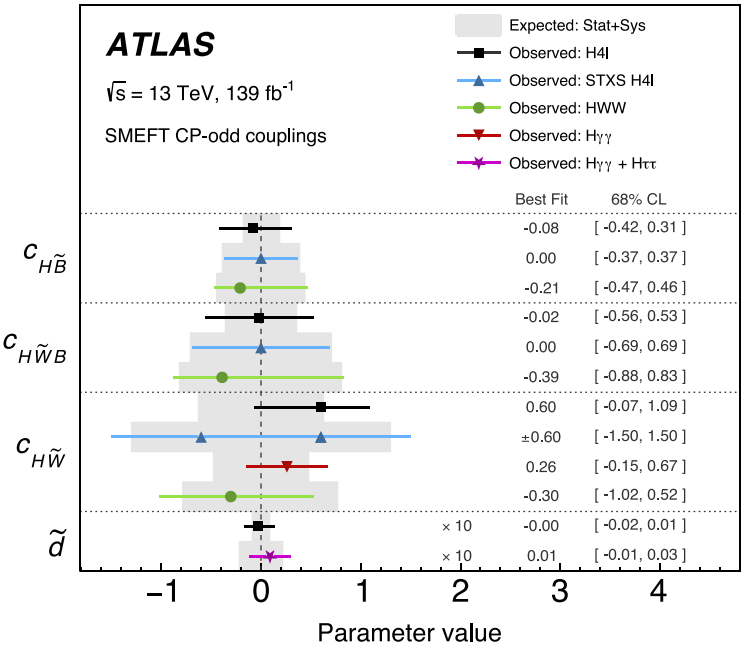

Fig. 29. Comparison of results extracted using the CP sensitive observables in the $H \to ZZ^* \to 4\ell$ channel, the $H \to WW^* \to e\nu\mu\nu$ differential cross-section measurement in the VBF production mode, the $H \to \gamma\gamma$ VBF measurement of $c_{H\tilde{W}}$ in the Warsaw basis, and the combined VBF measurement of $\tilde{d}$ in the $H \to \gamma\gamma$ and $H \to \tau\tau$ decay channels. Furthermore, the results based on the rate measurements in the $H \to ZZ^* \to 4\ell$ cross-section measurement of Ref. [112] ('STXS H4l') are added, which cannot distinguish between CP-odd and CP-even effects. The data points and 68% CL uncertainty bars show the observed values with statistical and systematic uncertainties. The $\tilde{d}$ best fit points and uncertainty bars are scaled by a factor of ten. In the $H \to ZZ^* \to 4\ell$ channel, only the linear parameterisation is considered (the effects of adding the quadratic terms are found to be negligible), while for the other analyses, the linear plus quadratic parameterisation is applied.

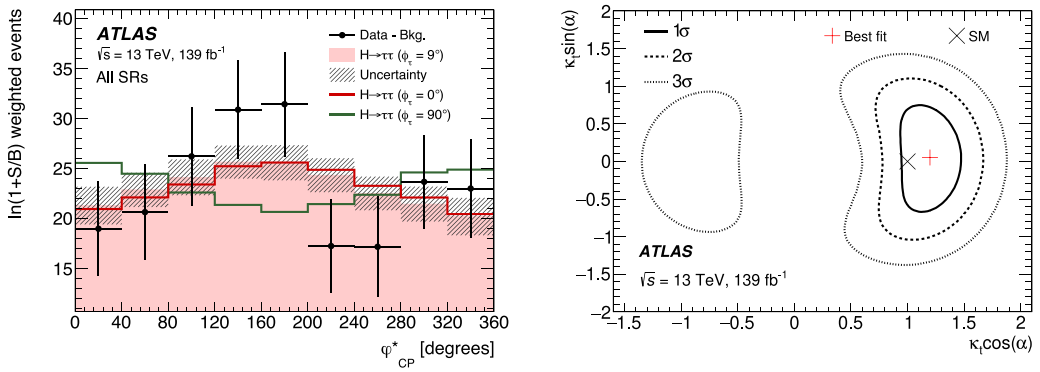

(a) (b)

Fig. 30. (a) Angle between the τ-lepton decay planes [176]. Events are weighted by $\ln(1+S/B)$, where S is the signal and B the background yield in the respective category. The best fit is shown in solid pink, while the red and green lines correspond to the predictions for the pure CP-even (scalar, SM) and pure CP-odd (pseudoscalar) hypotheses, respectively, all scaled to the best-fit $H \to \tau\tau$ yield. (b) Two-dimensional likelihood contours for $\kappa_t \cos\alpha$ and $\kappa_t \sin\alpha$, measured in the $H \to \gamma\gamma$ decay channel, with ggF and $H \to \gamma\gamma$ constrained by the Higgs boson coupling combination [177].

7.2. CP properties in interactions with fermions

The general effective Yukawa interaction between the Higgs boson and fermions, including a CP-odd term at tree level, can be parameterised as

$$\mathcal{L}_{HFF} = -\frac{m_F}{v}\kappa_F(\cos\alpha\,\bar{\psi}\psi + \sin\alpha\,\bar{\psi}i\gamma_5\psi)H. \tag{5}$$

Here, m_F is the fermion mass, v is the vacuum expectation value of the Higgs field, κ_F is the scaling factor for the Yukawa coupling, ψ are the fermion fields, and α is the CP-mixing angle. The SM corresponds to a CP-even coupling with $\alpha = 0$ and $\kappa_F = 1$ while a pure CP-odd coupling would be realised for $\alpha = 90°$. CP properties of the Higgs–τ-lepton and Higgs–top-quark couplings are probed.

The transverse spin components of the τ-leptons in the $H \to \tau\tau$ decays are affected by the CP-mixing angle α [176] and can be probed through the directions of the τ-lepton decay products. At least one of the τ-leptons is required to decay hadronically and decay planes are formed for each τ-lepton from the different visible decay products, i.e., leptons or pions, and, where necessary, the impact parameters of these objects. The angle φ^*_{CP} between these planes is calculated, which can be analytically related to α [166,167,178]. The event selection and background estimates follow the analysis discussed in Section 4. Categories are created to target VBF production and ggF production with Higgs bosons at high transverse momenta. A BDT classifier is used to further increase the purity of VBF events. In addition, $Z \to \tau\tau$ control regions are also formed. Fig. 30(a) shows the measured angle between the decay planes, which is used to extract $\phi_\tau = \alpha$.

Allowing for a free normalisation of the $H \to \tau\tau$ branching fraction, α is measured to be $9° \pm 16°$, with an expected value of $0° \pm 28°$ under the SM assumption. The pure CP-odd hypothesis is disfavoured at a level of 3.4σ.

The CP properties of the Higgs–top-quark couplings are probed in the $H \to \gamma\gamma$ [177] and $H \to b\bar{b}$ decay channels [179], using the $t\bar{t}H$ and tH production mechanisms. Both production rates and kinematic distributions depend on the CP properties, with the tH rate being particularly sensitive due to interference effects of diagrams. Furthermore, the ggF production and the $H \to \gamma\gamma$ decay rates are also affected, as there is a top-quark contribution in the loop diagrams.

For the $H \to \gamma\gamma$ channel, BDTs are used to identify the hadronic decay products for the reconstruction of the two top quarks, to reduce the background, and to separate CP-even and CP-odd contributions. The latter relies on kinematic distributions of the photons and top quarks and properties of the diphoton and $t\bar{t}$ systems, as well as various azimuthal angles. Events with at least one top quark candidate decaying semileptonically are separated from the fully hadronic events. A combined fit is performed over the $m_{\gamma\gamma}$ distributions in all signal regions and a pure CP-odd coupling of the Higgs boson to top quarks is excluded at 3.9σ, with $|\alpha| > 43°$ excluded at 95% CL. The likelihood contours as a function of $\kappa_t \cos\alpha$ and $\kappa_t \sin\alpha$ are shown in Fig. 30.

In the $H \to b\bar{b}$ case, either one or both of the top quarks are required to decay semileptonically. Signal candidate and control regions are formed based on the number of light- and heavy-flavour jets. The signal candidate regions are further split into signal and control regions with different $t\bar{t}H$ sensitivity. CP-sensitive observables are formed using the directions and azimuthal separation of the top quarks. A combined likelihood fit allows the mixing angle to be measured, resulting in $\alpha = (11\,^{+52}_{-73})°$.

In summary, no deviations from the CP-even hypothesis predicted by the SM are observed in the couplings of the Higgs boson to either bosons or fermions. The Run 2 data excludes CP-odd couplings to τ-leptons and top quarks at more than 3σ. Constraints are set on maximum mixing angles for the fermion couplings and on Wilson coefficients and matrix element mixing parameters for the boson couplings.

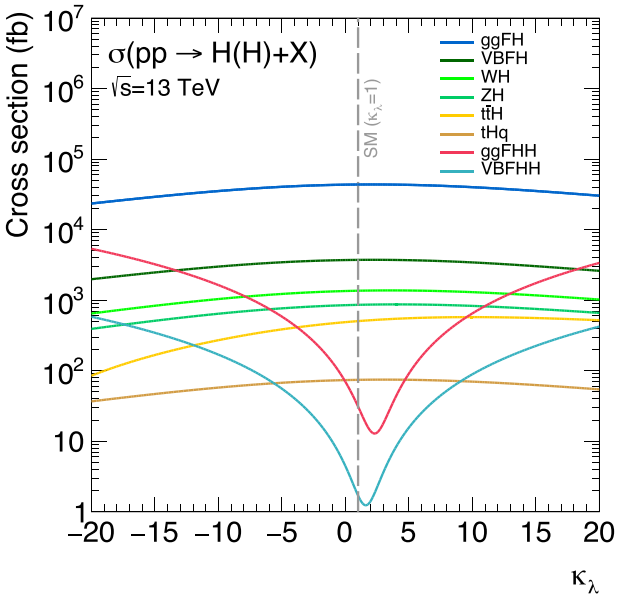

Fig. 31. Single-Higgs and double-Higgs boson production cross-sections as a function of κ_λ for $\sqrt{s} = 13$ TeV. The dashed line intercepts the values corresponding to the SM hypothesis ($\kappa_\lambda = 1$) [186].

8. The Higgs boson self-coupling

To completely understand the electroweak symmetry breaking mechanism, not only the properties of the Higgs boson, but also the Higgs field potential have to be probed experimentally. The Higgs field potential is of great interest from a cosmological perspective, as it determines the structure of the vacuum and influences the electroweak phase transition in the early universe [16,17]. A deviation of the Higgs boson self-coupling from the SM expectation might point to a first-order phase transition, a necessary condition for the electroweak baryogenesis mechanism, which in turn may help solve the matter–antimatter asymmetry puzzle. The Higgs field potential can be expressed as:

$$V(H) = \frac{1}{2} m_H^2 H^2 + \lambda_{HHH}\, v\, H^3 + \frac{1}{4}\lambda_{HHHH} H^4 + O(H^5)\,, \tag{6}$$

where m_H is the Higgs boson mass, v is the vacuum expectation value, and λ_{HHH} and λ_{HHHH} are the trilinear and quadrilinear Higgs boson self-couplings, respectively. In the SM, once m_H and the vacuum expectation value are known, the Higgs field potential and the Higgs boson self-couplings are fully determined:

$$O(H^5) = 0 \quad \text{and} \quad \lambda_{HHH}^{\text{SM}} = \lambda_{HHHH}^{\text{SM}} = \lambda\,, \quad \text{where} \quad \lambda = m_H^2/(2v^2) \sim 0.13\,. \tag{7}$$

To probe deviations from the Higgs boson self-coupling values within the SM Lagrangian structure, the self-coupling-modifier κ_λ is introduced as $\kappa_\lambda = \lambda_{HHH}/\lambda_{HHH}^{\text{SM}}$. Many BSM models predict changes in the trilinear and quadrilinear self-couplings and add additional higher-order terms to the Higgs field potential.

At the LHC, the Higgs boson trilinear self-interaction is directly accessible via the production of Higgs boson pairs (referred to as double-Higgs). The Higgs boson self-interaction also contributes to other processes via NLO EW corrections. In particular, it was shown [180–185] that single Higgs boson production cross-sections and branching ratios (referred to as single-Higgs) are modified if the Higgs boson self-coupling deviates from the SM prediction. Fig. 31 shows the expected effect of varying κ_λ on both the double- and single-Higgs boson production cross-sections. Additionally, BSM physics can give rise to resonant production of Higgs boson pairs mediated by a heavy scalar. More details of resonant double-Higgs searches can be found in Ref. [6].

8.1. Double Higgs boson production

Double Higgs boson production is sensitive to the Higgs boson trilinear self-coupling at LO. In the SM, the ggF *HH* process accounts for more than 90% of the Higgs boson pair-production at the LHC. The process with the second-highest cross-section at the LHC is VBF *HH* production. At LO, the ggF *HH* process proceeds through the destructive interference of two amplitudes: the box diagram in Fig. 2(a), which is proportional to the square of κ_t, and the triangle diagram in Fig. 2(b), which is proportional to the product of κ_t and κ_λ. The VBF *HH* process is described at LO by three Feynman diagrams: the two vector bosons radiated by the scattering quarks fuse into two Higgs bosons via a *HHVV* vertex (Fig. 2(c)),

with the corresponding amplitude proportional to $\kappa_{2V} = \lambda_{HHVV}/\lambda^{SM}_{HHVV}$; the vector bosons fuse into a virtual Higgs boson that decays into two Higgs bosons via a trilinear vertex (Fig. 2(d)), with the amplitude proportional to the product of κ_V and κ_λ; the vector bosons couple with two single Higgs bosons via two HVV interactions (Fig. 2(e)), with an amplitude proportional to the square of κ_V. Due to negative interference, the SM predicts double Higgs boson production to be a rare process, with a total cross-section that is more than a thousand times smaller than for single Higgs boson production (see Section 1.2 for the numerical values).

The various decays of the two Higgs bosons result in many different final states. However, the most sensitive decay channels for double Higgs boson production and its properties are those that contain at least one Higgs boson decaying into a bottom-quark pair [187–192], thanks to the large branching fraction. In particular, the most sensitive ones are the three HH decay channels $HH \to b\bar{b}b\bar{b}$, $HH \to b\bar{b}\tau^+\tau^-$, and $HH \to b\bar{b}\gamma\gamma$.

The $HH \to b\bar{b}b\bar{b}$ decay mode has the advantage of the largest SM HH decay branching fraction of 33.9%. However, the double-Higgs search in this final state is also affected by a larger SM background compared to the other HH analyses, due to the abundance of QCD multijet processes. The search for $HH \to b\bar{b}b\bar{b}$ [187] selects events that contain at least four b-tagged jets, which are split between VBF HH and ggF HH categories according to the properties of the additional jets in the event. A further selection aims to reduce the contamination from $t\bar{t}$ production in the two categories through a discriminant that quantifies the probability that an event contains a hadronic top-quark decay. Finally, in each category, the signal region is defined in a two-dimensional plane of the mass of the two Higgs boson candidates m_{H1} and m_{H2}, defined respectively as the one with the highest and lowest transverse momentum, by requiring that $X_{HH} < 1.6$ with X_{HH} defined as:

$$X_{HH} = \sqrt{\left(\frac{m_{H1} - 124\ \text{GeV}}{0.1\ m_{H1}}\right)^2 + \left(\frac{m_{H2} - 117\ \text{GeV}}{0.1\ m_{H2}}\right)^2}, \tag{8}$$

where 124 GeV and 117 GeV are determined as the peak of the m_{H1} and m_{H2} distributions for signal events in MC simulation. The HH invariant mass (m_{HH}) is used as a discriminating variable in the maximum-likelihood fit to extract the final results. The background, which is composed mostly of QCD multijet and $t\bar{t}$ processes, is evaluated with a fully data-driven method based on the extrapolation of the m_{HH} distribution from control regions, defined as the signal regions except that exactly two b-tagged jets are required in the events. To account for differences in kinematic properties between events with four and two b-tagged jets, a NN trained on data is used to reweight the m_{HH} distribution. The 95% CL upper limit on the observed (expected) double-Higgs production signal strength is $\mu_{HH} < 5.4$ (8.1).

ATLAS has also performed a dedicated search for $HH \to b\bar{b}b\bar{b}$ production via VBF HH in the boosted regime [188], which is particularly sensitive to BSM κ_{2V} variations. It results in 95% CL observed (expected) constraints on κ_{2V} equal to $0.52 < \kappa_{2V} < 1.52$ ($0.32 < \kappa_{2V} < 1.71$). Here, and in the following, unless explicitly stated otherwise, the Higgs boson couplings to the other particles are fixed to their SM expectations. The 95% CL upper limit on μ_{HH} and the constraints on κ_λ and κ_{2V}, obtained by the combination of the two $HH \to b\bar{b}b\bar{b}$ searches, are shown in Fig. 32 and in Table 2.

The $HH \to b\bar{b}\tau^+\tau^-$ decay mode has one of the largest branching fractions (7.3%) among the possible HH decay channels. The $HH \to b\bar{b}\tau^+\tau^-$ search [190] includes different signal regions targeting fully hadronic and semileptonic $\tau\tau$ final states. Events in the semileptonic channel are required to have exactly one electron or muon and one hadronically decaying τ-lepton with opposite charges. Events in the fully hadronic channel are required to have exactly two reconstructed hadronically decaying τ-leptons with opposite charge. In both channels, exactly two b-tagged jets are required. For each final state, the events are further split in different signal regions: one targeting VBF HH production, and two regions, dominated by ggF HH and defined by requiring $m_{HH} < 350$ GeV and $m_{HH} \geq 350$ GeV, respectively. The high mass region targets SM double-Higgs production, while the low-mass region is more sensitive to BSM values of κ_λ, as the double Higgs boson production cross-section would increase in this region if the value of κ_λ is different from one. The dominant backgrounds arise from Z + heavy flavour and $t\bar{t}$ production. Other relevant background contributions are due to events with a single Higgs boson decaying into $\tau^+\tau^-$: $t\bar{t}H$, ggF $+b\bar{b}$, $Z(\to b\bar{b})H$, and also $Z(\to \tau^+\tau^-)H(\to b\bar{b})$. A multivariate discriminant is trained separately in each signal region. The fit is performed simultaneously in the signal regions plus an additional control region that is used to constrain the normalisation of the Z + heavy flavour background component. It results in the best expected sensitivity for SM double-Higgs production in a single channel. Fig. 32 shows the final 95% CL upper limit on μ_{HH} and Table 2 presents the constraints on κ_λ and κ_{2V}.

The $HH \to b\bar{b}\gamma\gamma$ decay mode has a very small branching ratio (0.26%), but due to its experimentally clean signature allows for one of the most sensitive HH searches. The $HH \to b\bar{b}\gamma\gamma$ search [192] selects events with two photons and two b-tagged jets, each consistent with a SM Higgs boson decay. The dominant background arises from the SM continuum production of photon pairs and jets and from events with a single Higgs boson decaying into a pair of photons. The selected events are split into a low- and a high-mass region according to the value of the four-body mass $m^*_{b\bar{b}\gamma\gamma} = m_{b\bar{b}\gamma\gamma} - m_{b\bar{b}} - m_{\gamma\gamma} + 250$ GeV, where 250 GeV is about twice the Higgs boson mass. Compared to $m_{b\bar{b}\gamma\gamma}$, $m^*_{b\bar{b}\gamma\gamma}$ is chosen because it improves the four-object mass resolution. In each of the two mass regions, defined by $m^*_{b\bar{b}\gamma\gamma} < 350$ GeV and $m^*_{b\bar{b}\gamma\gamma} \geq 350$ GeV, respectively, a multivariate discriminant is used to separate the signal, which includes ggF HH and VBF HH production, from the background, and to define the categories which maximise the double-Higgs significance. The final results are obtained from a simultaneous fit to the diphoton invariant mass distribution in these categories, three in the high-mass region and four in the low-mass region. The 95% CL upper limit on μ_{HH} is shown in Fig. 32 and the constraints on κ_λ and κ_{2V} are summarised in Table 2.

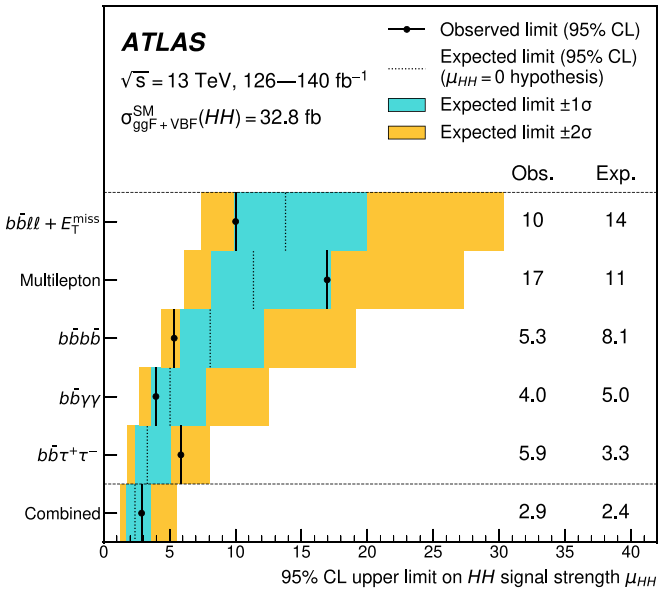

Fig. 32. Observed and expected 95% CL upper limits on μ_{HH} for double Higgs boson production in the $HH \to b\bar{b}\ell\ell + E_{\mathrm{T}}^{\mathrm{miss}}$, multilepton, $HH \to b\bar{b}\gamma\gamma$, $HH \to b\bar{b}\tau^+\tau^-$ and $HH \to b\bar{b}b\bar{b}$ decay channels and their statistical combination [193]. The expected limit is derived assuming $\mu_{HH} = 0$.

Table 2
Summary of the observed and expected constraints on κ_λ and κ_{2V} for the $HH \to b\bar{b}\gamma\gamma$, $HH \to b\bar{b}\tau^+\tau^-$, $HH \to b\bar{b}b\bar{b}$, multilepton and $HH \to b\bar{b}\ell\ell + E_{\mathrm{T}}^{\mathrm{miss}}$ analyses, and their combination [193]. In the fit, the Higgs boson couplings to the other particles are fixed to their SM expectations. The expected constraints are derived under the SM hypothesis.

Analysis	Obs. 95% CL	Exp. 95% CL	Obs. 68% CL
$HH \to b\bar{b}\gamma\gamma$	$-1.4 < \kappa_\lambda < 6.9$	$-2.9 < \kappa_\lambda < 7.8$	$\kappa_\lambda = 3.0^{+2.2}_{-2.5}$
$HH \to b\bar{b}\tau^+\tau^-$	$-3.2 < \kappa_\lambda < 9.0$	$-2.5 < \kappa_\lambda < 9.2$	$\kappa_\lambda = 0.0^{+3.3}_{-1.7}$
$HH \to b\bar{b}b\bar{b}$	$-3 < \kappa_\lambda < 11$	$-5 < \kappa_\lambda < 11$	$\kappa_\lambda = 5.8^{+3.0}_{-5.2}$
$HH \to$ multilepton	$-6 < \kappa_\lambda < 12$	$-4.5 < \kappa_\lambda < 9.6$	$\kappa_\lambda \in [-4.4, 0.6] \cup [4.3, 9.8]$
$HH \to b\bar{b}\ell\ell + E_{\mathrm{T}}^{\mathrm{miss}}$	$-6 < \kappa_\lambda < 13$	$-10 < \kappa_\lambda < 17$	$\kappa_\lambda = 3 \pm 6$
HH combination	$-1.2 < \kappa_\lambda < 7.2$	$-1.6 < \kappa_\lambda < 7.2$	$\kappa_\lambda = 3.8^{+2.1}_{-3.6}$
$HH \to b\bar{b}\gamma\gamma$	$-0.5 < \kappa_{2V} < 2.7$	$-1.1 < \kappa_{2V} < 3.3$	$\kappa_{2V} = 1.1 \pm 0.8$
$HH \to b\bar{b}\tau^+\tau^-$	$-0.5 < \kappa_{2V} < 2.7$	$-0.2 < \kappa_{2V} < 2.4$	$\kappa_{2V} = 0.4^{+1.9}_{-0.5}$
$HH \to b\bar{b}b\bar{b}$	$0.5 < \kappa_{2V} < 1.5$	$0.4 < \kappa_{2V} < 1.7$	$\kappa_{2V} = 1.01 \pm 0.23$
$HH \to$ multilepton	$-2.5 < \kappa_{2V} < 4.6$	$-1.9 < \kappa_{2V} < 4.1$	$\kappa_{2V} = -0.4^{+4.1}_{-1.2}$
$HH \to b\bar{b}\ell\ell + E_{\mathrm{T}}^{\mathrm{miss}}$	$-0.2 < \kappa_{2V} < 2.4$	$-0.5 < \kappa_{2V} < 2.7$	$\kappa_{2V} = 1.1 \pm 0.7$
HH combination	$0.6 < \kappa_{2V} < 1.5$	$0.4 < \kappa_{2V} < 1.6$	$\kappa_{2V} = 1.02^{+0.22}_{-0.23}$

The analyses in the $HH \to b\bar{b}b\bar{b}$, $HH \to b\bar{b}\tau^+\tau^-$ and $HH \to b\bar{b}\gamma\gamma$ decay channels are combined [193] to obtain more stringent constraints on the production cross-section, the Higgs boson self-coupling, and the $HHVV$ coupling. This combination includes also two other searches for double-Higgs production which target rarer or less sensitive final states: the search for HH events in $b\bar{b}ZZ^*$, VV^*VV^* ($V = W$ or Z), $VV^*\tau^+\tau^-$, $\tau^+\tau^-\tau^+\tau^-$, $\gamma\gamma VV^*$ and $\gamma\gamma\tau^+\tau^-$ decay channels with leptons in the final states (referred to as "multilepton") [194]; the search for $HH \to b\bar{b}\ell\ell + E_{\mathrm{T}}^{\mathrm{miss}}$, which probes the HH decay channels where one of the Higgs bosons decays to a b-quark pair and the other to either a boson pair (ZZ^*, WW^*) or a τ-lepton pair, which then decays to a pair of opposite-sign leptons and neutrinos [195]. The inclusion of these additional searches maximises the coverage over the combination of HH decays and improves the sensitivity to SM double-Higgs production by 4%.

The combination yields an observed 95% CL upper limit on μ_{HH} of 2.9, and an expected upper limit of 2.4 in the absence of HH production. The individual limits on the signal strength obtained from each channel and their combination are shown in Fig. 32. The best-fit value of the signal strength is $\mu_{HH} = 0.5^{+1.2}_{-1.0}$, which is compatible with the SM expectation with a p-value of 0.64. The observed (expected) significance for double-Higgs production is 0.4 (1.0) standard deviations, with respect to the hypothesis of no HH production. The 95% CL intervals for κ_λ and κ_{2V} are summarised in Table 2. The combination and the individual double-Higgs measurements are also interpreted in the context of effective field theory, as shown in Refs. [190,192,193,196].

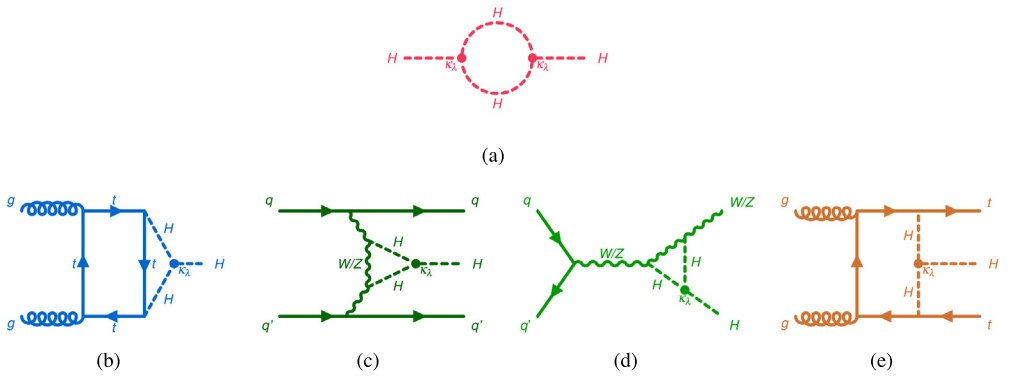

Fig. 33. Examples of one-loop λ_{HHH}-dependent diagrams for (a) the Higgs boson self-energy, and for single Higgs boson production in the (b) ggF, (c) VBF, (d) VH, and (e) $t\bar{t}H$ modes. The self-coupling vertex is indicated by the filled circle [197].

8.2. Self-coupling constraints from single Higgs boson measurements and combination with double Higgs boson searches

An alternative and complementary approach to study the Higgs boson self-coupling was proposed in Refs. [180–185]. Processes involving a single Higgs boson do not depend on λ_{HHH} at LO, but the Higgs trilinear self-coupling has to be taken into account in the calculation of the complete NLO EW corrections. In particular, λ_{HHH} contributes via Higgs boson self-energy loop corrections and additional diagrams, as illustrated for different production modes by the examples in Fig. 33.

A framework for a global fit to constrain the Higgs boson self-coupling is proposed in Refs. [180,181]. The SM predictions of the Higgs boson production and branching ratios are modified as:

$$\mu_{if}(\kappa_\lambda) = \mu_i(\kappa_\lambda) \times \mu_f(\kappa_\lambda) \equiv \frac{\sigma_i(\kappa_\lambda)}{\sigma_{\mathrm{SM},i}} \times \frac{\mathcal{B}_f(\kappa_\lambda)}{\mathcal{B}_{\mathrm{SM},f}} \,, \tag{9}$$

where μ_i and μ_f describe multiplicative corrections to the expected SM Higgs boson production cross-sections ($\sigma_{\mathrm{SM},i}$) and branching fractions ($\mathcal{B}_{\mathrm{SM},f}$) as a function of κ_λ. The functional dependence of $\mu_i(\kappa_\lambda)$ and $\mu_f(\kappa_\lambda)$ on κ_λ varies according to the production mode and the decay channel. Moreover, these functions depend on the kinematic region considered within each process, especially for the VH and $t\bar{t}H$ production modes. The cross-sections measured in different kinematic regions from the combined analysis in Section 6.3 are used to constrain κ_λ. While potential variations across kinematic regions are not considered for ggF, the differential effects of κ_λ for VBF, WH, ZH and $t\bar{t}H$ production modes are parameterised as reported in Ref. [186].

The observed (expected) 95% CL intervals for κ_λ from single Higgs boson measurements are $-4.0 < \kappa_\lambda < 10.3$ ($-5.2 < \kappa_\lambda < 11.5$) [198], which are not much looser than those obtained from the search for double Higgs boson production, despite the milder dependence of the single Higgs boson cross-sections on κ_λ. Moreover, since the two approaches are independent, they can be combined to provide the current most stringent 95% CL interval for κ_λ, equal to $-0.4 < \kappa_\lambda < 6.3$ [198]. This result and the following shown in this section, are based on the combination of a first version of the $HH \to b\bar{b}b\bar{b}$, $HH \to b\bar{b}\tau^+\tau^-$ and $HH \to b\bar{b}\gamma\gamma$ searches in the 140 fb^{-1} dataset [187,189,191], differently from the combination presented in the previous section which benefits from improved input analyses.

Double Higgs boson production does not only depend on κ_λ, but also has a significant dependence on κ_t because the two most important diagrams contributing to the ggF HH amplitude (see Fig. 2) contain the coupling of the Higgs boson to the top quark. Using only double Higgs boson analyses, it is not possible to simultaneously constrain κ_λ and κ_t without spoiling the sensitivity of the measurements of the two coupling-strength modifiers, as shown in Fig. 34. The inclusion of single Higgs boson measurements makes it possible to eliminate the degeneracy between κ_λ and κ_t and leads to a limit almost identical to that obtained by determining only κ_λ. The combination of single and double Higgs boson analyses allows a further generalisation of the fit model by simultaneously profiling κ_t, κ_b, κ_τ, and κ_V. The constraints on κ_λ in the different configurations are summarised in Table 3.

Although still not achieving the sensitivity required to probe the SM, the constraints of the trilinear Higgs boson self-coupling are starting to enter ranges predicted by BSM physics. They also have exceeded the expectations based on the Run 2 intermediate analyses [199–202]. This success can be attributed to new analysis techniques and improvements in the object identification, such as new algorithms for tagging heavy-flavour jets [203]. Future data taking will be critical to get closer to the first evidence of double Higgs boson production and increase the sensitivity to possible BSM effects on κ_λ.

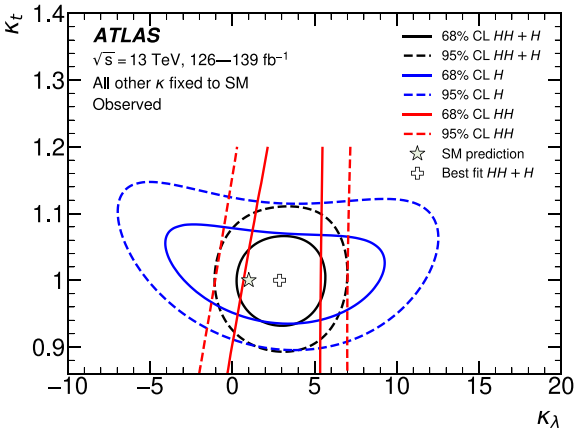

Fig. 34. Observed 68% (95%) CL contours in the κ_λ–κ_t plane from single (blue) and double (red) Higgs boson analyses and their combination (black) [198]. The Higgs boson couplings to the other particles are fixed to their SM expectations.

Table 3
Summary of observed and expected constraints on κ_λ and corresponding observed best-fit values with their uncertainties [198]. The *HH* combination is based on the earlier full Run 2 analyses performed by ATLAS.

	Floating parameters	Obs. 95% CL	Exp. 95% CL	Obs. value $^{+1\sigma}_{-1\sigma}$
HH combination	κ_λ	$-0.6 < \kappa_\lambda < 6.6$	$-2.1 < \kappa_\lambda < 7.8$	$\kappa_\lambda = 3.1^{+1.9}_{-2.0}$
Single-*H* combination	κ_λ	$-4.0 < \kappa_\lambda < 10.3$	$-5.2 < \kappa_\lambda < 11.5$	$\kappa_\lambda = 2.5^{+4.6}_{-3.9}$
$HH + H$ combination	κ_λ	$-0.4 < \kappa_\lambda < 6.3$	$-1.9 < \kappa_\lambda < 7.6$	$\kappa_\lambda = 3.0^{+1.8}_{-1.9}$
$HH + H$ combination	κ_λ, κ_t	$-0.4 < \kappa_\lambda < 6.3$	$-1.9 < \kappa_\lambda < 7.6$	$\kappa_\lambda = 3.0^{+1.8}_{-1.9}$
$HH + H$ combination	κ_λ, κ_t, κ_V, κ_b and κ_τ	$-1.4 < \kappa_\lambda < 6.1$	$-2.2 < \kappa_\lambda < 7.7$	$\kappa_\lambda = 2.3^{+2.1}_{-2.0}$

9. Conclusion and outlook

In Run 2 of the LHC (2015–2018), the ATLAS detector recorded an unprecedented amount of proton–proton collision data: 140 fb^{-1}, produced at a record centre-of-mass energy of 13 TeV. The analysis of these data significantly advances our understanding of the Higgs boson properties and its interactions with other particles.

The mass of the Higgs boson is not predicted by the SM and is a fundamental parameter in the calculation of its expected properties. It is measured to be 125.11 ± 0.11 GeV, which corresponds to a precision better than a permille, leading to negligible variations in the SM predictions for other Higgs boson properties compared to the current experimental uncertainties of the measurements. All the measurements, in particular the production cross-sections and decay branching fractions, show very good agreement with the SM predictions within the uncertainties.

Higgs boson production in association with a vector boson and its production in association with two top quarks is observed for the first time; together with the Run 1 discoveries, all major Higgs boson production modes at the LHC have now been observed. With the observation of $H \to \tau\tau$ and $H \to b\bar{b}$ decays, couplings to third generation fermions are now established, and the search for $H \to \mu\mu$, probing the Yukawa couplings to second generation fermions, yields a significance of 2σ. Evidence is found for $H \to \ell\ell\gamma$ decays, both for $H \to Z\gamma$ (in a combination of ATLAS and CMS analyses) and lepton pairs with low invariant masses.

Assuming the SM coupling structure, the Higgs boson couplings to the *W* and *Z* bosons are measured with uncertainties of about 6%, and the effective loop-induced couplings to photons and gluons with 6% and 7%, respectively. Couplings to τ-leptons are measured with uncertainties of 7%, and to the top and bottom quarks with about 12%. The measured uncertainty in the coupling to muons, which are the first second-generation fermions to be probed, is about 30%. Potential deviations from the SM predictions are also constrained within the framework of effective field theories. Searches for Higgs boson pair production achieve uncertainties in the *HH* cross-section of close to 100%, and reduce the possible range of the Higgs boson self-coupling (λ_{HHH}) to the interval $-0.4 < (\lambda_{HHH}/\lambda_{SM}) < 6.3$ at 95% CL.

Analyses of the data from Run 3 (2022–2025) and the High-Luminosity Runs of the LHC will build on the achieved results. Observation of the $H \to \ell\ell\gamma$ and $H \to \mu\mu$ decays are expected, as well as Higgs boson pair production, and the precision of the measured couplings and their structures will be significantly enhanced [204–206], further improving the characterisation of this key particle.

CRediT authorship contribution statement

ATLAS Collaboration: Writing – review & editing, Writing – original draft, Visualization, Validation, Supervision, Software, Resources, Project administration, Methodology, Investigation, Funding acquisition, Formal analysis, Data curation, Conceptualization.

Declaration of competing interest

The authors declare that they have no known competing financial interests or personal relationships that could have appeared to influence the work reported in this paper.

Acknowledgements

We thank CERN for the very successful operation of the LHC and its injectors, as well as the support staff at CERN and at our institutions worldwide without whom ATLAS could not be operated efficiently.

The crucial computing support from all WLCG partners is acknowledged gratefully, in particular from CERN, the ATLAS Tier-1 facilities at TRIUMF/SFU (Canada), NDGF (Denmark, Norway, Sweden), CC-IN2P3 (France), KIT/GridKA (Germany), INFN-CNAF (Italy), NL-T1 (Netherlands), PIC (Spain), RAL (UK) and BNL (USA), the Tier-2 facilities worldwide and large non-WLCG resource providers. Major contributors of computing resources are listed in Ref. [207].

We gratefully acknowledge the support of ANPCyT, Argentina; YerPhI, Armenia; ARC, Australia; BMWFW and FWF, Austria; ANAS, Azerbaijan; CNPq and FAPESP, Brazil; NSERC, NRC and CFI, Canada; CERN; ANID, Chile; CAS, MOST and NSFC, China; Minciencias, Colombia; MEYS CR, Czech Republic; DNRF and DNSRC, Denmark; IN2P3-CNRS and CEA-DRF/IRFU, France; SRNSFG, Georgia; BMBF, HGF and MPG, Germany; GSRI, Greece; RGC and Hong Kong SAR, China; ISF and Benoziyo Center, Israel; Istituto Nazionale di Fisica Nucleare, Italy; MEXT and JSPS, Japan; CNRST, Morocco; NWO, Netherlands; RCN, Norway; MNiSW, Poland; FCT, Portugal; MNE/IFA, Romania; MESTD, Serbia; MSSR, Slovakia; ARIS and MVZI, Slovenia; DSI/NRF, South Africa; MICIU/AEI, Spain; SRC and Wallenberg Foundation, Sweden; SERI, SNSF and Cantons of Bern and Geneva, Switzerland; NSTC, Taipei; TENMAK, Türkiye; STFC/UKRI, United Kingdom; DOE and NSF, United States of America.

Individual groups and members have received support from BCKDF, CANARIE, CRC and DRAC, Canada; PRIMUS 21/SCI/017, CERN-CZ and FORTE, Czech Republic; COST, ERC, ERDF, Horizon 2020, ICSC-NextGenerationEU and Marie Skłodowska-Curie Actions, European Union; Investissements d'Avenir Labex, Investissements d'Avenir Idex and ANR, France; DFG and AvH Foundation, Germany; Herakleitos, Thales and Aristeia programmes co-financed by EU-ESF and the Greek NSRF, Greece; BSF-NSF and MINERVA, Israel; Norwegian Financial Mechanism 2014–2021, Norway; NCN and NAWA, Poland; La Caixa Banking Foundation, CERCA Programme Generalitat de Catalunya and PROMETEO and GenT Programmes Generalitat Valenciana, Spain; Göran Gustafssons Stiftelse, Sweden; The Royal Society and Leverhulme Trust, United Kingdom.

In addition, individual members wish to acknowledge support from CERN: European Organisation for Nuclear Research (CERN PJAS); Chile: Agencia Nacional de Investigación *y* Desarrollo (FONDECYT 1190886, FONDECYT 1210400, FONDECYT 1230812, FONDECYT 1230987); China: Chinese Ministry of Science and Technology (MOST-2023YFA1605700), National Natural Science Foundation of China (NSFC - 12175119, NSFC 12275265, NSFC-12075060); Czech Republic: Czech Science Foundation (GACR - 24-11373S), Ministry of Education Youth and Sports (FORTE CZ.02.01.01/00/22_008/0004632), PRIMUS Research Programme (PRIMUS/21/SCI/017); EU: H2020 European Research Council (ERC - 101002463); European Union: European Research Council (ERC - 948254, ERC 101089007), Horizon 2020 Framework Programme (MUCCA - CHIST-ERA-19-XAI-00), European Union, Future Artificial Intelligence Research (FAIR-NextGenerationEU PE00000013), Italian Center for High Performance Computing, Big Data and Quantum Computing (ICSC, NextGenerationEU); France: Agence Nationale de la Recherche (ANR-20-CE31-0013, ANR-21-CE31-0013, ANR-21-CE31-0022, ANR-22-EDIR-0002), Investissements d'Avenir Labex (ANR-11-LABX-0012); Germany: Baden-Württemberg Stiftung (BW Stiftung-Postdoc Eliteprogramme), Deutsche Forschungsgemeinschaft (DFG - 469666862, DFG - CR 312/5-2); Italy: Istituto Nazionale di Fisica Nucleare (ICSC, NextGenerationEU), Ministero dell'Università e della Ricerca (PRIN - 20223N7F8K - PNRR M4.C2.1.1); Japan: Japan Society for the Promotion of Science (JSPS KAKENHI JP21H05085, JSPS KAKENHI JP22H01227, JSPS KAKENHI JP22H04944, JSPS KAKENHI JP22KK0227); Netherlands: Netherlands Organisation for Scientific Research (NWO Veni 2020 - VI.Veni.202.179); Norway: Research Council of Norway (RCN-314472); Poland: Polish National Agency for Academic Exchange (PPN/PPO/2020/1/00002/U/00001), Polish National Science Centre (NCN 2021/42/E/ST2/00350, NCN OPUS nr 2022/47/B/ST2/03059, NCN UMO-2019/34/E/ST2/00393, UMO-2020/37/B/ST2/01043, UMO-2021/40/C/ST2/00187, UMO-2022/47/O/ST2/00148); Slovenia: Slovenian Research Agency (ARIS grant J1-3010); Spain: Generalitat Valenciana (Artemisa, FEDER, IDIFEDER/2018/048), Ministry of Science and Innovation (MCIN & NextGenEU PCI2022-135018-2, MICIN & FEDER PID2021-125273NB, RYC2019-028510-I, RYC2020-030254-I, RYC2021-031273-I, RYC2022-038164-I), PROMETEO and GenT Programmes Generalitat Valenciana (CIDEGENT/2019/023, CIDEGENT/2019/027); Sweden: Swedish Research Council (Swedish Research Council 2023-04654, VR 2018-00482, VR 2022-03845, VR 2022-04683, VR 2023-03403, VR grant 2021-03651), Knut and Alice Wallenberg Foundation (KAW 2018.0157, KAW 2018.0458, KAW 2019.0447, KAW 2022.0358); Switzerland: Swiss National Science Foundation (SNSF - PCEFP2_194658); United Kingdom: Leverhulme Trust (Leverhulme Trust RPG-2020-004), Royal Society (NIF-R1-231091); United States of America: U.S. Department of Energy (ECA DE-AC02-76SF00515), Neubauer Family Foundation.

Appendix. The ATLAS collaboration

G. Aad[103], E. Aakvaag[16], B. Abbott[121], K. Abeling[55], N.J. Abicht[49], S.H. Abidi[29], M. Aboelela[44], A. Aboulhorma[35e], H. Abramowicz[153], H. Abreu[152], Y. Abulaiti[118], B.S. Acharya[69a,69b,k], A. Ackermann[63a], C. Adam Bourdarios[4], L. Adamczyk[86a], S.V. Addepalli[26], M.J. Addison[102], J. Adelman[116], A. Adiguzel[21c], T. Adye[135], A.A. Affolder[137], Y. Afik[39], M.N. Agaras[13], J. Agarwala[73a,73b], A. Aggarwal[101], C. Agheorghiesei[27c], A. Ahmad[36], F. Ahmadov[38,y], W.S. Ahmed[105], S. Ahuja[96], X. Ai[62e], G. Aielli[76a,76b], A. Aikot[164], M. Ait Tamlihat[35e], B. Aitbenchikh[35a], M. Akbiyik[101], T.P.A. Åkesson[99], A.V. Akimov[37], D. Akiyama[169], N.N. Akolkar[24], S. Aktas[21a], K. Al Khoury[41], G.L. Alberghi[23b], J. Albert[166], P. Albicocco[53], G.L. Albouy[60], S. Alderweireldt[52], Z.L. Alegria[122], M. Aleksa[36], I.N. Aleksandrov[38], C. Alexa[27b], T. Alexopoulos[10], F. Alfonsi[23b], M. Algren[56], M. Alhroob[143], B. Ali[133], H.M.J. Ali[92], S. Ali[31], S.W. Alibocus[93], M. Aliev[33c], G. Alimonti[71a], W. Alkakhi[55], C. Allaire[66], B.M.M. Allbrooke[148], J.F. Allen[52], C.A. Allendes Flores[138f], P.P. Allport[20], A. Aloisio[72a,72b], F. Alonso[91], C. Alpigiani[140], M. Alvarez Estevez[100], A. Alvarez Fernandez[101], M. Alves Cardoso[56], M.G. Alviggi[72a,72b], M. Aly[102], Y. Amaral Coutinho[83b], A. Ambler[105], C. Amelung[36], M. Amerl[102], C.G. Ames[110], D. Amidei[107], K.J. Amirie[156], S.P. Amor Dos Santos[131a], K.R. Amos[164], S. An[84], V. Ananiev[126], C. Anastopoulos[141], T. Andeen[11], J.K. Anders[36], S.Y. Andrean[47a,47b], A. Andreazza[71a,71b], S. Angelidakis[9], A. Angerami[41,aa], A.V. Anisenkov[37], A. Annovi[74a], C. Antel[56], E. Antipov[147], M. Antonelli[53], F. Anulli[75a], M. Aoki[84], T. Aoki[155], M.A. Aparo[148], L. Aperio Bella[48], C. Appelt[18], A. Apyan[26], S.J. Arbiol Val[87], C. Arcangeletti[53], A.T.H. Arce[51], E. Arena[93], J-F. Arguin[109], S. Argyropoulos[54], J.-H. Arling[48], O. Arnaez[4], H. Arnold[115], G. Artoni[75a,75b], H. Asada[112], K. Asai[119], S. Asai[155], N.A. Asbah[36], K. Assamagan[29], R. Astalos[28a], K.S.V. Astrand[99], S. Atashi[160], R.J. Atkin[33a], M. Atkinson[163], H. Atmani[35f], P.A. Atmasiddha[129], K. Augsten[133], S. Auricchio[72a,72b], A.D. Auriol[20], V.A. Austrup[102], G. Avolio[36], K. Axiotis[56], G. Azuelos[109,ae], D. Babal[28b], H. Bachacou[136], K. Bachas[154,o], A. Bachiu[34], F. Backman[47a,47b], A. Badea[39], T.M. Baer[107], P. Bagnaia[75a,75b], M. Bahmani[18], D. Bahner[54], K. Bai[124], J.T. Baines[135], L. Baines[95], O.K. Baker[173], E. Bakos[15], D. Bakshi Gupta[8], V. Balakrishnan[121], R. Balasubramanian[115], E.M. Baldin[37], P. Balek[86a], E. Ballabene[23b,23a], F. Balli[136], L.M. Baltes[63a], W.K. Balunas[32], J. Balz[101], E. Banas[87], M. Bandieramonte[130], A. Bandyopadhyay[24], S. Bansal[24], L. Barak[153], M. Barakat[48], E.L. Barberio[106], D. Barberis[57b,57a], M. Barbero[103], M.Z. Barel[115], K.N. Barends[33a], T. Barillari[111], M-S. Barisits[36], T. Barklow[145], P. Baron[123], D.A. Baron Moreno[102], A. Baroncelli[62a], G. Barone[29], A.J. Barr[127], J.D. Barr[97], F. Barreiro[100], J. Barreiro Guimarães da Costa[14a], U. Barron[153], M.G. Barros Teixeira[131a], S. Barsov[37], F. Bartels[63a], R. Bartoldus[145], A.E. Barton[92], P. Bartos[28a], A. Basan[101], M. Baselga[49], A. Bassalat[66,b], M.J. Basso[157a], R. Bate[165], R.L. Bates[59], S. Batlamous[100], B. Batool[143], M. Battaglia[137], D. Battulga[18], M. Bauce[75a,75b], M. Bauer[36], P. Bauer[24], L.T. Bazzano Hurrell[30], J.B. Beacham[51], T. Beau[128], J.Y. Beaucamp[91], P.H. Beauchemin[159], P. Bechtle[24], H.P. Beck[19,n], K. Becker[168], A.J. Beddall[82], V.A. Bednyakov[38], C.P. Bee[147], L.J. Beemster[15], T.A. Beermann[36], M. Begalli[83d], M. Begel[29], A. Behera[147], J.K. Behr[48], J.F. Beirer[36], F. Beisiegel[24], M. Belfkir[117b], G. Bella[153], L. Bellagamba[23b], A. Bellerive[34], P. Bellos[20], K. Beloborodov[37], D. Benchekroun[35a], F. Bendebba[35a], Y. Benhammou[153], K.C. Benkendorfer[61], L. Beresford[48], M. Beretta[53], E. Bergeaas Kuutmann[162], N. Berger[4], B. Bergmann[133], J. Beringer[17a], G. Bernardi[5], C. Bernius[145], F.U. Bernlochner[24], F. Bernon[36,103], A. Berrocal Guardia[13], T. Berry[96], P. Berta[134], A. Berthold[50], S. Bethke[111], A. Betti[75a,75b], A.J. Bevan[95], N.K. Bhalla[54], M. Bhamjee[33c], S. Bhatta[147], D.S. Bhattacharya[167], P. Bhattarai[145], K.D. Bhide[54], V.S. Bhopatkar[122], R.M. Bianchi[130], G. Bianco[23b,23a], O. Biebel[110], R. Bielski[124], M. Biglietti[77a], C.S. Billingsley[44], M. Bindi[55], A. Bingul[21b], C. Bini[75a,75b], A. Biondini[93], C.J. Birch-sykes[102], G.A. Bird[32], M. Birman[170], M. Biros[134], S. Biryukov[148], T. Bisanz[49], E. Bisceglie[43b,43a], J.P. Biswal[135], D. Biswas[143], I. Bloch[48], A. Blue[59], U. Blumenschein[95], J. Blumenthal[101], V.S. Bobrovnikov[37], M. Boehler[54], B. Boehm[167], D. Bogavac[36], A.G. Bogdanchikov[37], C. Bohm[47a], V. Boisvert[96], P. Bokan[36], T. Bold[86a], M. Bomben[5], M. Bona[95], M. Boonekamp[136], C.D. Booth[96], A.G. Borbély[59], I.S. Bordulev[37],

H.M. Borecka-Bielska[109], G. Borissov[92], D. Bortoletto[127], D. Boscherini[23b], M. Bosman[13], J.D. Bossio Sola[36], K. Bouaouda[35a], N. Bouchhar[164], L. Boudet[4], J. Boudreau[130], E.V. Bouhova-Thacker[92], D. Boumediene[40], R. Bouquet[57b,57a], A. Boveia[120], J. Boyd[36], D. Boye[29], I.R. Boyko[38], L. Bozianu[56], J. Bracinik[20], N. Brahimi[4], G. Brandt[172], O. Brandt[32], F. Braren[48], B. Brau[104], J.E. Brau[124], R. Brener[170], L. Brenner[115], R. Brenner[162], S. Bressler[170], D. Britton[59], D. Britzger[111], I. Brock[24], R. Brock[108], G. Brooijmans[41], E. Brost[29], L.M. Brown[166], L.E. Bruce[61], T.L. Bruckler[127], P.A. Bruckman de Renstrom[87], B. Brüers[48], A. Bruni[23b], G. Bruni[23b], M. Bruschi[23b], N. Bruscino[75a,75b], T. Buanes[16], Q. Buat[140], D. Buchin[111], A.G. Buckley[59], O. Bulekov[37], B.A. Bullard[145], S. Burdin[93], C.D. Burgard[49], A.M. Burger[36], B. Burghgrave[8], O. Burlayenko[54], J.T.P. Burr[32], C.D. Burton[11], J.C. Burzynski[144], E.L. Busch[41], V. Büscher[101], P.J. Bussey[59], J.M. Butler[25], C.M. Buttar[59], J.M. Butterworth[97], W. Buttinger[135], C.J. Buxo Vazquez[108], A.R. Buzykaev[37], S. Cabrera Urbán[164], L. Cadamuro[66], D. Caforio[58], H. Cai[130], Y. Cai[14a,14e], Y. Cai[14c], V.M.M. Cairo[36], O. Cakir[3a], N. Calace[36], P. Calafiura[17a], G. Calderini[128], P. Calfayan[68], G. Callea[59], L.P. Caloba[83b], D. Calvet[40], S. Calvet[40], M. Calvetti[74a,74b], R. Camacho Toro[128], S. Camarda[36], D. Camarero Munoz[26], P. Camarri[76a,76b], M.T. Camerlingo[72a,72b], D. Cameron[36], C. Camincher[166], M. Campanelli[97], A. Camplani[42], V. Canale[72a,72b], A.C. Canbay[3a], E. Canonero[96], J. Cantero[164], Y. Cao[163], F. Capocasa[26], M. Capua[43b,43a], A. Carbone[71a,71b], R. Cardarelli[76a], J.C.J. Cardenas[8], G. Carducci[43b,43a], T. Carli[36], G. Carlino[72a], J.I. Carlotto[13], B.T. Carlson[130,p], E.M. Carlson[166,157a], J. Carmignani[93], L. Carminati[71a,71b], A. Carnelli[136], M. Carnesale[75a,75b], S. Caron[114], E. Carquin[138f], S. Carrá[71a], G. Carratta[23b,23a], A.M. Carroll[124], T.M. Carter[52], M.P. Casado[13,h], M. Caspar[48], F.L. Castillo[4], L. Castillo Garcia[13], V. Castillo Gimenez[164], N.F. Castro[131a,131e], A. Catinaccio[36], J.R. Catmore[126], T. Cavaliere[4], V. Cavaliere[29], N. Cavalli[23b,23a], Y.C. Cekmecelioglu[48], E. Celebi[21a], S. Cella[36], F. Celli[127], M.S. Centonze[70a,70b], V. Cepaitis[56], K. Cerny[123], A.S. Cerqueira[83a], A. Cerri[148], L. Cerrito[76a,76b], F. Cerutti[17a], B. Cervato[143], A. Cervelli[23b], G. Cesarini[53], S.A. Cetin[82], D. Chakraborty[116], J. Chan[17a], W.Y. Chan[155], J.D. Chapman[32], E. Chapon[136], B. Chargeishvili[151b], D.G. Charlton[20], M. Chatterjee[19], C. Chauhan[134], Y. Che[14c], S. Chekanov[6], S.V. Chekulaev[157a], G.A. Chelkov[38,a], A. Chen[107], B. Chen[153], B. Chen[166], H. Chen[14c], H. Chen[29], J. Chen[62c], J. Chen[144], M. Chen[127], S. Chen[155], S.J. Chen[14c], X. Chen[62c,136], X. Chen[14b,ad], Y. Chen[62a], C.L. Cheng[171], H.C. Cheng[64a], S. Cheong[145], A. Cheplakov[38], E. Cheremushkina[48], E. Cherepanova[115], R. Cherkaoui El Moursli[35e], E. Cheu[7], K. Cheung[65], L. Chevalier[136], V. Chiarella[53], G. Chiarelli[74a], N. Chiedde[103], G. Chiodini[70a], A.S. Chisholm[20], A. Chitan[27b], M. Chitishvili[164], M.V. Chizhov[38,q], K. Choi[11], Y. Chou[140], E.Y.S. Chow[114], K.L. Chu[170], M.C. Chu[64a], X. Chu[14a,14e], J. Chudoba[132], J.J. Chwastowski[87], D. Cieri[111], K.M. Ciesla[86a], V. Cindro[94], A. Ciocio[17a], F. Cirotto[72a,72b], Z.H. Citron[170], M. Citterio[71a], D.A. Ciubotaru[27b], A. Clark[56], P.J. Clark[52], C. Clarry[156], J.M. Clavijo Columbie[48], S.E. Clawson[48], C. Clement[47a,47b], J. Clercx[48], Y. Coadou[103], M. Cobal[69a,69c], A. Coccaro[57b], R.F. Coelho Barrue[131a], R. Coelho Lopes De Sa[104], S. Coelli[71a], B. Cole[41], J. Collot[60], P. Conde Muiño[131a,131g], M.P. Connell[33c], S.H. Connell[33c], E.I. Conroy[127], F. Conventi[72a,af], H.G. Cooke[20], A.M. Cooper-Sarkar[127], F.A. Corchia[23b,23a], A. Cordeiro Oudot Choi[128], L.D. Corpe[40], M. Corradi[75a,75b], F. Corriveau[105,w], A. Cortes-Gonzalez[18], M.J. Costa[164], F. Costanza[4], D. Costanzo[141], B.M. Cote[120], J. Couthures[4], G. Cowan[96], K. Cranmer[171], D. Cremonini[23b,23a], S. Crépé-Renaudin[60], F. Cresciolli[128], M. Cristinziani[143], M. Cristoforetti[78a,78b], V. Croft[115], J.E. Crosby[122], G. Crosetti[43b,43a], A. Cueto[100], Z. Cui[7], W.R. Cunningham[59], F. Curcio[164], J.R. Curran[52], P. Czodrowski[36], M.M. Czurylo[36], M.J. Da Cunha Sargedas De Sousa[57b,57a], J.V. Da Fonseca Pinto[83b], C. Da Via[102], W. Dabrowski[86a], T. Dado[49], S. Dahbi[150], T. Dai[107], D. Dal Santo[19], C. Dallapiccola[104], M. Dam[42], G. D'amen[29], V. D'Amico[110], J. Damp[101], J.R. Dandoy[34], D. Dannheim[36], M. Danninger[144], V. Dao[36], G. Darbo[57b], S.J. Das[29,ag], F. Dattola[48], S. D'Auria[71a,71b], A. D'Avanzo[72a,72b], C. David[33a], T. Davidek[134], I. Dawson[95], H.A. Day-hall[133], K. De[8], R. De Asmundis[72a], N. De Biase[48], S. De Castro[23b,23a], N. De Groot[114], P. de Jong[115], H. De la Torre[116], A. De Maria[14c], A. De Salvo[75a], U. De Sanctis[76a,76b], F. De Santis[70a,70b], A. De Santo[148],

J.B. De Vivie De Regie[60], D.V. Dedovich[38], J. Degens[93], A.M. Deiana[44], F. Del Corso[23b,23a], J. Del Peso[100], F. Del Rio[63a], L. Delagrange[128], F. Deliot[136], C.M. Delitzsch[49], M. Della Pietra[72a,72b], D. Della Volpe[56], A. Dell'Acqua[36], L. Dell'Asta[71a,71b], M. Delmastro[4], P.A. Delsart[60], S. Demers[173], M. Demichev[38], S.P. Denisov[37], L. D'Eramo[40], D. Derendarz[87], F. Derue[128], P. Dervan[93], K. Desch[24], C. Deutsch[24], F.A. Di Bello[57b,57a], A. Di Ciaccio[76a,76b], L. Di Ciaccio[4], A. Di Domenico[75a,75b], C. Di Donato[72a,72b], A. Di Girolamo[36], G. Di Gregorio[36], A. Di Luca[78a,78b], B. Di Micco[77a,77b], R. Di Nardo[77a,77b], M. Diamantopoulou[34], F.A. Dias[115], T. Dias Do Vale[144], M.A. Diaz[138a,138b], F.G. Diaz Capriles[24], M. Didenko[164], E.B. Diehl[107], S. Díez Cornell[48], C. Diez Pardos[143], C. Dimitriadi[162,24], A. Dimitrievska[20], J. Dingfelder[24], I-M. Dinu[27b], S.J. Dittmeier[63b], F. Dittus[36], M. Divisek[134], F. Djama[103], T. Djobava[151b], C. Doglioni[102,99], A. Dohnalova[28a], J. Dolejsi[134], Z. Dolezal[134], K.M. Dona[39], M. Donadelli[83c], B. Dong[108], J. Donini[40], A. D'Onofrio[72a,72b], M. D'Onofrio[93], J. Dopke[135], A. Doria[72a], N. Dos Santos Fernandes[131a], P. Dougan[102], M.T. Dova[91], A.T. Doyle[59], M.A. Draguet[127], E. Dreyer[170], I. Drivas-koulouris[10], M. Drnevich[118], M. Drozdova[56], D. Du[62a], T.A. du Pree[115], F. Dubinin[37], M. Dubovsky[28a], E. Duchovni[170], G. Duckeck[110], O.A. Ducu[27b], D. Duda[52], A. Dudarev[36], E.R. Duden[26], M. D'uffizi[102], L. Duflot[66], M. Dührssen[36], I. Duminica[27g], A.E. Dumitriu[27b], M. Dunford[63a], S. Dungs[49], K. Dunne[47a,47b], A. Duperrin[103], H. Duran Yildiz[3a], M. Düren[58], A. Durglishvili[151b], B.L. Dwyer[116], G.I. Dyckes[17a], M. Dyndal[86a], B.S. Dziedzic[36], Z.O. Earnshaw[148], G.H. Eberwein[127], B. Eckerova[28a], S. Eggebrecht[55], E. Egidio Purcino De Souza[128], L.F. Ehrke[56], G. Eigen[16], K. Einsweiler[17a], T. Ekelof[162], P.A. Ekman[99], S. El Farkh[35b], Y. El Ghazali[35b], H. El Jarrari[36], A. El Moussaouy[109], V. Ellajosyula[162], M. Ellert[162], F. Ellinghaus[172], N. Ellis[36], J. Elmsheuser[29], M. Elsawy[117a], M. Elsing[36], D. Emeliyanov[135], Y. Enari[155], I. Ene[17a], S. Epari[13], P.A. Erland[87], M. Errenst[172], M. Escalier[66], C. Escobar[164], E. Etzion[153], G. Evans[131a], H. Evans[68], L.S. Evans[96], A. Ezhilov[37], S. Ezzarqtouni[35a], F. Fabbri[23b,23a], L. Fabbri[23b,23a], G. Facini[97], V. Fadeyev[137], R.M. Fakhrutdinov[37], D. Fakoudis[101], S. Falciano[75a], L.F. Falda Ulhoa Coelho[36], F. Fallavollita[111], J. Faltova[134], C. Fan[163], Y. Fan[14a], Y. Fang[14a,14e], M. Fanti[71a,71b], M. Faraj[69a,69b], Z. Farazpay[98], A. Farbin[8], A. Farilla[77a], T. Farooque[108], S.M. Farrington[52], F. Fassi[35e], D. Fassouliotis[9], M. Faucci Giannelli[76a,76b], W.J. Fawcett[32], L. Fayard[66], P. Federic[134], P. Federicova[132], O.L. Fedin[37,a], M. Feickert[171], L. Feligioni[103], D.E. Fellers[124], C. Feng[62b], M. Feng[14b], Z. Feng[115], M.J. Fenton[160], L. Ferencz[48], R.A.M. Ferguson[92], S.I. Fernandez Luengo[138f], P. Fernandez Martinez[13], M.J.V. Fernoux[103], J. Ferrando[92], A. Ferrari[162], P. Ferrari[115,114], R. Ferrari[73a], D. Ferrere[56], C. Ferretti[107], F. Fiedler[101], P. Fiedler[133], A. Filipčič[94], E.K. Filmer[1], F. Filthaut[114], M.C.N. Fiolhais[131a,131c,c], L. Fiorini[164], W.C. Fisher[108], T. Fitschen[102], P.M. Fitzhugh[136], I. Fleck[143], P. Fleischmann[107], T. Flick[172], M. Flores[33d,ab], L.R. Flores Castillo[64a], L. Flores Sanz De Acedo[36], F.M. Follega[78a,78b], N. Fomin[16], J.H. Foo[156], A. Formica[136], A.C. Forti[102], E. Fortin[36], A.W. Fortman[17a], M.G. Foti[17a], L. Fountas[9,i], D. Fournier[66], H. Fox[92], P. Francavilla[74a,74b], S. Francescato[61], S. Franchellucci[56], M. Franchini[23b,23a], S. Franchino[63a], D. Francis[36], L. Franco[114], V. Franco Lima[36], L. Franconi[48], M. Franklin[61], G. Frattari[26], Y.Y. Frid[153], J. Friend[59], N. Fritzsche[50], A. Froch[54], D. Froidevaux[36], J.A. Frost[127], Y. Fu[62a], S. Fuenzalida Garrido[138f], M. Fujimoto[103], K.Y. Fung[64a], E. Furtado De Simas Filho[83e], M. Furukawa[155], J. Fuster[164], A. Gabrielli[23b,23a], A. Gabrielli[156], P. Gadow[36], G. Gagliardi[57b,57a], L.G. Gagnon[17a], S. Gaid[161], S. Galantzan[153], E.J. Gallas[127], B.J. Gallop[135], K.K. Gan[120], S. Ganguly[155], Y. Gao[52], F.M. Garay Walls[138a,138b], B. Garcia[29], C. García[164], A. Garcia Alonso[115], A.G. Garcia Caffaro[173], J.E. García Navarro[164], M. Garcia-Sciveres[17a], G.L. Gardner[129], R.W. Gardner[39], N. Garelli[159], D. Garg[80], R.B. Garg[145], J.M. Gargan[52], C.A. Garner[156], C.M. Garvey[33a], V.K. Gassmann[159], G. Gaudio[73a], V. Gautam[13], P. Gauzzi[75a,75b], I.L. Gavrilenko[37], A. Gavrilyuk[37], C. Gay[165], G. Gaycken[48], E.N. Gazis[10], A.A. Geanta[27b], C.M. Gee[137], A. Gekow[120], C. Gemme[57b], M.H. Genest[60], A.D. Gentry[113], S. George[96], W.F. George[20], T. Geralis[46], P. Gessinger-Befurt[36], M.E. Geyik[172], M. Ghani[168], K. Ghorbanian[95], A. Ghosal[143], A. Ghosh[160], A. Ghosh[7], B. Giacobbe[23b], S. Giagu[75a,75b], T. Giani[115], P. Giannetti[74a], A. Giannini[62a], S.M. Gibson[96], M. Gignac[137], D.T. Gil[86b], A.K. Gilbert[86a],

B.J. Gilbert[41], D. Gillberg[34], G. Gilles[115], L. Ginabat[128], D.M. Gingrich[2,ae], M.P. Giordani[69a,69c], P.F. Giraud[136], G. Giugliarelli[69a,69c], D. Giugni[71a], F. Giuli[36], I. Gkialas[9,i], L.K. Gladilin[37], C. Glasman[100], G.R. Gledhill[124], G. Glemža[48], M. Glisic[124], I. Gnesi[43b,e], Y. Go[29], M. Goblirsch-Kolb[36], B. Gocke[49], D. Godin[109], B. Gokturk[21a], S. Goldfarb[106], T. Golling[56], M.G.D. Gololo[33g], D. Golubkov[37], J.P. Gombas[108], A. Gomes[131a,131b], G. Gomes Da Silva[143], A.J. Gomez Delegido[164], R. Gonçalo[131a], L. Gonella[20], A. Gongadze[151c], F. Gonnella[20], J.L. Gonski[145], R.Y. González Andana[52], S. González de la Hoz[164], R. Gonzalez Lopez[93], C. Gonzalez Renteria[17a], M.V. Gonzalez Rodrigues[48], R. Gonzalez Suarez[162], S. Gonzalez-Sevilla[56], L. Goossens[36], B. Gorini[36], E. Gorini[70a,70b], A. Gorišek[94], T.C. Gosart[129], A.T. Goshaw[51], M.I. Gostkin[38], S. Goswami[122], C.A. Gottardo[36], S.A. Gotz[110], M. Gouighri[35b], V. Goumarre[48], A.G. Goussiou[140], N. Govender[33c], I. Grabowska-Bold[86a], K. Graham[34], E. Gramstad[126], S. Grancagnolo[70a,70b], C.M. Grant[1,136], P.M. Gravila[27f], F.G. Gravili[70a,70b], H.M. Gray[17a], M. Greco[70a,70b], C. Grefe[24], I.M. Gregor[48], K.T. Greif[160], P. Grenier[145], S.G. Grewe[111], A.A. Grillo[137], K. Grimm[31], S. Grinstein[13,s], J.-F. Grivaz[66], E. Gross[170], J. Grosse-Knetter[55], J.C. Grundy[127], L. Guan[107], J.G.R. Guerrero Rojas[164], G. Guerrieri[69a,69c], F. Guescini[111], R. Gugel[101], J.A.M. Guhit[107], A. Guida[18], E. Guilloton[168], S. Guindon[36], F. Guo[14a,14e], J. Guo[62c], L. Guo[48], Y. Guo[107], R. Gupta[130], S. Gurbuz[24], S.S. Gurdasani[54], G. Gustavino[36], M. Guth[56], P. Gutierrez[121], L.F. Gutierrez Zagazeta[129], M. Gutsche[50], C. Gutschow[97], C. Gwenlan[127], C.B. Gwilliam[93], E.S. Haaland[126], A. Haas[118], M. Habedank[48], C. Haber[17a], H.K. Hadavand[8], A. Hadef[50], S. Hadzic[111], A.I. Hagan[92], J.J. Hahn[143], E.H. Haines[97], M. Haleem[167], J. Haley[122], J.J. Hall[141], G.D. Hallewell[103], L. Halser[19], K. Hamano[166], M. Hamer[24], G.N. Hamity[52], E.J. Hampshire[96], J. Han[62b], K. Han[62a], L. Han[14c], L. Han[62a], S. Han[17a], Y.F. Han[156], K. Hanagaki[84], M. Hance[137], D.A. Hangal[41], H. Hanif[144], M.D. Hank[129], J.B. Hansen[42], P.H. Hansen[42], K. Hara[158], D. Harada[56], T. Harenberg[172], S. Harkusha[37], M.L. Harris[104], Y.T. Harris[127], J. Harrison[13], N.M. Harrison[120], P.F. Harrison[168], N.M. Hartman[111], N.M. Hartmann[110], R.Z. Hasan[96,135], Y. Hasegawa[142], S. Hassan[16], R. Hauser[108], C.M. Hawkes[20], R.J. Hawkings[36], Y. Hayashi[155], S. Hayashida[112], D. Hayden[108], C. Hayes[107], R.L. Hayes[115], C.P. Hays[127], J.M. Hays[95], H.S. Hayward[93], F. He[62a], M. He[14a,14e], Y. He[139], Y. He[48], Y. He[97], N.B. Heatley[95], V. Hedberg[99], A.L. Heggelund[126], N.D. Hehir[95,*], C. Heidegger[54], K.K. Heidegger[54], W.D. Heidorn[81], J. Heilman[34], S. Heim[48], T. Heim[17a], J.G. Heinlein[129], J.J. Heinrich[124], L. Heinrich[111,ac], J. Hejbal[132], A. Held[171], S. Hellesund[16], C.M. Helling[165], S. Hellman[47a,47b], R.C.W. Henderson[92], L. Henkelmann[32], A.M. Henriques Correia[36], H. Herde[99], Y. Hernández Jiménez[147], L.M. Herrmann[24], T. Herrmann[50], G. Herten[54], R. Hertenberger[110], L. Hervas[36], M.E. Hesping[101], N.P. Hessey[157a], M. Hidaoui[35b], E. Hill[156], S.J. Hillier[20], J.R. Hinds[108], F. Hinterkeuser[24], M. Hirose[125], S. Hirose[158], D. Hirschbuehl[172], T.G. Hitchings[102], B. Hiti[94], J. Hobbs[147], R. Hobincu[27e], N. Hod[170], M.C. Hodgkinson[141], B.H. Hodkinson[127], A. Hoecker[36], D.D. Hofer[107], J. Hofer[48], T. Holm[24], M. Holzbock[111], L.B.A.H. Hommels[32], B.P. Honan[102], J.J. Hong[68], J. Hong[62c], T.M. Hong[130], B.H. Hooberman[163], W.H. Hopkins[6], M.C. Hoppesch[163], Y. Horii[112], S. Hou[150], A.S. Howard[94], J. Howarth[59], J. Hoya[6], M. Hrabovsky[123], A. Hrynevich[48], T. Hryn'ova[4], P.J. Hsu[65], S.-C. Hsu[140], T. Hsu[66], M. Hu[17a], Q. Hu[62a], S. Huang[64b], X. Huang[14a,14e], Y. Huang[141], Y. Huang[101], Y. Huang[14a], Z. Huang[102], Z. Hubacek[133], M. Huebner[24], F. Huegging[24], T.B. Huffman[127], C.A. Hugli[48], M. Huhtinen[36], S.K. Huiberts[16], R. Hulsken[105], N. Huseynov[12], J. Huston[108], J. Huth[61], R. Hyneman[145], G. Iacobucci[56], G. Iakovidis[29], L. Iconomidou-Fayard[66], J.P. Iddon[36], P. Iengo[72a,72b], R. Iguchi[155], T. Iizawa[127], Y. Ikegami[84], N. Ilic[156], H. Imam[35a], M. Ince Lezki[56], T. Ingebretsen Carlson[47a,47b], G. Introzzi[73a,73b], M. Iodice[77a], V. Ippolito[75a,75b], R.K. Irwin[93], M. Ishino[155], W. Islam[171], C. Issever[18,48], S. Istin[21a,ai], H. Ito[169], R. Iuppa[78a,78b], A. Ivina[170], J.M. Izen[45], V. Izzo[72a], P. Jacka[132], P. Jackson[1], C.S. Jagfeld[110], G. Jain[157a], P. Jain[48], K. Jakobs[54], T. Jakoubek[170], J. Jamieson[59], M. Javurkova[104], L. Jeanty[124], J. Jejelava[151a,z], P. Jenni[54,f], C.E. Jessiman[34], C. Jia[62b], J. Jia[147], X. Jia[61], X. Jia[14a,14e], Z. Jia[14c], C. Jiang[52], S. Jiggins[48], J. Jimenez Pena[13], S. Jin[14c], A. Jinaru[27b], O. Jinnouchi[139], P. Johansson[141], K.A. Johns[7], J.W. Johnson[137], D.M. Jones[148], E. Jones[48],

P. Jones[32], R.W.L. Jones[92], T.J. Jones[93], H.L. Joos[55,36], R. Joshi[120], J. Jovicevic[15], X. Ju[17a], J.J. Junggeburth[104], T. Junkermann[63a], A. Juste Rozas[13,s], M.K. Juzek[87], S. Kabana[138e], A. Kaczmarska[87], M. Kado[111], H. Kagan[120], M. Kagan[145], A. Kahn[129], C. Kahra[101], T. Kaji[155], E. Kajomovitz[152], N. Kakati[170], I. Kalaitzidou[54], C.W. Kalderon[29], N.J. Kang[137], D. Kar[33g], K. Karava[127], M.J. Kareem[157b], E. Karentzos[54], O. Karkout[115], S.N. Karpov[38], Z.M. Karpova[38], V. Kartvelishvili[92], A.N. Karyukhin[37], E. Kasimi[154], J. Katzy[48], S. Kaur[34], K. Kawade[142], M.P. Kawale[121], C. Kawamoto[88], T. Kawamoto[62a], E.F. Kay[36], F.I. Kaya[159], S. Kazakos[108], V.F. Kazanin[37], Y. Ke[147], J.M. Keaveney[33a], R. Keeler[166], G.V. Kehris[61], J.S. Keller[34], A.S. Kelly[97], J.J. Kempster[148], P.D. Kennedy[101], O. Kepka[132], B.P. Kerridge[135], S. Kersten[172], B.P. Kerševan[94], L. Keszeghova[28a], S. Ketabchi Haghighat[156], R.A. Khan[130], A. Khanov[122], A.G. Kharlamov[37], T. Kharlamova[37], E.E. Khoda[140], M. Kholodenko[37], T.J. Khoo[18], G. Khoriauli[167], J. Khubua[151b,*], Y.A.R. Khwaira[128], B. Kibirige[33g], D.W. Kim[47a,47b], Y.K. Kim[39], N. Kimura[97], M.K. Kingston[55], A. Kirchhoff[55], C. Kirfel[24], F. Kirfel[24], J. Kirk[135], A.E. Kiryunin[111], C. Kitsaki[10], O. Kivernyk[24], M. Klassen[159], C. Klein[34], L. Klein[167], M.H. Klein[44], S.B. Klein[56], U. Klein[93], P. Klimek[36], A. Klimentov[29], T. Klioutchnikova[36], P. Kluit[115], S. Kluth[111], E. Kneringer[79], T.M. Knight[156], A. Knue[49], R. Kobayashi[88], D. Kobylianskii[170], S.F. Koch[127], M. Kocian[145], P. Kodyš[134], D.M. Koeck[124], P.T. Koenig[24], T. Koffas[34], O. Kolay[50], I. Koletsou[4], T. Komarek[123], K. Köneke[54], A.X.Y. Kong[1], T. Kono[119], N. Konstantinidis[97], P. Kontaxakis[56], B. Konya[99], R. Kopeliansky[41], S. Koperny[86a], K. Korcyl[87], K. Kordas[154,d], A. Korn[97], S. Korn[55], I. Korolkov[13], N. Korotkova[37], B. Kortman[115], O. Kortner[111], S. Kortner[111], W.H. Kostecka[116], V.V. Kostyukhin[143], A. Kotsokechagia[136], A. Kotwal[51], A. Koulouris[36], A. Kourkoumeli-Charalampidi[73a,73b], C. Kourkoumelis[9], E. Kourlitis[111,ac], O. Kovanda[124], R. Kowalewski[166], W. Kozanecki[136], A.S. Kozhin[37], V.A. Kramarenko[37], G. Kramberger[94], P. Kramer[101], M.W. Krasny[128], A. Krasznahorkay[36], J.W. Kraus[172], J.A. Kremer[48], T. Kresse[50], J. Kretzschmar[93], K. Kreul[18], P. Krieger[156], S. Krishnamurthy[104], M. Krivos[134], K. Krizka[20], K. Kroeninger[49], H. Kroha[111], J. Kroll[132], J. Kroll[129], K.S. Krowpman[108], U. Kruchonak[38], H. Krüger[24], N. Krumnack[81], M.C. Kruse[51], O. Kuchinskaia[37], S. Kuday[3a], S. Kuehn[36], R. Kuesters[54], T. Kuhl[48], V. Kukhtin[38], Y. Kulchitsky[37,a], S. Kuleshov[138d,138b], M. Kumar[33g], N. Kumari[48], P. Kumari[157b], A. Kupco[132], T. Kupfer[49], A. Kupich[37], O. Kuprash[54], H. Kurashige[85], L.L. Kurchaninov[157a], O. Kurdysh[66], Y.A. Kurochkin[37], A. Kurova[37], M. Kuze[139], A.K. Kvam[104], J. Kvita[123], T. Kwan[105], N.G. Kyriacou[107], L.A.O. Laatu[103], C. Lacasta[164], F. Lacava[75a,75b], H. Lacker[18], D. Lacour[128], N.N. Lad[97], E. Ladygin[38], A. Lafarge[40], B. Laforge[128], T. Lagouri[173], F.Z. Lahbabi[35a], S. Lai[55], J.E. Lambert[166], S. Lammers[68], W. Lampl[7], C. Lampoudis[154,d], G. Lamprinoudis[101], A.N. Lancaster[116], E. Lançon[29], U. Landgraf[54], M.P.J. Landon[95], V.S. Lang[54], O.K.B. Langrekken[126], A.J. Lankford[160], F. Lanni[36], K. Lantzsch[24], A. Lanza[73a], J.F. Laporte[136], T. Lari[71a], F. Lasagni Manghi[23b], M. Lassnig[36], V. Latonova[132], A. Laudrain[101], A. Laurier[152], S.D. Lawlor[141], Z. Lawrence[102], R. Lazaridou[168], M. Lazzaroni[71a,71b], B. Le[102], E.M. Le Boulicaut[51], L.T. Le Pottier[17a], B. Leban[23b,23a], A. Lebedev[81], M. LeBlanc[102], F. Ledroit-Guillon[60], S.C. Lee[150], S. Lee[47a,47b], T.F. Lee[93], L.L. Leeuw[33c], H.P. Lefebvre[96], M. Lefebvre[166], C. Leggett[17a], G. Lehmann Miotto[36], M. Leigh[56], W.A. Leight[104], W. Leinonen[114], A. Leisos[154,r], M.A.L. Leite[83c], C.E. Leitgeb[18], R. Leitner[134], K.J.C. Leney[44], T. Lenz[24], S. Leone[74a], C. Leonidopoulos[52], A. Leopold[146], C. Leroy[109], R. Les[108], C.G. Lester[32], M. Levchenko[37], J. Levêque[4], L.J. Levinson[170], G. Levrini[23b,23a], M.P. Lewicki[87], C. Lewis[140], D.J. Lewis[4], A. Li[5], B. Li[62b], C. Li[62a], C-Q. Li[111], H. Li[62a], H. Li[62b], H. Li[14c], H. Li[14b], H. Li[62b], J. Li[62c], K. Li[140], L. Li[62c], M. Li[14a,14e], S. Li[14a,14e], S. Li[62d,62c], T. Li[5], X. Li[105], Z. Li[127], Z. Li[155], Z. Li[14a,14e], S. Liang[14a,14e], Z. Liang[14a], M. Liberatore[136], B. Liberti[76a], K. Lie[64c], J. Lieber Marin[83e], H. Lien[68], K. Lin[108], R.E. Lindley[7], J.H. Lindon[2], E. Lipeles[129], A. Lipniacka[16], A. Lister[165], J.D. Little[4], B. Liu[14a], B.X. Liu[14d], D. Liu[62d,62c], E.H.L. Liu[20], J.B. Liu[62a], J.K.K. Liu[32], K. Liu[62d], K. Liu[62d,62c], M. Liu[62a], M.Y. Liu[62a], P. Liu[14a], Q. Liu[62d,140,62c], X. Liu[62a], X. Liu[62b], Y. Liu[14d,14e], Y.L. Liu[62b], Y.W. Liu[62a], J. Llorente Merino[144], S.L. Lloyd[95], E.M. Lobodzinska[48], P. Loch[7], T. Lohse[18], K. Lohwasser[141], E. Loiacono[48], M. Lokajicek[132,*],

J.D. Lomas[20], J.D. Long[163], I. Longarini[160], R. Longo[163], I. Lopez Paz[67], A. Lopez Solis[48], N. Lorenzo Martinez[4], A.M. Lory[110], G. Löschcke Centeno[148], O. Loseva[37], X. Lou[47a,47b], X. Lou[14a,14e], A. Lounis[66], P.A. Love[92], G. Lu[14a,14e], M. Lu[66], S. Lu[129], Y.J. Lu[65], H.J. Lubatti[140], C. Luci[75a,75b], F.L. Lucio Alves[14c], F. Luehring[68], I. Luise[147], O. Lukianchuk[66], O. Lundberg[146], B. Lund-Jensen[146,*], N.A. Luongo[6], M.S. Lutz[36], A.B. Lux[25], D. Lynn[29], R. Lysak[132], E. Lytken[99], V. Lyubushkin[38], T. Lyubushkina[38], M.M. Lyukova[147], M. Firdaus M. Soberi[52], H. Ma[29], K. Ma[62a], L.L. Ma[62b], W. Ma[62a], Y. Ma[122], G. Maccarrone[53], J.C. MacDonald[101], P.C. Machado De Abreu Farias[83e], R. Madar[40], T. Madula[97], J. Maeda[85], T. Maeno[29], H. Maguire[141], V. Maiboroda[136], A. Maio[131a,131b,131d], K. Maj[86a], O. Majersky[48], S. Majewski[124], N. Makovec[66], V. Maksimovic[15], B. Malaescu[128], Pa. Malecki[87], V.P. Maleev[37], F. Malek[60,m], M. Mali[94], D. Malito[96], U. Mallik[80,*], S. Maltezos[10], S. Malyukov[38], J. Mamuzic[13], G. Mancini[53], M.N. Mancini[26], G. Manco[73a,73b], J.P. Mandalia[95], I. Mandić[94], L. Manhaes de Andrade Filho[83a], I.M. Maniatis[170], J. Manjarres Ramos[90], D.C. Mankad[170], A. Mann[110], S. Manzoni[36], L. Mao[62c], X. Mapekula[33c], A. Marantis[154,r], G. Marchiori[5], M. Marcisovsky[132], C. Marcon[71a], M. Marinescu[20], S. Marium[48], M. Marjanovic[121], A. Markhoos[54], M. Markovitch[66], E.J. Marshall[92], Z. Marshall[17a], S. Marti-Garcia[164], T.A. Martin[135], V.J. Martin[52], B. Martin dit Latour[16], L. Martinelli[75a,75b], M. Martinez[13,s], P. Martinez Agullo[164], V.I. Martinez Outschoorn[104], P. Martinez Suarez[13], S. Martin-Haugh[135], G. Martinovicova[134], V.S. Martoiu[27b], A.C. Martyniuk[97], A. Marzin[36], D. Mascione[78a,78b], L. Masetti[101], T. Mashimo[155], J. Masik[102], A.L. Maslennikov[37], P. Massarotti[72a,72b], P. Mastrandrea[74a,74b], A. Mastroberardino[43b,43a], T. Masubuchi[155], T. Mathisen[162], J. Matousek[134], N. Matsuzawa[155], J. Maurer[27b], A.J. Maury[66], B. Maček[94], D.A. Maximov[37], A.E. May[102], R. Mazini[150], I. Maznas[116], M. Mazza[108], S.M. Mazza[137], E. Mazzeo[71a,71b], C. Mc Ginn[29], J.P. Mc Gowan[166], S.P. Mc Kee[107], C.C. McCracken[165], E.F. McDonald[106], A.E. McDougall[115], J.A. Mcfayden[148], R.P. McGovern[129], G. Mchedlidze[151b], R.P. Mckenzie[33g], T.C. Mclachlan[48], D.J. Mclaughlin[97], S.J. McMahon[135], C.M. Mcpartland[93], R.A. McPherson[166,w], S. Mehlhase[110], A. Mehta[93], D. Melini[164], B.R. Mellado Garcia[33g], A.H. Melo[55], F. Meloni[48], A.M. Mendes Jacques Da Costa[102], H.Y. Meng[156], L. Meng[92], S. Menke[111], M. Mentink[36], E. Meoni[43b,43a], G. Mercado[116], S. Merianos[154], C. Merlassino[69a,69c], L. Merola[72a,72b], C. Meroni[71a,71b], J. Metcalfe[6], A.S. Mete[6], E. Meuser[101], C. Meyer[68], J-P. Meyer[136], R.P. Middleton[135], L. Mijović[52], G. Mikenberg[170], M. Mikestikova[132], M. Mikuž[94], H. Mildner[101], A. Milic[36], D.W. Miller[39], E.H. Miller[145], L.S. Miller[34], A. Milov[170], D.A. Milstead[47a,47b], T. Min[14c], A.A. Minaenko[37], I.A. Minashvili[151b], L. Mince[59], A.I. Mincer[118], B. Mindur[86a], M. Mineev[38], Y. Mino[88], L.M. Mir[13], M. Miralles Lopez[59], M. Mironova[17a], A. Mishima[155], M.C. Missio[114], A. Mitra[168], V.A. Mitsou[164], Y. Mitsumori[112], O. Miu[156], P.S. Miyagawa[95], T. Mkrtchyan[63a], M. Mlinarevic[97], T. Mlinarevic[97], M. Mlynarikova[36], S. Mobius[19], P. Mogg[110], M.H. Mohamed Farook[113], A.F. Mohammed[14a,14e], S. Mohapatra[41], G. Mokgatitswane[33g], L. Moleri[170], B. Mondal[143], S. Mondal[133], K. Mönig[48], E. Monnier[103], L. Monsonis Romero[164], J. Montejo Berlingen[13], M. Montella[120], F. Montereali[77a,77b], F. Monticelli[91], S. Monzani[69a,69c], N. Morange[66], A.L. Moreira De Carvalho[48], M. Moreno Llácer[164], C. Moreno Martinez[56], P. Morettini[57b], S. Morgenstern[36], M. Morii[61], M. Morinaga[155], F. Morodei[75a,75b], L. Morvaj[36], P. Moschovakos[36], B. Moser[36], M. Mosidze[151b], T. Moskalets[54], P. Moskvitina[114], J. Moss[31,j], P. Moszkowicz[86a], A. Moussa[35d], E.J.W. Moyse[104], O. Mtintsilana[33g], S. Muanza[103], J. Mueller[130], D. Muenstermann[92], R. Müller[19], G.A. Mullier[162], A.J. Mullin[32], J.J. Mullin[129], D.P. Mungo[156], D. Munoz Perez[164], F.J. Munoz Sanchez[102], M. Murin[102], W.J. Murray[168,135], M. Muškinja[94], C. Mwewa[29], A.G. Myagkov[37,a], A.J. Myers[8], G. Myers[107], M. Myska[133], B.P. Nachman[17a], O. Nackenhorst[49], K. Nagai[127], K. Nagano[84], J.L. Nagle[29,ag], E. Nagy[103], A.M. Nairz[36], Y. Nakahama[84], K. Nakamura[84], K. Nakkalil[5], H. Nanjo[125], E.A. Narayanan[113], I. Naryshkin[37], L. Nasella[71a,71b], M. Naseri[34], S. Nasri[117b], C. Nass[24], G. Navarro[22a], J. Navarro-Gonzalez[164], R. Nayak[153], A. Nayaz[18], P.Y. Nechaeva[37], S. Nechaeva[23b,23a], F. Nechansky[48], L. Nedic[127], T.J. Neep[20], A. Negri[73a,73b], M. Negrini[23b], C. Nellist[115], C. Nelson[105], K. Nelson[107], S. Nemecek[132], M. Nessi[36,g], M.S. Neubauer[163], F. Neuhaus[101], J. Neundorf[48], P.R. Newman[20], C.W. Ng[130],

Y.W.Y. Ng[48], B. Ngair[117a], H.D.N. Nguyen[109], R.B. Nickerson[127], R. Nicolaidou[136], J. Nielsen[137], M. Niemeyer[55], J. Niermann[55], N. Nikiforou[36], V. Nikolaenko[37,a], I. Nikolic-Audit[128], K. Nikolopoulos[20], P. Nilsson[29], I. Ninca[48], G. Ninio[153], A. Nisati[75a], N. Nishu[2], R. Nisius[111], J-E. Nitschke[50], E.K. Nkadimeng[33g], T. Nobe[155], T. Nommensen[149], M.B. Norfolk[141], R.R.B. Norisam[97], B.J. Norman[34], M. Noury[35a], J. Novak[94], T. Novak[94], L. Novotny[133], R. Novotny[113], L. Nozka[123], K. Ntekas[160], N.M.J. Nunes De Moura Junior[83b], J. Ocariz[128], A. Ochi[85], I. Ochoa[131a], S. Oerdek[48,t], J.T. Offermann[39], A. Ogrodnik[134], A. Oh[102], C.C. Ohm[146], H. Oide[84], R. Oishi[155], M.L. Ojeda[48], Y. Okumura[155], L.F. Oleiro Seabra[131a], S.A. Olivares Pino[138d], G. Oliveira Correa[13], D. Oliveira Damazio[29], D. Oliveira Goncalves[83a], J.L. Oliver[160], Ö.O. Öncel[54], A.P. O'Neill[19], A. Onofre[131a,131e], P.U.E. Onyisi[11], M.J. Oreglia[39], G.E. Orellana[91], D. Orestano[77a,77b], N. Orlando[13], R.S. Orr[156], V. O'Shea[59], L.M. Osojnak[129], R. Ospanov[62a], G. Otero y Garzon[30], H. Otono[89], P.S. Ott[63a], G.J. Ottino[17a], M. Ouchrif[35d], F. Ould-Saada[126], T. Ovsiannikova[140], M. Owen[59], R.E. Owen[135], V.E. Ozcan[21a], F. Ozturk[87], N. Ozturk[8], S. Ozturk[82], H.A. Pacey[127], A. Pacheco Pages[13], C. Padilla Aranda[13], G. Padovano[75a,75b], S. Pagan Griso[17a], G. Palacino[68], A. Palazzo[70a,70b], J. Pampel[24], J. Pan[173], T. Pan[64a], D.K. Panchal[11], C.E. Pandini[115], J.G. Panduro Vazquez[135], H.D. Pandya[1], H. Pang[14b], P. Pani[48], G. Panizzo[69a,69c], L. Panwar[128], L. Paolozzi[56], S. Parajuli[163], A. Paramonov[6], C. Paraskevopoulos[53], D. Paredes Hernandez[64b], A. Pareti[73a,73b], K.R. Park[41], T.H. Park[156], M.A. Parker[32], F. Parodi[57b,57a], E.W. Parrish[116], V.A. Parrish[52], J.A. Parsons[41], U. Parzefall[54], B. Pascual Dias[109], L. Pascual Dominguez[100], E. Pasqualucci[75a], S. Passaggio[57b], F. Pastore[96], P. Patel[87], U.M. Patel[51], J.R. Pater[102], T. Pauly[36], C.I. Pazos[159], J. Pearkes[145], M. Pedersen[126], R. Pedro[131a], S.V. Peleganchuk[37], O. Penc[36], E.A. Pender[52], G.D. Penn[173], K.E. Penski[110], M. Penzin[37], B.S. Peralva[83d], A.P. Pereira Peixoto[140], L. Pereira Sanchez[145], D.V. Perepelitsa[29,ag], E. Perez Codina[157a], M. Perganti[10], H. Pernegger[36], O. Perrin[40], K. Peters[48], R.F.Y. Peters[102], B.A. Petersen[36], T.C. Petersen[42], E. Petit[103], V. Petousis[133], C. Petridou[154,d], T. Petru[134], A. Petrukhin[143], M. Pettee[17a], N.E. Pettersson[36], A. Petukhov[37], K. Petukhova[134], R. Pezoa[138f], L. Pezzotti[36], G. Pezzullo[173], T.M. Pham[171], T. Pham[106], P.W. Phillips[135], G. Piacquadio[147], E. Pianori[17a], F. Piazza[124], R. Piegaia[30], D. Pietreanu[27b], A.D. Pilkington[102], M. Pinamonti[69a,69c], J.L. Pinfold[2], B.C. Pinheiro Pereira[131a], A.E. Pinto Pinoargote[136,136], L. Pintucci[69a,69c], K.M. Piper[148], A. Pirttikoski[56], D.A. Pizzi[34], L. Pizzimento[64b], A. Pizzini[115], M.-A. Pleier[29], V. Pleskot[134], E. Plotnikova[38], G. Poddar[95], R. Poettgen[99], L. Poggioli[128], I. Pokharel[55], S. Polacek[134], G. Polesello[73a], A. Poley[144,157a], A. Polini[23b], C.S. Pollard[168], Z.B. Pollock[120], E. Pompa Pacchi[75a,75b], N.I. Pond[97], D. Ponomarenko[114], L. Pontecorvo[36], S. Popa[27a], G.A. Popeneciu[27d], A. Poreba[36], D.M. Portillo Quintero[157a], S. Pospisil[133], M.A. Postill[141], P. Postolache[27c], K. Potamianos[168], P.A. Potepa[86a], I.N. Potrap[38], C.J. Potter[32], H. Potti[1], J. Poveda[164], M.E. Pozo Astigarraga[36], A. Prades Ibanez[164], J. Pretel[54], D. Price[102], M. Primavera[70a], M.A. Principe Martin[100], R. Privara[123], T. Procter[59], M.L. Proffitt[140], N. Proklova[129], K. Prokofiev[64c], G. Proto[111], J. Proudfoot[6], M. Przybycien[86a], W.W. Przygoda[86b], A. Psallidas[46], J.E. Puddefoot[141], D. Pudzha[37], D. Pyatiizbyantseva[37], J. Qian[107], D. Qichen[102], Y. Qin[13], T. Qiu[52], A. Quadt[55], M. Queitsch-Maitland[102], G. Quetant[56], R.P. Quinn[165], G. Rabanal Bolanos[61], D. Rafanoharana[54], F. Raffaeli[76a,76b], F. Ragusa[71a,71b], J.L. Rainbolt[39], J.A. Raine[56], S. Rajagopalan[29], E. Ramakoti[37], I.A. Ramirez-Berend[34], K. Ran[48,14e], N.P. Rapheeha[33g], H. Rasheed[27b], V. Raskina[128], D.F. Rassloff[63a], A. Rastogi[17a], S. Rave[101], B. Ravina[55], I. Ravinovich[170], M. Raymond[36], A.L. Read[126], N.P. Readioff[141], D.M. Rebuzzi[73a,73b], G. Redlinger[29], A.S. Reed[111], K. Reeves[26], J.A. Reidelsturz[172], D. Reikher[153], A. Rej[49], C. Rembser[36], M. Renda[27b], M.B. Rendel[111], F. Renner[48], A.G. Rennie[160], A.L. Rescia[48], S. Resconi[71a], M. Ressegotti[57b,57a], S. Rettie[36], J.G. Reyes Rivera[108], E. Reynolds[17a], O.L. Rezanova[37], P. Reznicek[134], H. Riani[35d], N. Ribaric[92], E. Ricci[78a,78b], R. Richter[111], S. Richter[47a,47b], E. Richter-Was[86b], M. Ridel[128], S. Ridouani[35d], P. Rieck[118], P. Riedler[36], E.M. Riefel[47a,47b], J.O. Rieger[115], M. Rijssenbeek[147], M. Rimoldi[36], L. Rinaldi[23b,23a], T.T. Rinn[29], M.P. Rinnagel[110], G. Ripellino[162], I. Riu[13], J.C. Rivera Vergara[166], F. Rizatdinova[122], E. Rizvi[95], B.R. Roberts[17a], S.H. Robertson[105,w], D. Robinson[32],

C.M. Robles Gajardo[138f], M. Robles Manzano[101], A. Robson[59], A. Rocchi[76a,76b], C. Roda[74a,74b], S. Rodriguez Bosca[36], Y. Rodriguez Garcia[22a], A. Rodriguez Rodriguez[54], A.M. Rodríguez Vera[116], S. Roe[36], J.T. Roemer[160], A.R. Roepe-Gier[137], J. Roggel[172], O. Røhne[126], R.A. Rojas[104], C.P.A. Roland[128], J. Roloff[29], A. Romaniouk[37], E. Romano[73a,73b], M. Romano[23b], A.C. Romero Hernandez[163], N. Rompotis[93], L. Roos[128], S. Rosati[75a], B.J. Rosser[39], E. Rossi[127], E. Rossi[72a,72b], L.P. Rossi[61], L. Rossini[54], R. Rosten[120], M. Rotaru[27b], B. Rottler[54], C. Rougier[90], D. Rousseau[66], D. Rousso[48], A. Roy[163], S. Roy-Garand[156], A. Rozanov[103], Z.M.A. Rozario[59], Y. Rozen[152], A. Rubio Jimenez[164], A.J. Ruby[93], V.H. Ruelas Rivera[18], T.A. Ruggeri[1], A. Ruggiero[127], A. Ruiz-Martinez[164], A. Rummler[36], Z. Rurikova[54], N.A. Rusakovich[38], H.L. Russell[166], G. Russo[75a,75b], J.P. Rutherfoord[7], S. Rutherford Colmenares[32], M. Rybar[134], E.B. Rye[126], A. Ryzhov[44], J.A. Sabater Iglesias[56], P. Sabatini[164], H.F-W. Sadrozinski[137], F. Safai Tehrani[75a], B. Safarzadeh Samani[135], S. Saha[1], M. Sahinsoy[111], A. Saibel[164], M. Saimpert[136], M. Saito[155], T. Saito[155], A. Sala[71a,71b], D. Salamani[36], A. Salnikov[145], J. Salt[164], A. Salvador Salas[153], D. Salvatore[43b,43a], F. Salvatore[148], A. Salzburger[36], D. Sammel[54], E. Sampson[92], D. Sampsonidis[154,d], D. Sampsonidou[124], J. Sánchez[164], V. Sanchez Sebastian[164], H. Sandaker[126], C.O. Sander[48], J.A. Sandesara[104], M. Sandhoff[172], C. Sandoval[22b], L. Sanfilippo[63a], D.P.C. Sankey[135], T. Sano[88], A. Sansoni[53], L. Santi[75a,75b], C. Santoni[40], H. Santos[131a,131b], A. Santra[170], E. Sanzani[23b,23a], K.A. Saoucha[161], J.G. Saraiva[131a,131d], J. Sardain[7], O. Sasaki[84], K. Sato[158], C. Sauer[63b], E. Sauvan[4], P. Savard[156,ae], R. Sawada[155], C. Sawyer[135], L. Sawyer[98], C. Sbarra[23b], A. Sbrizzi[23b,23a], T. Scanlon[97], J. Schaarschmidt[140], U. Schäfer[101], A.C. Schaffer[66,44], D. Schaile[110], R.D. Schamberger[147], C. Scharf[18], M.M. Schefer[19], V.A. Schegelsky[37], D. Scheirich[134], M. Schernau[160], C. Scheulen[55], C. Schiavi[57b,57a], M. Schioppa[43b,43a], B. Schlag[145], K.E. Schleicher[54], S. Schlenker[36], J. Schmeing[172], M.A. Schmidt[172], K. Schmieden[101], C. Schmitt[101], N. Schmitt[101], S. Schmitt[48], L. Schoeffel[136], A. Schoening[63b], P.G. Scholer[34], E. Schopf[127], M. Schott[24], J. Schovancova[36], S. Schramm[56], T. Schroer[56], H-C. Schultz-Coulon[63a], M. Schumacher[54], B.A. Schumm[137], Ph. Schune[136], A.J. Schuy[140], H.R. Schwartz[137], A. Schwartzman[145], T.A. Schwarz[107], Ph. Schwemling[136], R. Schwienhorst[108], A. Sciandra[29], G. Sciolla[26], F. Scuri[74a], C.D. Sebastiani[93], K. Sedlaczek[116], S.C. Seidel[113], A. Seiden[137], B.D. Seidlitz[41], C. Seitz[48], J.M. Seixas[83b], G. Sekhniaidze[72a], L. Selem[60], N. Semprini-Cesari[23b,23a], D. Sengupta[56], V. Senthilkumar[164], L. Serin[66], M. Sessa[76a,76b], H. Severini[121], F. Sforza[57b,57a], A. Sfyrla[56], Q. Sha[14a], E. Shabalina[55], A.H. Shah[32], R. Shaheen[146], J.D. Shahinian[129], D. Shaked Renous[170], L.Y. Shan[14a], M. Shapiro[17a], A. Sharma[36], A.S. Sharma[165], P. Sharma[80], P.B. Shatalov[37], K. Shaw[148], S.M. Shaw[102], Q. Shen[62c,5], D.J. Sheppard[144], P. Sherwood[97], L. Shi[97], X. Shi[14a], C.O. Shimmin[173], J.D. Shinner[96], I.P.J. Shipsey[127,*], S. Shirabe[89], M. Shiyakova[38,u], M.J. Shochet[39], J. Shojaii[106], D.R. Shope[126], B. Shrestha[121], S. Shrestha[120,ah], M.J. Shroff[166], P. Sicho[132], A.M. Sickles[163], E. Sideras Haddad[33g], A.C. Sidley[115], A. Sidoti[23b], F. Siegert[50], Dj. Sijacki[15], F. Sili[91], J.M. Silva[52], M.V. Silva Oliveira[29], S.B. Silverstein[47a], S. Simion[66], R. Simoniello[36], E.L. Simpson[102], H. Simpson[148], L.R. Simpson[107], N.D. Simpson[99], S. Simsek[82], S. Sindhu[55], P. Sinervo[156], S. Singh[156], S. Sinha[48], S. Sinha[102], M. Sioli[23b,23a], I. Siral[36], E. Sitnikova[48], J. Sjölin[47a,47b], A. Skaf[55], E. Skorda[20], P. Skubic[121], M. Slawinska[87], V. Smakhtin[170], B.H. Smart[135], S.Yu. Smirnov[37], Y. Smirnov[37], L.N. Smirnova[37,a], O. Smirnova[99], A.C. Smith[41], D.R. Smith[160], E.A. Smith[39], H.A. Smith[127], J.L. Smith[102], R. Smith[145], M. Smizanska[92], K. Smolek[133], A.A. Snesarev[37], S.R. Snider[156], H.L. Snoek[115], S. Snyder[29], R. Sobie[166,w], A. Soffer[153], C.A. Solans Sanchez[36], E.Yu. Soldatov[37], U. Soldevila[164], A.A. Solodkov[37], S. Solomon[26], A. Soloshenko[38], K. Solovieva[54], O.V. Solovyanov[40], P. Sommer[36], A. Sonay[13], W.Y. Song[157b], A. Sopczak[133], A.L. Sopio[97], F. Sopkova[28b], J.D. Sorenson[113], I.R. Sotarriva Alvarez[139], V. Sothilingam[63a], O.J. Soto Sandoval[138c,138b], S. Sottocornola[68], R. Soualah[161], Z. Soumaimi[35e], D. South[48], N. Soybelman[170], S. Spagnolo[70a,70b], M. Spalla[111], D. Sperlich[54], G. Spigo[36], S. Spinali[92], D.P. Spiteri[59], M. Spousta[134], E.J. Staats[34], R. Stamen[63a], A. Stampekis[20], M. Standke[24], E. Stanecka[87], W. Stanek-Maslouska[48], M.V. Stange[50], B. Stanislaus[17a], M.M. Stanitzki[48], B. Stapf[48], E.A. Starchenko[37],

G.H. Stark[137], J. Stark[90], P. Staroba[132], P. Starovoitov[63a], S. Stärz[105], R. Staszewski[87], G. Stavropoulos[46], J. Steentoft[162], P. Steinberg[29], B. Stelzer[144,157a], H.J. Stelzer[130], O. Stelzer-Chilton[157a], H. Stenzel[58], T.J. Stevenson[148], G.A. Stewart[36], J.R. Stewart[122], M.C. Stockton[36], G. Stoicea[27b], M. Stolarski[131a], S. Stonjek[111], A. Straessner[50], J. Strandberg[146], S. Strandberg[47a,47b], M. Stratmann[172], M. Strauss[121], T. Strebler[103], P. Strizenec[28b], R. Ströhmer[167], D.M. Strom[124], R. Stroynowski[44], A. Strubig[47a,47b], S.A. Stucci[29], B. Stugu[16], J. Stupak[121], N.A. Styles[48], D. Su[145], S. Su[62a], W. Su[62d], X. Su[62a], D. Suchy[28a], K. Sugizaki[155], V.V. Sulin[37], M.J. Sullivan[93], D.M.S. Sultan[127], L. Sultanaliyeva[37], S. Sultansoy[3b], T. Sumida[88], S. Sun[107], S. Sun[171], O. Sunneborn Gudnadottir[162], N. Sur[103], M.R. Sutton[148], H. Suzuki[158], M. Svatos[132], M. Swiatlowski[157a], T. Swirski[167], I. Sykora[28a], M. Sykora[134], T. Sykora[134], D. Ta[101], K. Tackmann[48,t], A. Taffard[160], R. Tafirout[157a], J.S. Tafoya Vargas[66], Y. Takubo[84], M. Talby[103], A.A. Talyshev[37], K.C. Tam[64b], N.M. Tamir[153], A. Tanaka[155], J. Tanaka[155], R. Tanaka[66], M. Tanasini[147], Z. Tao[165], S. Tapia Araya[138f], S. Tapprogge[101], A. Tarek Abouelfadl Mohamed[108], S. Tarem[152], K. Tariq[14a], G. Tarna[27b], G.F. Tartarelli[71a], M.J. Tartarin[90], P. Tas[134], M. Tasevsky[132], E. Tassi[43b,43a], A.C. Tate[163], G. Tateno[155], Y. Tayalati[35e,v], G.N. Taylor[106], W. Taylor[157b], A.S. Tee[171], R. Teixeira De Lima[145], P. Teixeira-Dias[96], J.J. Teoh[156], K. Terashi[155], J. Terron[100], S. Terzo[13], M. Testa[53], R.J. Teuscher[156,w], A. Thaler[79], O. Theiner[56], N. Themistokleous[52], T. Theveneaux-Pelzer[103], O. Thielmann[172], D.W. Thomas[96], J.P. Thomas[20], E.A. Thompson[17a], P.D. Thompson[20], E. Thomson[129], R.E. Thornberry[44], C. Tian[62a], Y. Tian[55], V. Tikhomirov[37,a], Yu.A. Tikhonov[37], S. Timoshenko[37], D. Timoshyn[134], E.X.L. Ting[1], P. Tipton[173], S.H. Tlou[33g], K. Todome[139], S. Todorova-Nova[134], S. Todt[50], L. Toffolin[69a,69c], M. Togawa[84], J. Tojo[89], S. Tokár[28a], K. Tokushuku[84], O. Toldaiev[68], R. Tombs[32], M. Tomoto[84,112], L. Tompkins[145,l], K.W. Topolnicki[86b], E. Torrence[124], H. Torres[90], E. Torró Pastor[164], M. Toscani[30], C. Tosciri[39], M. Tost[11], D.R. Tovey[141], A. Traeet[16], I.S. Trandafir[27b], T. Trefzger[167], A. Tricoli[29], I.M. Trigger[157a], S. Trincaz-Duvoid[128], D.A. Trischuk[26], B. Trocmé[60], L. Truong[33c], M. Trzebinski[87], A. Trzupek[87], F. Tsai[147], M. Tsai[107], A. Tsiamis[154,d], P.V. Tsiareshka[37], S. Tsigaridas[157a], A. Tsirigotis[154,r], V. Tsiskaridze[156], E.G. Tskhadadze[151a], M. Tsopoulou[154], Y. Tsujikawa[88], I.I. Tsukerman[37], V. Tsulaia[17a], S. Tsuno[84], K. Tsuri[119], D. Tsybychev[147], Y. Tu[64b], A. Tudorache[27b], V. Tudorache[27b], A.N. Tuna[61], S. Turchikhin[57b,57a], I. Turk Cakir[3a], R. Turra[71a], T. Turtuvshin[38,x], P.M. Tuts[41], S. Tzamarias[154,d], E. Tzovara[101], F. Ukegawa[158], P.A. Ulloa Poblete[138c,138b], E.N. Umaka[29], G. Unal[36], A. Undrus[29], G. Unel[160], J. Urban[28b], P. Urrejola[138a], G. Usai[8], R. Ushioda[139], M. Usman[109], Z. Uysal[82], V. Vacek[133], B. Vachon[105], T. Vafeiadis[36], A. Vaitkus[97], C. Valderanis[110], E. Valdes Santurio[47a,47b], M. Valente[157a], S. Valentinetti[23b,23a], A. Valero[164], E. Valiente Moreno[164], A. Vallier[90], J.A. Valls Ferrer[164], D.R. Van Arneman[115], T.R. Van Daalen[140], A. Van Der Graaf[49], P. Van Gemmeren[6], M. Van Rijnbach[36], S. Van Stroud[97], I. Van Vulpen[115], P. Vana[134], M. Vanadia[76a,76b], W. Vandelli[36], E.R. Vandewall[122], D. Vannicola[153], L. Vannoli[53], R. Vari[75a], E.W. Varnes[7], C. Varni[17b], T. Varol[150], D. Varouchas[66], L. Varriale[164], K.E. Varvell[149], M.E. Vasile[27b], L. Vaslin[84], G.A. Vasquez[166], A. Vasyukov[38], R. Vavricka[101], T. Vazquez Schroeder[36], J. Veatch[31], V. Vecchio[102], M.J. Veen[104], I. Veliscek[29], L.M. Veloce[156], F. Veloso[131a,131c], S. Veneziano[75a], A. Ventura[70a,70b], S. Ventura Gonzalez[136], A. Verbytskyi[111], M. Verducci[74a,74b], C. Vergis[95], M. Verissimo De Araujo[83b], W. Verkerke[115], J.C. Vermeulen[115], C. Vernieri[145], M. Vessella[104], M.C. Vetterli[144,ae], A. Vgenopoulos[154,d], N. Viaux Maira[138f], T. Vickey[141], O.E. Vickey Boeriu[141], G.H.A. Viehhauser[127], L. Vigani[63b], M. Villa[23b,23a], M. Villaplana Perez[164], E.M. Villhauer[52], E. Vilucchi[53], M.G. Vincter[34], A. Visibile[115], C. Vittori[36], I. Vivarelli[23b,23a], E. Voevodina[111], F. Vogel[110], J.C. Voigt[50], P. Vokac[133], Yu. Volkotrub[86b], J. Von Ahnen[48], E. Von Toerne[24], B. Vormwald[36], V. Vorobel[134], K. Vorobev[37], M. Vos[164], K. Voss[143], M. Vozak[115], L. Vozdecky[121], N. Vranjes[15], M. Vranjes Milosavljevic[15], M. Vreeswijk[115], N.K. Vu[62d,62c], R. Vuillermet[36], O. Vujinovic[101], I. Vukotic[39], S. Wada[158], C. Wagner[104], J.M. Wagner[17a], W. Wagner[172], S. Wahdan[172], H. Wahlberg[91], M. Wakida[112], J. Walder[135], R. Walker[110], W. Walkowiak[143], A. Wall[129], E.J. Wallin[99], T. Wamorkar[6], A.Z. Wang[137], C. Wang[101], C. Wang[11], H. Wang[17a], J. Wang[64c], R. Wang[61],

R. Wang[6], S.M. Wang[150], S. Wang[62b], S. Wang[14a], T. Wang[62a], W.T. Wang[80], W. Wang[14a], X. Wang[14c], X. Wang[163], X. Wang[62c], Y. Wang[62d], Y. Wang[14c], Z. Wang[107], Z. Wang[62d,51,62c], Z. Wang[107], A. Warburton[105], R.J. Ward[20], N. Warrack[59], S. Waterhouse[96], A.T. Watson[20], H. Watson[59], M.F. Watson[20], E. Watton[59,135], G. Watts[140], B.M. Waugh[97], J.M. Webb[54], C. Weber[29], H.A. Weber[18], M.S. Weber[19], S.M. Weber[63a], C. Wei[62a], Y. Wei[54], A.R. Weidberg[127], E.J. Weik[118], J. Weingarten[49], C. Weiser[54], C.J. Wells[48], T. Wenaus[29], B. Wendland[49], T. Wengler[36], N.S. Wenke[111], N. Wermes[24], M. Wessels[63a], A.M. Wharton[92], A.S. White[61], A. White[8], M.J. White[1], D. Whiteson[160], L. Wickremasinghe[125], W. Wiedenmann[171], M. Wielers[135], C. Wiglesworth[42], D.J. Wilbern[121], H.G. Wilkens[36], J.J.H. Wilkinson[32], D.M. Williams[41], H.H. Williams[129], S. Williams[32], S. Willocq[104], B.J. Wilson[102], P.J. Windischhofer[39], F.I. Winkel[30], F. Winklmeier[124], B.T. Winter[54], J.K. Winter[102], M. Wittgen[145], M. Wobisch[98], T. Wojtkowski[60], Z. Wolffs[115], J. Wollrath[160], M.W. Wolter[87], H. Wolters[131a,131c], M.C. Wong[137], E.L. Woodward[41], S.D. Worm[48], B.K. Wosiek[87], K.W. Woźniak[87], S. Wozniewski[55], K. Wraight[59], C. Wu[20], M. Wu[14d], M. Wu[114], S.L. Wu[171], X. Wu[56], Y. Wu[62a], Z. Wu[4], J. Wuerzinger[111,ac], T.R. Wyatt[102], B.M. Wynne[52], S. Xella[42], L. Xia[14c], M. Xia[14b], J. Xiang[64c], M. Xie[62a], S. Xin[14a,14e], A. Xiong[124], J. Xiong[17a], D. Xu[14a], H. Xu[62a], L. Xu[62a], R. Xu[129], T. Xu[107], Y. Xu[14b], Z. Xu[52], Z. Xu[14c], B. Yabsley[149], S. Yacoob[33a], Y. Yamaguchi[139], E. Yamashita[155], H. Yamauchi[158], T. Yamazaki[17a], Y. Yamazaki[85], J. Yan[62c], S. Yan[59], Z. Yan[104], H.J. Yang[62c,62d], H.T. Yang[62a], S. Yang[62a], T. Yang[64c], X. Yang[36], X. Yang[14a], Y. Yang[44], Y. Yang[62a], Z. Yang[62a], W-M. Yao[17a], H. Ye[14c], H. Ye[55], J. Ye[14a], S. Ye[29], X. Ye[62a], Y. Yeh[97], I. Yeletskikh[38], B. Yeo[17b], M.R. Yexley[97], T.P. Yildirim[127], P. Yin[41], K. Yorita[169], S. Younas[27b], C.J.S. Young[36], C. Young[145], C. Yu[14a,14e], Y. Yu[62a], M. Yuan[107], R. Yuan[62d,62c], L. Yue[97], M. Zaazoua[62a], B. Zabinski[87], E. Zaid[52], Z.K. Zak[87], T. Zakareishvili[164], N. Zakharchuk[34], S. Zambito[56], J.A. Zamora Saa[138d,138b], J. Zang[155], D. Zanzi[54], O. Zaplatilek[133], C. Zeitnitz[172], H. Zeng[14a], J.C. Zeng[163], D.T. Zenger Jr[26], O. Zenin[37], T. Ženiš[28a], S. Zenz[95], S. Zerradi[35a], D. Zerwas[66], M. Zhai[14a,14e], D.F. Zhang[141], J. Zhang[62b], J. Zhang[6], K. Zhang[14a,14e], L. Zhang[62a], L. Zhang[14c], P. Zhang[14a,14e], R. Zhang[171], S. Zhang[107], S. Zhang[90], T. Zhang[155], X. Zhang[62c], X. Zhang[62b], Y. Zhang[62c], Y. Zhang[97], Y. Zhang[14c], Z. Zhang[17a], Z. Zhang[66], H. Zhao[140], T. Zhao[62b], Y. Zhao[137], Z. Zhao[62a], Z. Zhao[62a], A. Zhemchugov[38], J. Zheng[14c], K. Zheng[163], X. Zheng[62a], Z. Zheng[145], D. Zhong[163], B. Zhou[107], H. Zhou[7], N. Zhou[62c], Y. Zhou[14b], Y. Zhou[14c], Y. Zhou[7], C.G. Zhu[62b], J. Zhu[107], X. Zhu[62d], Y. Zhu[62c], Y. Zhu[62a], X. Zhuang[14a], K. Zhukov[37], N.I. Zimine[38], J. Zinsser[63b], M. Ziolkowski[143], L. Živković[15], A. Zoccoli[23b,23a], K. Zoch[61], T.G. Zorbas[141], O. Zormpa[46], W. Zou[41], L. Zwalinski[36].

[1]Department of Physics, University of Adelaide, Adelaide; Australia.
[2]Department of Physics, University of Alberta, Edmonton AB; Canada.
[3(a)]Department of Physics, Ankara University, Ankara; [(b)]Division of Physics, TOBB University of Economics and Technology, Ankara; Türkiye.
[4]LAPP, Université Savoie Mont Blanc, CNRS/IN2P3, Annecy; France.
[5]APC, Université Paris Cité, CNRS/IN2P3, Paris; France.
[6]High Energy Physics Division, Argonne National Laboratory, Argonne IL; United States of America.
[7]Department of Physics, University of Arizona, Tucson AZ; United States of America.
[8]Department of Physics, University of Texas at Arlington, Arlington TX; United States of America.
[9]Physics Department, National and Kapodistrian University of Athens, Athens; Greece.
[10]Physics Department, National Technical University of Athens, Zografou; Greece.
[11]Department of Physics, University of Texas at Austin, Austin TX; United States of America.
[12]Institute of Physics, Azerbaijan Academy of Sciences, Baku; Azerbaijan.
[13]Institut de Física d'Altes Energies (IFAE), Barcelona Institute of Science and Technology, Barcelona; Spain.
[14(a)]Institute of High Energy Physics, Chinese Academy of Sciences, Beijing; [(b)]Physics Department, Tsinghua University, Beijing; [(c)]Department of Physics, Nanjing University, Nanjing; [(d)]School of Science, Shenzhen Campus of Sun Yat-sen University; [(e)]University of Chinese Academy of Science (UCAS), Beijing; China.
[15]Institute of Physics, University of Belgrade, Belgrade; Serbia.
[16]Department for Physics and Technology, University of Bergen, Bergen; Norway.
[17(a)]Physics Division, Lawrence Berkeley National Laboratory, Berkeley CA; [(b)]University of California, Berkeley CA; United States of America.

[18]Institut für Physik, Humboldt Universität zu Berlin, Berlin; Germany.
[19]Albert Einstein Center for Fundamental Physics and Laboratory for High Energy Physics, University of Bern, Bern; Switzerland.
[20]School of Physics and Astronomy, University of Birmingham, Birmingham; United Kingdom.
[21(a)]Department of Physics, Bogazici University, Istanbul; [(b)]Department of Physics Engineering, Gaziantep University, Gaziantep; [(c)]Department of Physics, Istanbul University, Istanbul; Türkiye.
[22(a)]Facultad de Ciencias *y* Centro de Investigaciónes, Universidad Antonio Nariño, Bogotá; [(b)]Departamento de Física, Universidad Nacional de Colombia, Bogotá; Colombia.
[23(a)]Dipartimento di Fisica e Astronomia A. Righi, Università di Bologna, Bologna; [(b)]INFN Sezione di Bologna; Italy.
[24]Physikalisches Institut, Universität Bonn, Bonn; Germany.
[25]Department of Physics, Boston University, Boston MA; United States of America.
[26]Department of Physics, Brandeis University, Waltham MA; United States of America.
[27(a)]Transilvania University of Brasov, Brasov; [(b)]Horia Hulubei National Institute of Physics and Nuclear Engineering, Bucharest; [(c)]Department of Physics, Alexandru Ioan Cuza University of Iasi, Iasi; [(d)]National Institute for Research and Development of Isotopic and Molecular Technologies, Physics Department, Cluj-Napoca; [(e)]National University of Science and Technology Politechnica, Bucharest; [(f)]West University in Timisoara, Timisoara; [(g)]Faculty of Physics, University of Bucharest, Bucharest; Romania.
[28(a)]Faculty of Mathematics, Physics and Informatics, Comenius University, Bratislava; [(b)]Department of Subnuclear Physics, Institute of Experimental Physics of the Slovak Academy of Sciences, Kosice; Slovak Republic.
[29]Physics Department, Brookhaven National Laboratory, Upton NY; United States of America.
[30]Universidad de Buenos Aires, Facultad de Ciencias Exactas *y* Naturales, Departamento de Física, *y* CONICET, Instituto de Física de Buenos Aires (IFIBA), Buenos Aires; Argentina.
[31]California State University, CA; United States of America.
[32]Cavendish Laboratory, University of Cambridge, Cambridge; United Kingdom.
[33(a)]Department of Physics, University of Cape Town, Cape Town; [(b)]iThemba Labs, Western Cape; [(c)]Department of Mechanical Engineering Science, University of Johannesburg, Johannesburg; [(d)]National Institute of Physics, University of the Philippines Diliman (Philippines); [(e)]University of South Africa, Department of Physics, Pretoria; [(f)]University of Zululand, KwaDlangezwa; [(g)]School of Physics, University of the Witwatersrand, Johannesburg; South Africa.
[34]Department of Physics, Carleton University, Ottawa ON; Canada.
[35(a)]Faculté des Sciences Ain Chock, Université Hassan II de Casablanca; [(b)]Faculté des Sciences, Université Ibn-Tofail, Kénitra; [(c)]Faculté des Sciences Semlalia, Université Cadi Ayyad, LPHEA-Marrakech; [(d)]LPMR, Faculté des Sciences, Université Mohamed Premier, Oujda; [(e)]Faculté des sciences, Université Mohammed V, Rabat; [(f)]Institute of Applied Physics, Mohammed VI Polytechnic University, Ben Guerir; Morocco.
[36]CERN, Geneva; Switzerland.
[37]Affiliated with an institute covered by a cooperation agreement with CERN.
[38]Affiliated with an international laboratory covered by a cooperation agreement with CERN.
[39]Enrico Fermi Institute, University of Chicago, Chicago IL; United States of America.
[40]LPC, Université Clermont Auvergne, CNRS/IN2P3, Clermont-Ferrand; France.
[41]Nevis Laboratory, Columbia University, Irvington NY; United States of America.
[42]Niels Bohr Institute, University of Copenhagen, Copenhagen; Denmark.
[43(a)]Dipartimento di Fisica, Università della Calabria, Rende; [(b)]INFN Gruppo Collegato di Cosenza, Laboratori Nazionali di Frascati; Italy.
[44]Physics Department, Southern Methodist University, Dallas TX; United States of America.
[45]Physics Department, University of Texas at Dallas, Richardson TX; United States of America.
[46]National Centre for Scientific Research "Demokritos", Agia Paraskevi; Greece.
[47(a)]Department of Physics, Stockholm University; [(b)]Oskar Klein Centre, Stockholm; Sweden.
[48]Deutsches Elektronen-Synchrotron DESY, Hamburg and Zeuthen; Germany.
[49]Fakultät Physik, Technische Universität Dortmund, Dortmund; Germany.
[50]Institut für Kern- und Teilchenphysik, Technische Universität Dresden, Dresden; Germany.
[51]Department of Physics, Duke University, Durham NC; United States of America.
[52]SUPA - School of Physics and Astronomy, University of Edinburgh, Edinburgh; United Kingdom.
[53]INFN e Laboratori Nazionali di Frascati, Frascati; Italy.
[54]Physikalisches Institut, Albert-Ludwigs-Universität Freiburg, Freiburg; Germany.
[55]II. Physikalisches Institut, Georg-August-Universität Göttingen, Göttingen; Germany.
[56]Département de Physique Nucléaire et Corpusculaire, Université de Genève, Genève; Switzerland.
[57(a)]Dipartimento di Fisica, Università di Genova, Genova; [(b)]INFN Sezione di Genova; Italy.
[58]II. Physikalisches Institut, Justus-Liebig-Universität Giessen, Giessen; Germany.
[59]SUPA - School of Physics and Astronomy, University of Glasgow, Glasgow; United Kingdom.
[60]LPSC, Université Grenoble Alpes, CNRS/IN2P3, Grenoble INP, Grenoble; France.
[61]Laboratory for Particle Physics and Cosmology, Harvard University, Cambridge MA; United States of America.
[62(a)]Department of Modern Physics and State Key Laboratory of Particle Detection and Electronics, University of Science and Technology of China, Hefei; [(b)]Institute of Frontier and Interdisciplinary Science and Key Laboratory of Particle Physics

and Particle Irradiation (MOE), Shandong University, Qingdao; [c]School of Physics and Astronomy, Shanghai Jiao Tong University, Key Laboratory for Particle Astrophysics and Cosmology (MOE), SKLPPC, Shanghai; [d]Tsung-Dao Lee Institute, Shanghai; [e]School of Physics, Zhengzhou University; China.
63[a]Kirchhoff-Institut für Physik, Ruprecht-Karls-Universität Heidelberg, Heidelberg; [b]Physikalisches Institut, Ruprecht-Karls-Universität Heidelberg, Heidelberg; Germany.
64[a]Department of Physics, Chinese University of Hong Kong, Shatin, N.T., Hong Kong; [b]Department of Physics, University of Hong Kong, Hong Kong; [c]Department of Physics and Institute for Advanced Study, Hong Kong University of Science and Technology, Clear Water Bay, Kowloon, Hong Kong; China.
65Department of Physics, National Tsing Hua University, Hsinchu; Taiwan.
66IJCLab, Université Paris-Saclay, CNRS/IN2P3, 91405, Orsay; France.
67Centro Nacional de Microelectrónica (IMB-CNM-CSIC), Barcelona; Spain.
68Department of Physics, Indiana University, Bloomington IN; United States of America.
69[a]INFN Gruppo Collegato di Udine, Sezione di Trieste, Udine; [b]ICTP, Trieste; [c]Dipartimento Politecnico di Ingegneria e Architettura, Università di Udine, Udine; Italy.
70[a]INFN Sezione di Lecce; [b]Dipartimento di Matematica e Fisica, Università del Salento, Lecce; Italy.
71[a]INFN Sezione di Milano; [b]Dipartimento di Fisica, Università di Milano, Milano; Italy.
72[a]INFN Sezione di Napoli; [b]Dipartimento di Fisica, Università di Napoli, Napoli; Italy.
73[a]INFN Sezione di Pavia; [b]Dipartimento di Fisica, Università di Pavia, Pavia; Italy.
74[a]INFN Sezione di Pisa; [b]Dipartimento di Fisica E. Fermi, Università di Pisa, Pisa; Italy.
75[a]INFN Sezione di Roma; [b]Dipartimento di Fisica, Sapienza Università di Roma, Roma; Italy.
76[a]INFN Sezione di Roma Tor Vergata; [b]Dipartimento di Fisica, Università di Roma Tor Vergata, Roma; Italy.
77[a]INFN Sezione di Roma Tre; [b]Dipartimento di Matematica e Fisica, Università Roma Tre, Roma; Italy.
78[a]INFN-TIFPA; [b]Università degli Studi di Trento, Trento; Italy.
79Universität Innsbruck, Department of Astro and Particle Physics, Innsbruck; Austria.
80University of Iowa, Iowa City IA; United States of America.
81Department of Physics and Astronomy, Iowa State University, Ames IA; United States of America.
82Istinye University, Sariyer, Istanbul; Türkiye.
83[a]Departamento de Engenharia Elétrica, Universidade Federal de Juiz de Fora (UFJF), Juiz de Fora; [b]Universidade Federal do Rio De Janeiro COPPE/EE/IF, Rio de Janeiro; [c]Instituto de Física, Universidade de São Paulo, São Paulo; [d]Rio de Janeiro State University, Rio de Janeiro; [e]Federal University of Bahia, Bahia; Brazil.
84KEK, High Energy Accelerator Research Organisation, Tsukuba; Japan.
85Graduate School of Science, Kobe University, Kobe; Japan.
86[a]AGH University of Krakow, Faculty of Physics and Applied Computer Science, Krakow; [b]Marian Smoluchowski Institute of Physics, Jagiellonian University, Krakow; Poland.
87Institute of Nuclear Physics Polish Academy of Sciences, Krakow; Poland.
88Faculty of Science, Kyoto University, Kyoto; Japan.
89Research Center for Advanced Particle Physics and Department of Physics, Kyushu University, Fukuoka ; Japan.
90L2IT, Université de Toulouse, CNRS/IN2P3, UPS, Toulouse; France.
91Instituto de Física La Plata, Universidad Nacional de La Plata and CONICET, La Plata; Argentina.
92Physics Department, Lancaster University, Lancaster; United Kingdom.
93Oliver Lodge Laboratory, University of Liverpool, Liverpool; United Kingdom.
94Department of Experimental Particle Physics, Jožef Stefan Institute and Department of Physics, University of Ljubljana, Ljubljana; Slovenia.
95School of Physics and Astronomy, Queen Mary University of London, London; United Kingdom.
96Department of Physics, Royal Holloway University of London, Egham; United Kingdom.
97Department of Physics and Astronomy, University College London, London; United Kingdom.
98Louisiana Tech University, Ruston LA; United States of America.
99Fysiska institutionen, Lunds universitet, Lund; Sweden.
100Departamento de Física Teorica C-15 and CIAFF, Universidad Autónoma de Madrid, Madrid; Spain.
101Institut für Physik, Universität Mainz, Mainz; Germany.
102School of Physics and Astronomy, University of Manchester, Manchester; United Kingdom.
103CPPM, Aix-Marseille Université, CNRS/IN2P3, Marseille; France.
104Department of Physics, University of Massachusetts, Amherst MA; United States of America.
105Department of Physics, McGill University, Montreal QC; Canada.
106School of Physics, University of Melbourne, Victoria; Australia.
107Department of Physics, University of Michigan, Ann Arbor MI; United States of America.
108Department of Physics and Astronomy, Michigan State University, East Lansing MI; United States of America.
109Group of Particle Physics, University of Montreal, Montreal QC; Canada.
110Fakultät für Physik, Ludwig-Maximilians-Universität München, München; Germany.
111Max–Planck-Institut für Physik (Werner-Heisenberg-Institut), München; Germany.
112Graduate School of Science and Kobayashi-Maskawa Institute, Nagoya University, Nagoya; Japan.

[113]Department of Physics and Astronomy, University of New Mexico, Albuquerque NM; United States of America.
[114]Institute for Mathematics, Astrophysics and Particle Physics, Radboud University/Nikhef, Nijmegen; Netherlands.
[115]Nikhef National Institute for Subatomic Physics and University of Amsterdam, Amsterdam; Netherlands.
[116]Department of Physics, Northern Illinois University, DeKalb IL; United States of America.
[117(a)]New York University Abu Dhabi, Abu Dhabi; [(b)]United Arab Emirates University, Al Ain; United Arab Emirates.
[118]Department of Physics, New York University, New York NY; United States of America.
[119]Ochanomizu University, Otsuka, Bunkyo-ku, Tokyo; Japan.
[120]Ohio State University, Columbus OH; United States of America.
[121]Homer L. Dodge Department of Physics and Astronomy, University of Oklahoma, Norman OK; United States of America.
[122]Department of Physics, Oklahoma State University, Stillwater OK; United States of America.
[123]Palacký University, Joint Laboratory of Optics, Olomouc; Czech Republic.
[124]Institute for Fundamental Science, University of Oregon, Eugene, OR; United States of America.
[125]Graduate School of Science, Osaka University, Osaka; Japan.
[126]Department of Physics, University of Oslo, Oslo; Norway.
[127]Department of Physics, Oxford University, Oxford; United Kingdom.
[128]LPNHE, Sorbonne Université, Université Paris Cité, CNRS/IN2P3, Paris; France.
[129]Department of Physics, University of Pennsylvania, Philadelphia PA; United States of America.
[130]Department of Physics and Astronomy, University of Pittsburgh, Pittsburgh PA; United States of America.
[131(a)]Laboratório de Instrumentação e Física Experimental de Partículas - LIP, Lisboa; [(b)]Departamento de Física, Faculdade de Ciências, Universidade de Lisboa, Lisboa; [(c)]Departamento de Física, Universidade de Coimbra, Coimbra; [(d)]Centro de Física Nuclear da Universidade de Lisboa, Lisboa; [(e)]Departamento de Física, Universidade do Minho, Braga; [(f)]Departamento de Física Teórica *y* del Cosmos, Universidad de Granada, Granada (Spain); [(g)]Departamento de Física, Instituto Superior Técnico, Universidade de Lisboa, Lisboa; Portugal.
[132]Institute of Physics of the Czech Academy of Sciences, Prague; Czech Republic.
[133]Czech Technical University in Prague, Prague; Czech Republic.
[134]Charles University, Faculty of Mathematics and Physics, Prague; Czech Republic.
[135]Particle Physics Department, Rutherford Appleton Laboratory, Didcot; United Kingdom.
[136]IRFU, CEA, Université Paris-Saclay, Gif-sur-Yvette; France.
[137]Santa Cruz Institute for Particle Physics, University of California Santa Cruz, Santa Cruz CA; United States of America.
[138(a)]Departamento de Física, Pontificia Universidad Católica de Chile, Santiago; [(b)]Millennium Institute for Subatomic physics at high energy frontier (SAPHIR), Santiago; [(c)]Instituto de Investigación Multidisciplinario en Ciencia *y* Tecnología, *y* Departamento de Física, Universidad de La Serena; [(d)]Universidad Andres Bello, Department of Physics, Santiago; [(e)]Instituto de Alta Investigación, Universidad de Tarapacá, Arica; [(f)]Departamento de Física, Universidad Técnica Federico Santa María, Valparaíso; Chile.
[139]Department of Physics, Institute of Science, Tokyo; Japan.
[140]Department of Physics, University of Washington, Seattle WA; United States of America.
[141]Department of Physics and Astronomy, University of Sheffield, Sheffield; United Kingdom.
[142]Department of Physics, Shinshu University, Nagano; Japan.
[143]Department Physik, Universität Siegen, Siegen; Germany.
[144]Department of Physics, Simon Fraser University, Burnaby BC; Canada.
[145]SLAC National Accelerator Laboratory, Stanford CA; United States of America.
[146]Department of Physics, Royal Institute of Technology, Stockholm; Sweden.
[147]Departments of Physics and Astronomy, Stony Brook University, Stony Brook NY; United States of America.
[148]Department of Physics and Astronomy, University of Sussex, Brighton; United Kingdom.
[149]School of Physics, University of Sydney, Sydney; Australia.
[150]Institute of Physics, Academia Sinica, Taipei; Taiwan.
[151(a)]E. Andronikashvili Institute of Physics, Iv. Javakhishvili Tbilisi State University, Tbilisi; [(b)]High Energy Physics Institute, Tbilisi State University, Tbilisi; [(c)]University of Georgia, Tbilisi; Georgia.
[152]Department of Physics, Technion, Israel Institute of Technology, Haifa; Israel.
[153]Raymond and Beverly Sackler School of Physics and Astronomy, Tel Aviv University, Tel Aviv; Israel.
[154]Department of Physics, Aristotle University of Thessaloniki, Thessaloniki; Greece.
[155]International Center for Elementary Particle Physics and Department of Physics, University of Tokyo, Tokyo; Japan.
[156]Department of Physics, University of Toronto, Toronto ON; Canada.
[157(a)]TRIUMF, Vancouver BC; [(b)]Department of Physics and Astronomy, York University, Toronto ON; Canada.
[158]Division of Physics and Tomonaga Center for the History of the Universe, Faculty of Pure and Applied Sciences, University of Tsukuba, Tsukuba; Japan.
[159]Department of Physics and Astronomy, Tufts University, Medford MA; United States of America.
[160]Department of Physics and Astronomy, University of California Irvine, Irvine CA; United States of America.
[161]University of Sharjah, Sharjah; United Arab Emirates.
[162]Department of Physics and Astronomy, University of Uppsala, Uppsala; Sweden.
[163]Department of Physics, University of Illinois, Urbana IL; United States of America.

[164]Instituto de Física Corpuscular (IFIC), Centro Mixto Universidad de Valencia - CSIC, Valencia; Spain.
[165]Department of Physics, University of British Columbia, Vancouver BC; Canada.
[166]Department of Physics and Astronomy, University of Victoria, Victoria BC; Canada.
[167]Fakultät für Physik und Astronomie, Julius-Maximilians-Universität Würzburg, Würzburg; Germany.
[168]Department of Physics, University of Warwick, Coventry; United Kingdom.
[169]Waseda University, Tokyo; Japan.
[170]Department of Particle Physics and Astrophysics, Weizmann Institute of Science, Rehovot; Israel.
[171]Department of Physics, University of Wisconsin, Madison WI; United States of America.
[172]Fakultät für Mathematik und Naturwissenschaften, Fachgruppe Physik, Bergische Universität Wuppertal, Wuppertal; Germany.
[173]Department of Physics, Yale University, New Haven CT; United States of America.
[a] Also Affiliated with an institute covered by a cooperation agreement with CERN.
[b] Also at An-Najah National University, Nablus; Palestine.
[c] Also at Borough of Manhattan Community College, City University of New York, New York NY; United States of America.
[d] Also at Center for Interdisciplinary Research and Innovation (CIRI-AUTH), Thessaloniki; Greece.
[e] Also at Centro Studi e Ricerche Enrico Fermi; Italy.
[f] Also at CERN, Geneva; Switzerland.
[g] Also at Département de Physique Nucléaire et Corpusculaire, Université de Genève, Genève; Switzerland.
[h] Also at Departament de Fisica de la Universitat Autonoma de Barcelona, Barcelona; Spain.
[i] Also at Department of Financial and Management Engineering, University of the Aegean, Chios; Greece.
[j] Also at Department of Physics, California State University, Sacramento; United States of America.
[k] Also at Department of Physics, King's College London, London; United Kingdom.
[l] Also at Department of Physics, Stanford University, Stanford CA; United States of America.
[m] Also at Department of Physics, Stellenbosch University; South Africa.
[n] Also at Department of Physics, University of Fribourg, Fribourg; Switzerland.
[o] Also at Department of Physics, University of Thessaly; Greece.
[p] Also at Department of Physics, Westmont College, Santa Barbara; United States of America.
[q] Also at Faculty of Physics, Sofia University, 'St. Kliment Ohridski', Sofia; Bulgaria.
[r] Also at Hellenic Open University, Patras; Greece.
[s] Also at Institucio Catalana de Recerca i Estudis Avancats, ICREA, Barcelona; Spain.
[t] Also at Institut für Experimentalphysik, Universität Hamburg, Hamburg; Germany.
[u] Also at Institute for Nuclear Research and Nuclear Energy (INRNE) of the Bulgarian Academy of Sciences, Sofia; Bulgaria.
[v] Also at Institute of Applied Physics, Mohammed VI Polytechnic University, Ben Guerir; Morocco.
[w] Also at Institute of Particle Physics (IPP); Canada.
[x] Also at Institute of Physics and Technology, Mongolian Academy of Sciences, Ulaanbaatar; Mongolia.
[y] Also at Institute of Physics, Azerbaijan Academy of Sciences, Baku; Azerbaijan.
[z] Also at Institute of Theoretical Physics, Ilia State University, Tbilisi; Georgia.
[aa] Also at Lawrence Livermore National Laboratory, Livermore; United States of America.
[ab] Also at National Institute of Physics, University of the Philippines Diliman (Philippines); Philippines.
[ac] Also at Technical University of Munich, Munich; Germany.
[ad] Also at The Collaborative Innovation Center of Quantum Matter (CICQM), Beijing; China.
[ae] Also at TRIUMF, Vancouver BC; Canada.
[af] Also at Università di Napoli Parthenope, Napoli; Italy.
[ag] Also at University of Colorado Boulder, Department of Physics, Colorado; United States of America.
[ah] Also at Washington College, Chestertown, MD; United States of America.
[ai] Also at Yeditepe University, Physics Department, Istanbul; Türkiye.
* Deceased

References

[1] ATLAS Collaboration, Observation of a new particle in the search for the standard model Higgs boson with the ATLAS detector at the LHC, Phys. Lett. B 716 (2012) 1, arXiv:1207.7214 [hep-ex].
[2] CMS Collaboration, Observation of a new boson at a mass of 125 GeV with the CMS experiment at the LHC, Phys. Lett. B 716 (2012) 30, arXiv:1207.7235 [hep-ex].
[3] ATLAS Collaboration, The ATLAS experiment at the CERN large hadron collider, JINST 3 (2008) S08003.
[4] CMS Collaboration, The CMS experiment at the CERN LHC, JINST 3 (2008) S08004.
[5] ATLAS Collaboration, Luminosity determination in pp collisions at $\sqrt{s} = 13$ TeV using the ATLAS detector at the LHC, Eur. Phys. J. C 83 (2023) 982, arXiv:2212.09379 [hep-ex].
[6] ATLAS Collaboration, ATLAS searches for additional scalars and exotic Higgs boson decays with the LHC run 2 dataset, 2024, CERN-EP-2024-94.
[7] S. Weinberg, A model of leptons, Phys. Rev. Lett. 19 (1967) 1264–1266.
[8] S.L. Glashow, Partial symmetries of weak interactions, Nuclear Phys. 22 (1961) 579–588.
[9] A. Salam, Weak and electromagnetic interactions, Conf. Proc. C 680519 (1968) 367–377.
[10] G. 't Hooft, M. Veltman, Regularization and renormalization of gauge fields, Nuclear Phys. B 44 (1972) 189–213.
[11] P.W. Higgs, Broken symmetries, massless particles and gauge fields, Phys. Lett. 12 (1964) 132–133.

[12] P.W. Higgs, Broken symmetries and the masses of gauge bosons, in: J.C. Taylor (Ed.), Phys. Rev. Lett. 13 (1964) 508–509.
[13] F. Englert, R. Brout, Broken symmetry and the mass of gauge vector mesons, in: J.C. Taylor (Ed.), Phys. Rev. Lett. 13 (1964) 321–323.
[14] G.S. Guralnik, C.R. Hagen, T.W.B. Kibble, Global conservation laws and massless particles, in: J.C. Taylor (Ed.), Phys. Rev. Lett. 13 (1964) 585–587.
[15] T.W.B. Kibble, Symmetry breaking in nonabelian gauge theories, in: J.C. Taylor (Ed.), Phys. Rev. 155 (1967) 1554–1561.
[16] G. Degrassi, et al., Higgs mass and vacuum stability in the standard model at NNLO, JHEP 08 (2012) 098, arXiv:1205.6497 [hep-ph].
[17] M. Reichert, et al., Probing baryogenesis through the Higgs boson self-coupling, Phys. Rev. D 97 (7) (2018) 075008, arXiv:1711.00019 [hep-ph].
[18] D. de Florian, et al., Handbook of LHC Higgs cross sections: 4. Deciphering the nature of the Higgs sector, 2017, http://dx.doi.org/10.23731/CYRM-2017-002, arXiv:1610.07922 [hep-ph].
[19] ATLAS Collaboration, A detailed map of Higgs boson interactions by the ATLAS experiment ten years after the discovery, Nature 607 (7917) (2022) 52–59, arXiv:2207.00092 [hep-ex].
[20] ATLAS and CMS Collaborations, Combined measurement of the Higgs boson mass in pp collisions at $\sqrt{s} = 7$ and 8 TeV with the ATLAS and CMS experiments, Phys. Rev. Lett. 114 (2015) 191803, arXiv:1503.07589 [hep-ex].
[21] C. Anastasiou, et al., High precision determination of the gluon fusion Higgs boson cross-section at the LHC, JHEP 05 (2016) 058, arXiv:1602.00695 [hep-ph].
[22] C. Anastasiou, C. Duhr, F. Dulat, F. Herzog, B. Mistlberger, Higgs boson gluon-fusion production in QCD at three loops, Phys. Rev. Lett. 114 (2015) 212001, arXiv:1503.06056 [hep-ph].
[23] F. Dulat, A. Lazopoulos, B. Mistlberger, Ihixs 2 – inclusive Higgs cross sections, Comput. Phys. Comm. 233 (2018) 243–260, arXiv:1802.00827 [hep-ph].
[24] R.V. Harlander, K.J. Ozeren, Finite top mass effects for hadronic Higgs production at next-to-next-to-leading order, JHEP 11 (2009) 088, arXiv:0909.3420 [hep-ph].
[25] R.V. Harlander, K.J. Ozeren, Top mass effects in Higgs production at next-to-next-to-leading order QCD: Virtual corrections, Phys. Lett. B 679 (2009) 467–472, arXiv:0907.2997 [hep-ph].
[26] R.V. Harlander, H. Mantler, S. Marzani, K.J. Ozeren, Higgs production in gluon fusion at next-to-next-to-leading order QCD for finite top mass, Eur. Phys. J. C 66 (2010) 359–372, arXiv:0912.2104 [hep-ph].
[27] A. Pak, M. Rogal, M. Steinhauser, Finite top quark mass effects in NNLO Higgs boson production at LHC, JHEP 02 (2010) 025, arXiv:0911.4662 [hep-ph].
[28] S. Actis, G. Passarino, C. Sturm, S. Uccirati, NLO electroweak corrections to Higgs boson production at hadron colliders, Phys. Lett. B 670 (2008) 12–17, arXiv:0809.1301 [hep-ph].
[29] S. Actis, G. Passarino, C. Sturm, S. Uccirati, NNLO computational techniques: The cases $H \to \gamma\gamma$ and $H \to gg$, Nuclear Phys. B 811 (2009) 182–273, arXiv:0809.3667 [hep-ph].
[30] M. Bonetti, K. Melnikov, L. Tancredi, Higher order corrections to mixed QCD-EW contributions to Higgs boson production in gluon fusion, Phys. Rev. D 97 (5) (2018) 056017, arXiv:1801.10403 [hep-ph].
[31] U. Aglietti, R. Bonciani, G. Degrassi, A. Vicini, Two-loop light fermion contribution to Higgs production and decays, Phys. Lett. B 595 (2004) 432–441, arXiv:hep-ph/0404071.
[32] E. Bagnaschi, G. Degrassi, P. Slavich, A. Vicini, Higgs production via gluon fusion in the POWHEG approach in the SM and in the MSSM, JHEP 02 (2012) 088, arXiv:1111.2854 [hep-ph].
[33] K. Hamilton, P. Nason, G. Zanderighi, Finite quark-mass effects in the NNLOPS POWHEG+MiNLO Higgs generator, JHEP 05 (2015) 140, arXiv:1501.04637 [hep-ph].
[34] M. Ciccolini, A. Denner, S. Dittmaier, Strong and electroweak corrections to the production of a Higgs boson + 2 jets via weak interactions at the large hadron collider, Phys. Rev. Lett. 99 (2007) 161803, arXiv:0707.0381 [hep-ph].
[35] M. Ciccolini, A. Denner, S. Dittmaier, Electroweak and QCD corrections to Higgs production via vector-boson fusion at the CERN LHC, Phys. Rev. D 77 (2008) 013002, arXiv:0710.4749 [hep-ph].
[36] P. Bolzoni, F. Maltoni, S.-O. Moch, M. Zaro, Higgs boson production via vector-boson fusion at next-to-next-to-leading order in QCD, Phys. Rev. Lett. 105 (2010) 011801, arXiv:1003.4451 [hep-ph].
[37] O. Brein, R.V. Harlander, T.J.E. Zirke, Vh@nnlo – Higgs strahlung at hadron colliders, Comput. Phys. Comm. 184 (2013) 998–1003, arXiv:1210.5347 [hep-ph].
[38] R.V. Harlander, J. Klappert, S. Liebler, L. Simon, Vh@nnlo-v2: new physics in Higgs strahlung, JHEP 05 (2018) 089, arXiv:1802.04817 [hep-ph].
[39] O. Brein, A. Djouadi, R. Harlander, NNLO QCD corrections to the Higgs-strahlung processes at hadron colliders, Phys. Lett. B 579 (2004) 149–156, arXiv:hep-ph/0307206.
[40] O. Brein, R.V. Harlander, M. Wiesemann, T. Zirke, Top-quark mediated effects in hadronic Higgs-strahlung, Eur. Phys. J. C 72 (2012) 1868, arXiv:1111.0761 [hep-ph].
[41] L. Altenkamp, S. Dittmaier, R.V. Harlander, H. Rzehak, T.J.E. Zirke, Gluon-induced Higgs-strahlung at next-to-leading order QCD, JHEP 02 (2013) 078, arXiv:1211.5015 [hep-ph].
[42] R.V. Harlander, A. Kulesza, V. Theeuwes, T. Zirke, Soft gluon resummation for gluon-induced Higgs strahlung, JHEP 11 (2014) 082, arXiv:1410.0217 [hep-ph].
[43] A. Denner, S. Dittmaier, S. Kallweit, A. Mück, HAWK 2.0: A Monte Carlo program for Higgs production in vector-boson fusion and Higgs strahlung at hadron colliders, Comput. Phys. Comm. 195 (2015) 161–171, arXiv:1412.5390 [hep-ph].
[44] M.L. Ciccolini, S. Dittmaier, M. Krämer, Electroweak radiative corrections to associated WH and ZH production at hadron colliders, Phys. Rev. D 68 (2003) 073003, arXiv:hep-ph/0306234 [hep-ph].
[45] A. Denner, S. Dittmaier, S. Kallweit, A. Mück, Electroweak corrections to Higgs-strahlung off W/Z bosons at the tevatron and the LHC with HAWK, JHEP 03 (2012) 075, arXiv:1112.5142 [hep-ph].
[46] W. Beenakker, et al., NLO QCD corrections to $t\bar{t}H$ production in hadron collisions, Nucl. Phys. B 653 (2003) 151–203, arXiv:hep-ph/0211352.
[47] S. Dawson, C. Jackson, L. Orr, L. Reina, D. Wackeroth, Associated Higgs boson production with top quarks at the CERN large hadron collider: NLO QCD corrections, Phys. Rev. D 68 (2003) 034022, arXiv:hep-ph/0305087.
[48] Y. Zhang, W.-G. Ma, R.-Y. Zhang, C. Chen, L. Guo, QCD nlo and EW NLO corrections to $t\bar{t}H$ production with top quark decays at hadron collider, Phys. Lett. B 738 (2014) 1–5, arXiv:1407.1110 [hep-ph].
[49] S. Frixione, V. Hirschi, D. Pagani, H.-S. Shao, M. Zaro, Electroweak and QCD corrections to top-pair hadroproduction in association with heavy bosons, JHEP 06 (2015) 184, arXiv:1504.03446 [hep-ph].
[50] S. Dawson, C. Jackson, L. Reina, D. Wackeroth, Exclusive Higgs boson production with bottom quarks at hadron colliders, Phys. Rev. D 69 (2004) 074027, arXiv:hep-ph/0311067.
[51] S. Dittmaier, M. Krämer, M. Spira, Higgs radiation off bottom quarks at the Fermilab Tevatron and the CERN LHC, Phys. Rev. D 70 (2004) 074010, arXiv:hep-ph/0309204.
[52] R. Harlander, M. Krämer, M. Schumacher, Bottom-quark associated Higgs-boson production: reconciling the four- and five-flavour scheme approach, 2011, arXiv:1112.3478 [hep-ph].

[53] F. Demartin, F. Maltoni, K. Mawatari, M. Zaro, Higgs production in association with a single top quark at the LHC, Eur. Phys. J. C 75 (2015) 267, arXiv:1504.00611 [hep-ph].
[54] F. Demartin, B. Maier, F. Maltoni, K. Mawatari, M. Zaro, tWH associated production at the LHC, Eur. Phys. J. C 77 (1) (2017) 34, arXiv:1607.05862 [hep-ph].
[55] M. Grazzini, et al., Higgs boson pair production at NNLO with top quark mass effects, JHEP 05 (2018) 059, arXiv:1803.02463 [hep-ph].
[56] G. Heinrich, S.P. Jones, M. Kerner, G. Luisoni, L. Scyboz, Probing the trilinear Higgs boson coupling in di-Higgs production at NLO QCD including parton shower effects, JHEP 06 (2019) 066, arXiv:1903.08137 [hep-ph].
[57] S. Dawson, S. Dittmaier, M. Spira, Neutral Higgs-boson pair production at hadron colliders: QCD corrections, Phys. Rev. D 58 (1998) 115012, arXiv:hep-ph/9805244 [hep-ph].
[58] S. Borowka, et al., Higgs boson pair production in gluon fusion at next-to-leading order with full top-quark mass dependence, Phys. Rev. Lett. 117 (1) (2016) 012001, arXiv:1604.06447 [hep-ph].
[59] J. Baglio, et al., Gluon fusion into Higgs pairs at NLO QCD and the top mass scheme, Eur. Phys. J. C 79 (6) (2019) 459, arXiv:1811.05692 [hep-ph].
[60] R. Bonciani, G. Degrassi, P.P. Giardino, R. Gröber, Analytical method for next-to-leading-order QCD corrections to double-Higgs production, Phys. Rev. Lett. 121 (16) (2018) 162003, arXiv:1806.11564 [hep-ph].
[61] D. de Florian, J. Mazzitelli, Higgs boson pair production at next-to-next-to-leading order in QCD, Phys. Rev. Lett. 111 (2013) 201801, arXiv:1309.6594 [hep-ph].
[62] D.Y. Shao, C.S. Li, H.T. Li, J. Wang, Threshold resummation effects in Higgs boson pair production at the LHC, JHEP 07 (2013) 169, arXiv:1301.1245 [hep-ph].
[63] D. de Florian, J. Mazzitelli, Higgs pair production at next-to-next-to-leading logarithmic accuracy at the LHC, JHEP 09 (2015) 053, arXiv:1505.07122 [hep-ph].
[64] J. Baglio, et al., $gg \to HH$: Combined uncertainties, Phys. Rev. D 103.
[65] F.A. Dreyer, A. Karlberg, Vector-boson fusion Higgs pair production at N^{3}LO, Phys. Rev. D 98 (2018) 114016, arXiv:1811.07906.
[66] J. Baglio, et al., The measurement of the Higgs self-coupling at the LHC: theoretical status, JHEP 04 (4) (2013) 151, arXiv:1212.5581.
[67] L.-S. Ling, et al., NNLO QCD corrections to Higgs pair production via vector boson fusion at hadron colliders, Phys. Rev. D 89.
[68] A. Djouadi, J. Kalinowski, M. Spira, HDECAY: A program for Higgs boson decays in the standard model and its supersymmetric extension, Comput. Phys. Comm. 108 (1998) 56–74, arXiv:hep-ph/9704448.
[69] M. Spira, QCD effects in Higgs physics, Fortschr. Phys. 46 (1998) 203–284, arXiv:hep-ph/9705337.
[70] A. Bredenstein, A. Denner, S. Dittmaier, M.M. Weber, Precise predictions for the Higgs-boson decay $H \to WW/ZZ \to 4$ leptons, Phys. Rev. D 74 (2006) 013004, arXiv:hep-ph/0604011.
[71] A. Bredenstein, A. Denner, S. Dittmaier, M.M. Weber, Radiative corrections to the semileptonic and hadronic Higgs-boson decays H → W W / Z Z → 4 fermions, JHEP 02 (2007) 080, arXiv:hep-ph/0611234.
[72] L. Mihaila, B. Schmidt, M. Steinhauser, $\Gamma(H \to b\bar{b})$ To order $\alpha\alpha_s$, Phys. Lett. B 751 (2015) 442–447, arXiv:1509.02294 [hep-ph].
[73] P. Nason, A new method for combining NLO QCD with shower Monte Carlo algorithms, JHEP 11 (2004) 040, arXiv:hep-ph/0409146.
[74] S. Frixione, P. Nason, C. Oleari, Matching NLO QCD computations with parton shower simulations: the POWHEG method, JHEP 11 (2007) 070, arXiv:0709.2092 [hep-ph].
[75] S. Alioli, P. Nason, C. Oleari, E. Re, A general framework for implementing NLO calculations in shower Monte Carlo programs: the POWHEG BOX, JHEP 06 (2010) 043, arXiv:1002.2581 [hep-ph].
[76] K. Hamilton, P. Nason, E. Re, G. Zanderighi, NNLOPS simulation of Higgs boson production, JHEP 10 (2013) 222, arXiv:1309.0017 [hep-ph].
[77] S. Catani, M. Grazzini, Next-to-next-to-leading-order subtraction formalism in hadron collisions and its application to Higgs-boson production at the large hadron collider, Phys. Rev. Lett. 98 (2007) 222002, arXiv:hep-ph/0703012.
[78] P. Nason, C. Oleari, NLO Higgs boson production via vector-boson fusion matched with shower in POWHEG, JHEP 02 (2010) 037, arXiv:0911.5299 [hep-ph].
[79] G. Cullen, et al., Automated one-loop calculations with gosam, Eur. Phys. J. C 72 (2012) 1889, arXiv:1111.2034 [hep-ph].
[80] H.B. Hartanto, B. Jäger, L. Reina, D. Wackeroth, Higgs boson production in association with top quarks in the POWHEG BOX, Phys. Rev. D 91 (9) (2015) 094003, arXiv:1501.04498 [hep-ph].
[81] J. Alwall, et al., The automated computation of tree-level and next-to-leading order differential cross sections, and their matching to parton shower simulations, JHEP 07 (2014) 079, arXiv:1405.0301 [hep-ph].
[82] ATLAS Collaboration, The ATLAS simulation infrastructure, Eur. Phys. J. C 70 (2010) 823, arXiv:1005.4568 [physics.ins-det].
[83] S. Agostinelli, et al., GEANT4 - a simulation toolkit, Nucl. Instrum. Methods A 506 (2003) 250.
[84] R. Barate, et al., Search for the standard model Higgs boson at LEP, Phys. Lett. B 565 (2003) 61–75, arXiv:hep-ex/0306033.
[85] CDF and D0 Collaborations, Higgs boson studies at the tevatron, Phys. Rev. D 88 (5) (2013) 052014, arXiv:1303.6346 [hep-ex].
[86] ALEPH, CDF, D0, DELPHI, L3, OPAL, SLD, LEP Electroweak Working Group, Tevatron Electroweak Working Group, SLD Electroweak, Heavy Flavour Groups, Precision electroweak measurements and constraints on the standard model, 2010, arXiv:1012.2367 [hep-ex].
[87] M. Baak, et al., Updated status of the global electroweak fit and constraints on new physics, Eur. Phys. J. C 72 (2012) 2003, arXiv:1107.0975 [hep-ph].
[88] ATLAS and CMS Collaborations, Measurements of the Higgs boson production and decay rates and constraints on its couplings from a combined ATLAS and CMS analysis of the LHC pp collision data at $\sqrt{s} = 7$ and 8 TeV, JHEP 08 (2016) 045, arXiv:1606.02266 [hep-ex].
[89] ATLAS Collaboration, Measurements of fiducial and differential cross sections for Higgs boson production in the diphoton decay channel at $\sqrt{s} = 8$ TeV with ATLAS, JHEP 09 (2014) 112, arXiv:1407.4222 [hep-ex].
[90] ATLAS Collaboration, Fiducial and differential cross sections of Higgs boson production measured in the four-lepton decay channel in pp collisions at $\sqrt{s} = 8$ TeV with the ATLAS detector, Phys. Lett. B 738 (2014) 234, arXiv:1408.3226 [hep-ex].
[91] ATLAS Collaboration, Measurements of the total and differential Higgs boson production cross sections combining the $H \to \gamma\gamma$ and $H \to ZZ^* \to 4\ell$ decay channels at $\sqrt{s} = 8$ TeV with the ATLAS detector, Phys. Rev. Lett. 115 (2015) 091801, arXiv:1504.05833 [hep-ex].
[92] ATLAS Collaboration, Measurement of fiducial differential cross sections of gluon-fusion production of Higgs bosons decaying to $WW^* \to e\nu\mu\nu$ with the ATLAS detector at $\sqrt{s} = 8$ TeV, JHEP 08 (2016) 104, arXiv:1604.02997 [hep-ex].
[93] L.D. Landau, On the angular momentum of a system of two photons, Dokl. Akad. Nauk SSSR 60 (2) (1948) 207–209.
[94] C.-N. Yang, Selection rules for the dematerialization of a particle into two photons, Phys. Rev. 77 (1950) 242–245.
[95] ATLAS Collaboration, Study of the spin and parity of the Higgs boson in diboson decays with the ATLAS detector, Eur. Phys. J. C 75 (2015) 476, arXiv:1506.05669 [hep-ex].
[96] ATLAS Collaboration, Test of CP invariance in vector-boson fusion production of the Higgs boson using the *optimal observable* method in the ditau decay channel with the ATLAS detector, Eur. Phys. J. C 76 (2016) 658, arXiv:1602.04516 [hep-ex].
[97] ATLAS Collaboration, Constraints on the off-shell Higgs boson signal strength in the high-mass ZZ and WW final states with the ATLAS detector, Eur. Phys. J. C 75 (2015) 335, arXiv:1503.01060 [hep-ex].
[98] N. Kauer, G. Passarino, Inadequacy of zero-width approximation for a light Higgs boson signal, JHEP 08 (2012) 116, arXiv:1206.4803 [hep-ph].

[99] F. Caola, K. Melnikov, Constraining the Higgs boson width with ZZ production at the LHC, Phys. Rev. D 88 (2013) 054024, arXiv:1307.4935 [hep-ph].
[100] J.M. Campbell, R.K. Ellis, C. Williams, Bounding the Higgs width at the LHC using full analytic results for $gg \to e^-e^+\mu^-\mu^+$, JHEP 04 (2014) 060, arXiv:1311.3589 [hep-ph].
[101] J.M. Campbell, R.K. Ellis, C. Williams, Bounding the Higgs width at the LHC: Complementary results from $H \to WW$, Phys. Rev. D 89 (5) (2014) 053011, arXiv:1312.1628 [hep-ph].
[102] Gfitter Group, J. Haller, et al., Update of the global electroweak fit and constraints on two-Higgs-doublet models, Eur. Phys. J. C 78 (8) (2018) 675, arXiv:1803.01853 [hep-ph].
[103] M. Sher, Electroweak Higgs potential and vacuum stability, Phys. Rep. 179 (1989) 273–418.
[104] ATLAS Collaboration, Measurement of the Higgs boson mass with $H \to \gamma\gamma$ decays in 140 fb^{-1} of $\sqrt{s} = 13$ TeV pp collisions with the ATLAS detector, Phys. Lett. B 847 (2023) 138315, arXiv:2308.07216 [hep-ex].
[105] M.J. Oreglia, A Study of the Reactions $\psi' \to \gamma\gamma\psi$, Appendix D (SLAC-0236, Ph.D. thesis), SLAC, 1980, URL www.slac.stanford.edu/cgi-wrap/getdoc/slac-r-236.pdf.
[106] ATLAS Collaboration, Measurement of the Higgs boson mass in the $H \to ZZ^* \to 4\ell$ and $H \to \gamma\gamma$ channels with $\sqrt{s} = 13$ TeV pp collisions using the ATLAS detector, Phys. Lett. B 784 (2018) 345, arXiv:1806.00242 [hep-ex].
[107] ATLAS Collaboration, Electron and photon energy calibration with the ATLAS detector using LHC run 2 data, JINST 19 (02) (2023) P02009, arXiv:2309.05471 [hep-ex].
[108] ATLAS Collaboration, Measurement of the Higgs boson mass in the $H \to ZZ^* \to 4\ell$ decay channel using 139 fb^{-1} of $\sqrt{s}$=13 TeV pp collisions recorded by the ATLAS detector at the LHC, Phys. Lett. B 843 (2023) 137880, arXiv:2207.00320 [hep-ex].
[109] ATLAS Collaboration, Combined measurement of the Higgs boson mass from the $H \to \gamma\gamma$ and $H \to ZZ^* \to 4\ell$ decay channels with the ATLAS detector using $\sqrt{s} = 7, 8,$ and 13 TeV pp collision data, Phys. Rev. Lett. 131 (2023) 251802, arXiv:2308.04775 [hep-ex].
[110] ATLAS Collaboration, Evidence of off-shell Higgs boson production from ZZ leptonic decay channels and constraints on its total width with the ATLAS detector, Phys. Lett. B 846 (2023) 138223, arXiv:2304.01532 [hep-ex].
[111] ATLAS Collaboration, Constraints on the off-shell Higgs boson signal strength in the high-mass ZZ and WW final states with the ATLAS detector, Eur. Phys. J. C 75 (7) (2015) 335, arXiv:1503.01060 [hep-ex].
[112] ATLAS Collaboration, Higgs boson production cross-section measurements and their EFT interpretation in the 4ℓ decay channel at $\sqrt{s} = 13$ TeV with the ATLAS detector, Eur. Phys. J. C 80 (2020) 957, arXiv:2004.03447 [hep-ex].
[113] ATLAS Collaboration, Measurements of the Higgs boson inclusive and differential fiducial cross-sections in the diphoton decay channel with pp collisions at $\sqrt{s} = 13$ TeV with the ATLAS detector, JHEP 08 (2022) 027, arXiv:2202.00487 [hep-ex].
[114] ATLAS Collaboration, Measurements of the Higgs boson inclusive and differential fiducial cross sections in the 4ℓ decay channel at $\sqrt{s} = 13$ TeV, Eur. Phys. J. C 80 (2020) 942, arXiv:2004.03969 [hep-ex].
[115] ATLAS Collaboration, Measurement of the total and differential Higgs boson production cross-sections at $\sqrt{s} = 13$ TeV with the ATLAS detector by combining the $H \to ZZ^* \to 4\ell$ and $H \to \gamma\gamma$ decay channels, JHEP 05 (2023) 028, arXiv:2207.08615 [hep-ex].
[116] ATLAS Collaboration, Direct constraint on the Higgs-charm coupling from a search for Higgs boson decays into charm quarks with the ATLAS detector, Eur. Phys. J. C 82 (2022) 717, arXiv:2201.11428 [hep-ex].
[117] D. Curtin, et al., Exotic decays of the 125 GeV Higgs boson, Phys. Rev. D 90 (7) (2014) 075004, arXiv:1312.4992 [hep-ph].
[118] D. Curtin, R. Essig, S. Gori, J. Shelton, Illuminating dark photons with high-energy colliders, JHEP 02 (2015) 157, arXiv:1412.0018 [hep-ph].
[119] M. González-Alonso, A. Greljo, G. Isidori, D. Marzocca, Pseudo-observables in Higgs decays, Eur. Phys. J. C 75 (2015) 128, arXiv:1412.6038 [hep-ph].
[120] ATLAS Collaboration, Measurements of differential cross sections of Higgs boson production through gluon fusion in the $H \to WW^* \to e\nu\mu\nu$ final state at $\sqrt{s} = 13$ TeV with the ATLAS detector, Eur. Phys. J. C 83 (9) (2023) 774, arXiv:2301.06822 [hep-ex].
[121] ATLAS Collaboration, Integrated and differential fiducial cross-section measurements for the vector boson fusion production of the Higgs boson in the $H \to WW^* \to e\nu\mu\nu$ decay channel at 13 TeV with the ATLAS detector, Phys. Rev. D 108 (2023) 072003, arXiv:2304.03053 [hep-ex].
[122] A. Tikhonov, Solution of incorrectly formulated problems and the regularization method, Sov. Math. Dokl. 5 (1963) 1035/1038, URL https://ci.nii.ac.jp/naid/10004315593/en/.
[123] ATLAS Collaboration, Cross-section measurements of the Higgs boson decaying into a pair of τ-leptons in proton–proton collisions at $\sqrt{s} = 13$ TeV with the ATLAS detector, Phys. Rev. D 99 (2019) 072001, arXiv:1811.08856 [hep-ex].
[124] A. Elagin, P. Murat, A. Pranko, A. Safonov, A new mass reconstruction technique for resonances decaying to $\tau\tau$, Nucl. Instrum. Methods A 654 (2011) 481–489, arXiv:1012.4686 [hep-ex].
[125] ATLAS Collaboration, Measurements of Higgs boson production cross-sections in the $H \to \tau^+\tau^-$ decay channel in pp collisions at $\sqrt{s} = 13$ TeV with the ATLAS detector, JHEP 08 (2022) 175, arXiv:2201.08269 [hep-ex].
[126] ATLAS Collaboration, Observation of Higgs boson production in association with a top quark pair at the LHC with the ATLAS detector, Phys. Lett. B 784 (2018) 173, arXiv:1806.00425 [hep-ex].
[127] LHC Higgs Cross Section Working Group, S. Heinemeyer, et al., Handbook of LHC Higgs Cross Sections: 3. Higgs Properties, CERN-2013-004, CERN, Geneva, 2013, arXiv:1307.1347 [hep-ph].
[128] ATLAS Collaboration, Search for the standard model Higgs boson produced in association with top quarks and decaying into a $b\bar{b}$ pair in pp collisions at $\sqrt{s} = 13$ TeV with the ATLAS detector, Phys. Rev. D 97 (2018) 072016, arXiv:1712.08895 [hep-ex].
[129] ATLAS Collaboration, Evidence for the associated production of the Higgs boson and a top quark pair with the ATLAS detector, Phys. Rev. D 97 (2018) 072003, arXiv:1712.08891 [hep-ex].
[130] ATLAS Collaboration, Measurement of Higgs boson decay into b-quarks in associated production with a top-quark pair in pp collisions at $\sqrt{s} = 13$ TeV with the ATLAS detector, JHEP 06 (2022) 097, arXiv:2111.06712 [hep-ex].
[131] ATLAS Collaboration, Measurement of the properties of Higgs boson production at $\sqrt{s} = 13$ TeV in the $H \to \gamma\gamma$ channel using 139 fb^{-1} of pp collision data with the ATLAS experiment, JHEP 07 (2023) 088, arXiv:2207.00348 [hep-ex].
[132] ATLAS Collaboration, Observation of $H \to b\bar{b}$ decays and VH production with the ATLAS detector, Phys. Lett. B 786 (2018) 59, arXiv:1808.08238 [hep-ex].
[133] ATLAS Collaboration, Measurements of WH and ZH production in the $H \to b\bar{b}$ decay channel in pp collisions at 13 TeV with the ATLAS detector, Eur. Phys. J. C 81 (2021) 178, arXiv:2007.02873 [hep-ex].
[134] ATLAS Collaboration, Combination of measurements of Higgs boson production in association with a W or Z boson in the $b\bar{b}$ decay channel with the ATLAS experiment at $\sqrt{s} = 13$ TeV, 2021, URL https://cds.cern.ch/record/2782535.
[135] ATLAS Collaboration, Measurement of the associated production of a Higgs boson decaying into b-quarks with a vector boson at high transverse momentum in pp collisions at $\sqrt{s} = 13$ TeV with the ATLAS detector, Phys. Lett. B 816 (2021) 136204, arXiv:2008.02508 [hep-ex].
[136] ATLAS Collaboration, Measurements of Higgs bosons decaying to bottom quarks from vector boson fusion production with the ATLAS experiment at $\sqrt{s} = 13$ TeV, Eur. Phys. J. C 81 (2021) 537, arXiv:2011.08280 [hep-ex].
[137] ATLAS Collaboration, Constraints on Higgs boson production with large transverse momentum using $H \to b\bar{b}$ decays in the ATLAS detector, Phys. Rev. D 105 (2022) 092003, arXiv:2111.08340 [hep-ex].

[138] Fermilab Lattice, MILC, and TUMQCD Collaborations, A. Bazavov, et al., Up-, down-, strange-, charm-, and bottom-quark masses from four-flavor lattice QCD, Phys. Rev. D 98 (5) (2018) 054517, arXiv:1802.04248 [hep-lat].
[139] ATLAS Collaboration, A search for the dimuon decay of the standard model Higgs boson with the ATLAS detector, Phys. Lett. B 812 (2021) 135980, arXiv:2007.07830 [hep-ex].
[140] A. Kachanovich, U. Nierste, I. Nišandžić, Higgs boson decay into a lepton pair and a photon revisited, Phys. Rev. D 101 (7) (2020) 073003, arXiv:2001.06516 [hep-ph].
[141] A.Y. Korchin, V.A. Kovalchuk, Angular distribution and forward–backward asymmetry of the Higgs-boson decay to photon and lepton pair, Eur. Phys. J. C 74 (11) (2014) 3141, arXiv:1408.0342 [hep-ph].
[142] Y. Chen, A. Falkowski, I. Low, R. Vega-Morales, New observables for CP violation in Higgs decays, Phys. Rev. D 90 (11) (2014) 113006, arXiv:1405.6723 [hep-ph].
[143] ATLAS Collaboration, Evidence for Higgs boson decays to a low-mass dilepton system and a photon in pp collisions at $\sqrt{s} = 13$ TeV with the ATLAS detector, Phys. Lett. B 819 (2021) 136412, arXiv:2103.10322 [hep-ex].
[144] ATLAS Collaboration, A search for the $Z\gamma$ decay mode of the Higgs boson in pp collisions at $\sqrt{s} = 13$ TeV with the ATLAS detector, Phys. Lett. B 809 (2020) 135754, arXiv:2005.05382 [hep-ex].
[145] ATLAS Collaboration, Searches for exclusive Higgs and Z boson decays into a vector quarkonium state and a photon using 139 fb^{-1} of ATLAS $\sqrt{s} = 13$ TeV proton–proton collision data, Eur. Phys. J. C 83 (9) (2023) 781, arXiv:2208.03122 [hep-ex].
[146] CMS Collaboration, Search for Higgs boson decays to a Z boson and a photon in proton–proton collisions at $\sqrt{s} = 13$ TeV, JHEP 05 (2023) 233, arXiv:2204.12945 [hep-ex].
[147] ATLAS and CMS Collaborations, Evidence for the Higgs boson decay to a Z boson and a photon at the LHC, Phys. Rev. Lett. 132 (2024) 021803, arXiv:2309.03501 [hep-ex].
[148] Y. Sun, H.-R. Chang, D.-N. Gao, Higgs decays to $\gamma l^+ l^-$ in the standard model, JHEP 05 (2013) 061, arXiv:1303.2230 [hep-ph].
[149] ATLAS Collaboration, Measurements of Higgs boson production by gluon–gluon fusion and vector-boson fusion using $H \to WW^* \to e\nu\mu\nu$ decays in pp collisions at $\sqrt{s} = 13$ TeV with the ATLAS detector, Phys. Rev. D 108 (2023) 032005, arXiv:2207.00338 [hep-ex].
[150] ATLAS Collaboration, Measurement of the production cross section for a Higgs boson in association with a vector boson in the $H \to WW^* \to \ell\nu\ell\nu$ channel in pp collisions at $\sqrt{s} = 13$ TeV with the ATLAS detector, Phys. Lett. B 798 (2019) 134949, arXiv:1903.10052 [hep-ex].
[151] ATLAS Collaboration, Search for invisible Higgs-boson decays in events with vector-boson fusion signatures using 139 fb^{-1} of proton–proton data recorded by the ATLAS experiment, JHEP 08 (2022) 104, arXiv:2202.07953 [hep-ex].
[152] ATLAS Collaboration, Search for associated production of a Z boson with an invisibly decaying Higgs boson or dark matter candidates at $\sqrt{s} = 13$ TeV with the ATLAS detector, Phys. Lett. B 829 (2022) 137066, arXiv:2111.08372 [hep-ex].
[153] The ATLAS Collaboration, The CMS Collaboration, The LHC Higgs Combination Group, Procedure for the LHC Higgs boson search combination in summer 2011, 2011, URL https://cds.cern.ch/record/1375842.
[154] Particle Data Group, R.L. Workman, et al., Review of particle physics, PTEP 2022 (2022) 083C01.
[155] J.R. Andersen, et al., Les houches 2015: Physics at TeV colliders, standard model working group report, 9th les houches workshop on physics at TeV colliders, 2016, arXiv:1605.04692 [hep-ph].
[156] N. Berger, et al., Simplified template cross sections - stage 1.1, 2019, arXiv:1906.02754 [hep-ph].
[157] S. Amoroso, et al., Les Houches 2019: Physics at TeV Colliders, Standard Model Working Group Report, 11th Les Houches Workshop on Physics at TeV Colliders, 2020, arXiv:2003.01700 [hep-ph].
[158] ATLAS Collaboration, Interpretations of the ATLAS measurements of Higgs boson production and decay rates and differential cross-sections in pp collisions at $\sqrt{s} = 13$ TeV, 2024, arXiv:2402.05742 [hep-ex].
[159] I. Brivio, M. Trott, The Standard Model as an Effective Field Theory, Phys. Rep. 793 (2019) 1–98, arXiv:1706.08945 [hep-ph].
[160] B. Grzadkowski, M. Iskrzyński, M. Misiak, J. Rosiek, Dimension-six terms in the standard model Lagrangian, JHEP 10 (2010) 085, arXiv:1008.4884 [hep-ph].
[161] I. Brivio, Y. Jiang, M. Trott, The SMEFTsim package, theory and tools, JHEP 12 (2017) 070, arXiv:1709.06492 [hep-ph].
[162] I. Brivio, SMEFTsim 3.0 — a practical guide, JHEP 04 (2021) 073, arXiv:2012.11343 [hep-ph].
[163] LHC Higgs Cross Section Working Group, Off-shell Higgs Interpretations Task Force : Models and Effective Field Theories Subgroup Report, LHCHWG-2022-001, CERN, Geneva, 2022, URL https://cds.cern.ch/record/2801789.
[164] K. Hagiwara, S. Ishihara, R. Szalapski, D. Zeppenfeld, Low energy effects of new interactions in the electroweak boson sector, Phys. Rev. D 48 (1993) 2182–2203.
[165] ATLAS Collaboration, Interpretations of the ATLAS measurements of Higgs boson production and decay rates and differential cross-sections in pp collisions at $\sqrt{s} = 13$ TeV, 2023, URL https://cds.cern.ch/record/2870216.
[166] S. Berge, W. Bernreuther, S. Kirchner, Determination of the Higgs CP-mixing angle in the tau decay channels at the LHC including the Drell–Yan background, Eur. Phys. J. C 74 (11) (2014) 3164, arXiv:1408.0798 [hep-ph].
[167] S. Berge, W. Bernreuther, S. Kirchner, Determination of the Higgs CP-mixing angle in the tau decay channels, Nucl. Part. Phys. Proc. 273–275 (2016) 841–845, arXiv:1410.6362 [hep-ph].
[168] C. Zhang, S. Willenbrock, Effective-field-theory approach to top-quark production and decay, Phys. Rev. D 83 (2011) 034006, arXiv:1008.3869 [hep-ph].
[169] ATLAS Collaboration, Test of CP-invariance of the Higgs boson in vector-boson fusion production and its decay into four leptons, JHEP 05 (2024) 105.
[170] D. Atwood, A. Soni, Analysis for magnetic moment and electric dipole moment form factors of the top quark via $e^+e^- \to t\bar{t}$, Phys. Rev. D 45 (1992) 2405–2413.
[171] M. Davier, L. Duflot, F. Le Diberder, A. Rougé, The optimal method for the measurement of tau polarization, Phys. Lett. B 306 (1993) 411–417.
[172] M. Diehl, O. Nachtmann, Optimal observables for the measurement of three gauge boson couplings in $e^+e^- \to W^+W^-$, Z. Phys. C 62 (1994) 397–412.
[173] ATLAS Collaboration, Test of CP invariance in vector-boson fusion production of the Higgs boson in the $H \to \tau\tau$ channel in proton–proton collisions at $\sqrt{s} = 13$ TeV with the ATLAS detector, Phys. Lett. B 805 (2020) 135426, arXiv:2002.05315 [hep-ex].
[174] ATLAS Collaboration, Test of CP invariance in Higgs boson vector-boson-fusion production using the $H \to \gamma\gamma$ channel with the ATLAS detector, Phys. Rev. Lett. 131 (2023) 061802, arXiv:2208.02338 [hep-ex].
[175] ATLAS Collaboration, Constraints on Higgs boson properties using $WW^*(\to e\nu\mu\nu)jj$ production in 36.1 fb^{-1} of $\sqrt{s} = 13$ TeV pp collisions with the ATLAS detector, Eur. Phys. J. C 82 (2022) 622, arXiv:2109.13808 [hep-ex].
[176] ATLAS Collaboration, Measurement of the CP properties of Higgs boson interactions with τ-leptons with the ATLAS detector, Eur. Phys. J. C 83 (7) (2023) 563, arXiv:2212.05833 [hep-ex].
[177] ATLAS Collaboration, CP Properties of Higgs boson interactions with top quarks in the $t\bar{t}H$ and tH processes using $H \to \gamma\gamma$ with the ATLAS detector, Phys. Rev. Lett. 125 (2020) 061802, arXiv:2004.04545 [hep-ex].
[178] M. Krämer, J. Kühn, M.L. Stong, P.M. Zerwas, Prospects of measuring the parity of Higgs particles, Z. Phys. C 64 (1994) 21–30, arXiv:hep-ph/9404280.

[179] ATLAS Collaboration, Probing the *CP* nature of the top-Higgs Yukawa coupling in $t\bar{t}H$ and tH events with $H \to b\bar{b}$ decays using the ATLAS detector at the LHC, Phys. Lett. B 849 (2023) 138469, arXiv:2303.05974 [hep-ex].
[180] G. Degrassi, P.P. Giardino, F. Maltoni, D. Pagani, Probing the Higgs self coupling via single Higgs production at the LHC, JHEP 12 (2016) 080, arXiv:1607.04251 [hep-ph].
[181] F. Maltoni, D. Pagani, A. Shivaji, X. Zhao, Trilinear Higgs coupling determination via single-Higgs differential measurements at the LHC, Eur. Phys. J. C 77 (12) (2017) 887, arXiv:1709.08649 [hep-ph].
[182] S. Di Vita, C. Grojean, G. Panico, M. Riembau, T. Vantalon, A global view on the Higgs self-coupling, JHEP 09 (2017) 069, arXiv:1704.01953 [hep-ph].
[183] M. Gorbahn, U. Haisch, Indirect probes of the trilinear Higgs coupling: $gg \to h$ and $h \to \gamma\gamma$, JHEP 10 (2016) 094, arXiv:1607.03773 [hep-ph].
[184] W. Bizoń, M. Gorbahn, U. Haisch, G. Zanderighi, Constraints on the trilinear Higgs coupling from vector boson fusion and associated Higgs production at the LHC, JHEP 07 (2017) 083, arXiv:1610.05771 [hep-ph].
[185] M. McCullough, An indirect model-dependent probe of the Higgs self-coupling, Phys. Rev. D 90 (1) (2014) 015001, arXiv:1312.3322 [hep-ph].
[186] LHC Higgs Cross Section Working Group, Modelling of the Single-Higgs Simplified Template Cross-Sections (STXS 1.2) for the Determination of the Higgs Boson Trilinear Self-Coupling, Tech. Rep. LHCHWG-2022-002, CERN, 2022, URL https://cds.cern.ch/record/2803606.
[187] ATLAS Collaboration, Search for nonresonant pair production of Higgs bosons in the $b\bar{b}b\bar{b}$ final state in pp collisions at $\sqrt{s}$=13 TeV with the ATLAS detector, Phys. Rev. D 108 (5) (2023) 052003, arXiv:2301.03212 [hep-ex].
[188] ATLAS Collaboration, Search for pair production of boosted Higgs bosons via vector-boson fusion in the $b\bar{b}b\bar{b}$ final state using *pp* collisions at $\sqrt{s} = 13$ TeV with the ATLAS detector, Phys. Lett. B 858 (2024) 139007.
[189] ATLAS Collaboration, Search for resonant and non-resonant Higgs boson pair production in the $b\bar{b}\tau^+\tau^-$ decay channel using 13 TeV *pp* collision data from the ATLAS detector, JHEP 07 (2023) 040, arXiv:2209.10910 [hep-ex].
[190] ATLAS Collaboration, Search for the non-resonant production of Higgs boson pairs via gluon fusion and vector-boson fusion in the $b\bar{b}\tau^+\tau^-$ final state in proton–proton collisions at $\sqrt{s} = 13$ TeV with the ATLAS detector, Phys. Rev. D 110 (3) (2024) 032012, arXiv:2404.12660 [hep-ex].
[191] ATLAS Collaboration, Search for Higgs boson pair production in the two bottom quarks plus two photons final state in *pp* collisions at $\sqrt{s} = 13$ TeV with the ATLAS detector, Phys. Rev. D 106 (5) (2022) 052001, arXiv:2112.11876 [hep-ex].
[192] ATLAS Collaboration, Studies of new Higgs boson interactions through nonresonant *HH* production in the $b\bar{b}\gamma\gamma$ final state in *pp* collisions at $\sqrt{s} = 13$ TeV with the ATLAS detector, JHEP 01 (2024) 066, arXiv:2310.12301 [hep-ex].
[193] ATLAS Collaboration, Combination of searches for Higgs boson pair production in *pp* collisions at $\sqrt{s} = 13$ TeV with the ATLAS detector, Phys. Rev. Lett. 133 (10) (2024) 101801, arXiv:2406.09971 [hep-ex].
[194] ATLAS Collaboration, Search for non-resonant Higgs boson pair production in final states with leptons, taus, and photons in *pp* collisions at $\sqrt{s}$=13 TeV with the ATLAS detector, JHEP 08 (2024) 164, arXiv:2405.20040 [hep-ex].
[195] ATLAS Collaboration, Search for non-resonant Higgs boson pair production in the $2b + 2\ell + E_{\mathrm{T}}^{\mathrm{miss}}$ final state in *pp* collisions at $\sqrt{s} = 13$TeV with the ATLAS detector, JHEP 02 (2024) 037, arXiv:2310.11286 [hep-ex].
[196] ATLAS Collaboration, HEFT interpretations of Higgs boson pair searches in $b\bar{b}\gamma\gamma$ and $b\bar{b}\tau^+\tau^-$ final states and of their combination in ATLAS, 2022, URL https://cds.cern.ch/record/2806411.
[197] ATLAS Collaboration, Constraints on the Higgs boson self-coupling from single- and double-Higgs production with the ATLAS detector using pp collisions at $\sqrt{s}$=13 TeV, Phys. Lett. B 843 (2023) 137745, arXiv:2211.01216 [hep-ex].
[198] ATLAS Collaboration, Constraints on the Higgs boson self-coupling from single- and double-Higgs production with the ATLAS detector using *pp* collisions at $\sqrt{s} = 13$ TeV, Phys. Lett. B 843 (2023) 137745, arXiv:2211.01216 [hep-ex].
[199] ATLAS Collaboration, Search for Higgs boson pair production in the $\gamma\gamma b\bar{b}$ final state with 13 TeV *pp* collision data collected by the ATLAS experiment, JHEP 11 (2018) 040, arXiv:1807.04873 [hep-ex].
[200] ATLAS Collaboration, Search for resonant and nonresonant Higgs boson pair production in the $b\bar{b}\tau^+\tau^-$ decay channel in *pp* collisions at $\sqrt{s} = 13$ TeV with the ATLAS detector, Phys. Rev. Lett. 121 (2018) 191801, arXiv:1808.00336 [hep-ex].
[201] ATLAS Collaboration, Search for pair production of Higgs bosons in the $b\bar{b}b\bar{b}$ final state using proton–proton collisions at $\sqrt{s} = 13$ TeV with the ATLAS detector, JHEP 01 (2019) 030, arXiv:1804.06174 [hep-ex].
[202] ATLAS Collaboration, Search for Higgs boson pair production in the $b\bar{b}WW^*$ decay mode at $\sqrt{s} = 13$ TeV with the ATLAS detector, JHEP 04 (2019) 092, arXiv:1811.04671 [hep-ex].
[203] ATLAS Collaboration, ATLAS flavour-tagging algorithms for the LHC run 2 pp collision dataset, Eur. Phys. J. C 83 (7) (2023) 681, arXiv:2211.16345 [physics.data-an].
[204] ATLAS and CMS Collaborations, Addendum to the report on the physics at the HL-LHC, and perspectives for the HE-LHC: Collection of notes from ATLAS and CMS, CERN Yellow Rep. Monogr. 7 (2019) Addendum, arXiv:1902.10229 [hep-ex].
[205] ATLAS and CMS Collaborations, Snowmass white paper contribution: Physics with the phase-2 ATLAS and CMS detectors, 2022, URL https://cds.cern.ch/record/2805993.
[206] ATLAS Collaboration, HL-LHC prospects for the measurement of Higgs boson pair production in the $b\bar{b}b\bar{b}$ final state and combination with the $b\bar{b}\gamma\gamma$ and $b\bar{b}\tau^+\tau^-$ final states at the ATLAS experiment, 2022, URL https://cds.cern.ch/record/2841244.
[207] ATLAS Collaboration, ATLAS computing acknowledgements, 2023, URL https://cds.cern.ch/record/2869272.